Phase Change Material Thermal Energy Storage for a Supercritical Water Desalination System

By

Emre U. Bal

May 2024

Director of Thesis: Dr. Tarek Abdel-Salam

Major Department: Engineering

ABSTRACT

Due to the growing population and increasing demand for clean water, new solutions are being developed to access clean water. Supercritical water desalination (SCWD) is one of the solutions still developing. However, SCWD is a process that consumes high energy. This thesis presents a comprehensive study on the integration of a phase change material (PCM) thermal energy storage (TES) system into an SCWD system. The objective of this research is to address the pressing issues of energy consumption and environmental sustainability in the desalination process by harnessing renewable solar energy and leveraging the latent heat storage capacity of PCM.

By incorporating PCM energy storage, the availability of stored thermal energy during periods of high demand is ensured, further enhancing the energy efficiency and resilience of the system. The proposed integration of PCM thermal energy storage for preheating an SCWD system aims to reduce energy consumption from the furnace and minimize the environmental impact of the SCWD process by introducing a sustainable solar energy source.

The research approach encompasses experimental analysis, numerical simulations, and data processing. The experiment focuses on investigating the heat transfer occurring in the PCM storage tank, specifically from the PCM to the fluid, with various data parameters such as temperatures, pressures, and flow rates being recorded. MATLAB is employed to simulate the SCWD process, while the System Advisor Model (SAM) is utilized to collect and process weather data for solar energy analysis. The numerical analysis encompasses performance assessment and economic evaluation of the integrated system.

This study aims to propose a novel strategy for enhancing the sustainability and energy efficiency of SCWD systems through the integration of renewable energy sources. It provides valuable insights into the influence of PCMs on solar thermal energy utilization in SCWD. Furthermore, the findings contribute to a better understanding of the impact of this integration on the performance and cost of SCWD. The results of this research are crucial for the development and implementation of efficient and environmentally friendly desalination technologies.

Phase Change Material Thermal Energy Storage for a Supercritical Water Desalination System

A Thesis

Presented to the Faculty of the Department of Engineering

East Carolina University

In Partial Fulfillment of the Requirements for the Degree

Master of Science in Mechanical Engineering

By

Emre U. Bal

May 2024

Director of Thesis: Tarek Abdel-Salam, PhD

Thesis Committee Members:

Tarek Abdel-Salam, PhD

Kurabachew Duba, PhD

Jinbo Chen, PhD

Acknowledgements

I would like to express my heartfelt gratitude to my family and friends who have supported me throughout my journey to completing this thesis. Your unwavering love, encouragement, and understanding have been instrumental in my success.

First and foremost, I would like to thank my wife, my parents, and my brother for their constant belief in me and their unconditional support. Your guidance, sacrifices, and endless encouragement have been the driving force behind my accomplishments. I would also like to extend my appreciation to my uncle for his invaluable support and mentorship.

I am deeply indebted to my advisor, Dr. Tarek Abdel-Salam, for their guidance, expertise, and continuous support throughout the entire research process. Their wealth of knowledge, insightful feedback, and unwavering commitment to excellence have been invaluable in shaping the direction of this thesis. I am grateful for their mentorship and for providing me with the opportunity to grow both academically and personally.

Finally, I would like to extend my thanks to Gabriel Glosson for his assistance on the MATLAB simulation, and Michael Trapani and Kenneth Weddle for their help with the experimental work.

Contents

List of Tables

List of Figures

List of Abbreviations

CSP	Concentrated Solar Power
EES	Electrical Energy Storage
EPA	Environmental Protection Agency
FNPT	Female National Pipe Thread
HP	High Pressure
LMTD	Logarithmic Mean Temperature Difference
MED	Multi-Effect Distillation
MSF	Multi-Stage Flash Distillation
NIST	National Institute of Standards and Technology
NREL	National Renewable Energy Laboratory
NSRDB	National Solar Radiation Database
NTU	Number of Transfer Units
PCM	Phase Change Material
PV	Photovoltaic
REFPROP	Reference Fluid Thermodynamic and Transport Properties Database
RO	Reverse Osmosis
SAM	System Advisor Model
SCWD	Supercritical Water Desalination
TES	Thermal Energy Storage
TMY	Typical Meteorological Year
ZLD	Zero Liquid Discharge

Nomenclature

A	Surface area (m^2)
C_{max}	Maximum heat capacity rate
C_{min}	Minimum heat capacity rate
C_p	Specific Heat (kJ/kg.K)
d	Thickness (m)
h	Convective heat transfer coefficient ($W/m^2.K$)
H	Enthalpy (kJ/kg)
H_f	Specific Enthalpy (kJ/kg)
k	Thermal conductivity (W/m.K)
Q	Rate of heat transfer (W)
Q_{actual}	Actual heat transfer rate (W)
Q_{max}	Maximum heat transfer rate (W)
R	Thermal Resistance
T_∞	Ambient Temperature (K)
T_s	Surface temperature (K)
U	Overall heat transfer coefficient ($W/m^2.K$)
ε	Heat exchanger effectiveness
σ	Stefan-Boltzmann constant ($5.67x10^{-8}$ $W/m^2.K^4$)

Chapter 1

Introduction

As the global population continues to increase, the demand for energy automatically increases, and so does the need for clean, pure water. Fossil-fuel-based energy sources which is commonly over-used in the past, are not only finite but also significantly high greenhouse gas emissions and environmental degradation. By transitioning to renewable energy, the escalating energy requirements can be addressed while reducing the carbon footprint and mitigating the impacts of global warming and climate change as well. Moreover, access to clean, pure water has become a major issue due to population growth, water pollution, climate change, poor sanitation, etc.

One of the solutions to the problem of not being able to access clean water resources in the world is desalination. Desalination is the process of removing salt and other impurities from seawater or brackish water to produce freshwater suitable for human use or other purposes. Since the majority of the Earth's water supply is in the form of salt water in oceans and seas, the primary objective of desalination is to convert saline water into potable water. There are several desalination methods. However, all desalination methods require a lot of energy which may lead to high operating costs and bad environmental impacts. According to the data, there are more than 15,000 desalination plants in the world that produce approximately 95 million m^3 of fresh water per day [1].

Nearly all desalination plants are located along the coast, and brine waste is usually dumped into the seas or oceans. The new regulations have increased the demand for zero-liquid discharge (ZLD) technology by necessitating the development of new methods for treating brine streams.

Supercritical water desalination is a ZLD technology that uses supercritical conditions (Temperature > 374 °C, Pressure > 22.1 MPa) and the non-polar nature of water to separate salt from water [2] The characteristics of water drastically change under supercritical conditions, making inorganic materials insoluble in water [3]. This technology has an advantage over traditional desalination methods in that it is adaptable to a variety of brine streams with variable concentrations. For a feed concentration of 3.5 wt% NaCl, the recovery of drinking water can be almost 95% (mass basis) depending on the separation parameters [4]. However, supercritical water desalination is a desalination method that requires a high temperature which is around 450 °C, and it makes the process energy intensive [5]. According to the enthalpy calculations conducted in the research by Odu et al., the required amount of thermal energy estimation for a supercritical water desalination process at 460 °C and 300 bar for 3.5 wt% NaCl feed is 450 MJ/m^3 [6].

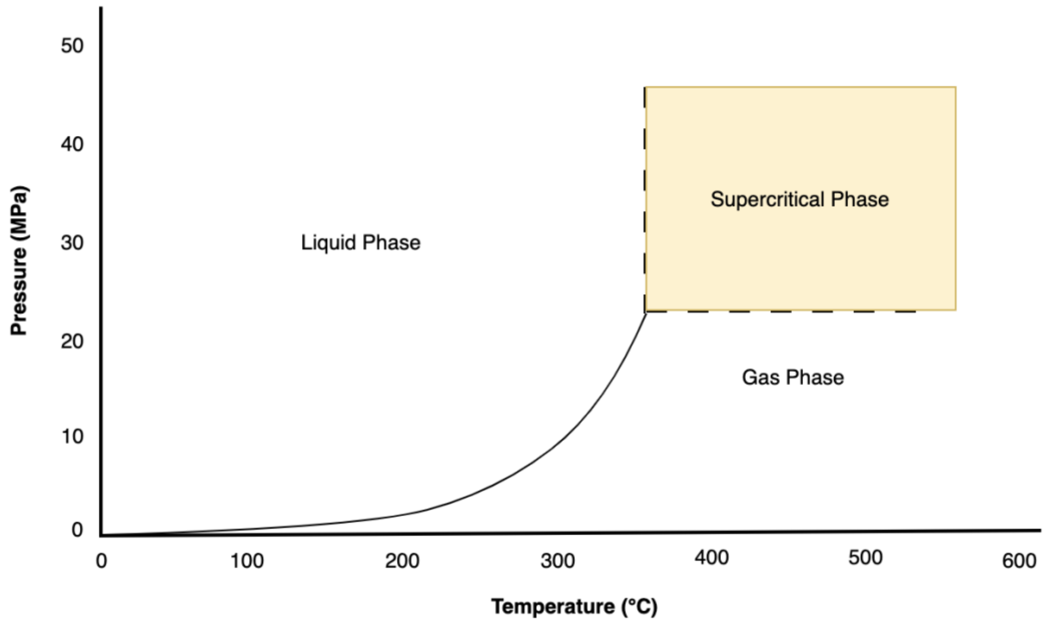

Figure 1: Phase diagram of water

This high energy requirement for supercritical water desalination leads to a heavy reliance on fossil fuels, which have long been the world's primary energy source. The use of fossil fuels comes with a significant environmental cost, with carbon emissions and other environmental impacts leading to concerns over climate change, global warming, and sustainability. In response to these challenges, renewable energy sources have emerged as a viable alternative to fossil fuels. Renewable energy sources, such as solar, wind, hydroelectric, and geothermal power, offer a promising solution to mitigate the bad environmental impact and combat climate change. Transitioning to these sustainable alternatives is crucial for a greener and more resilient future, reducing the carbon footprint and ensuring the long-term well-being of our planet. Among the search for sustainable alternatives, solar energy has emerged as a frontrunner. Harnessing the power of the sun through photovoltaic panels and solar thermal systems, solar energy presents an eco-friendly and abundant solution to meet the growing energy needs while significantly reducing carbon emissions and combating climate change. One potential approach to overcome the problem of high energy requirements for supercritical water desalination is integrating solar energy into desalination. Solar energy is abundant in many regions, and its use can significantly reduce the reliance on fossil fuels. When it comes to renewable energy sources like solar power, energy storage becomes a crucial aspect of the equation. Energy storage methods allow to store excess energy generated during peak production times and use it during periods of low or no energy generation. One significant method of energy storage, particularly relevant to solar energy, is thermal energy storage.

Thermal energy storage systems operate by capturing the excess heat generated by solar panels during the available periods and storing it for later use when solar energy is not accessible, such as during cloudy days or nighttime. TES systems have been widely studied and developed for decades, and they are recognized as a viable option to support the integration of renewable energy sources. These systems can store the captured thermal energy in various forms, including high-temperature liquids, molten salts, or phase-change materials. When energy demand increases, the stored thermal energy can be released to generate electricity or provide heating for several purposes including residential and industrial purposes. TES systems store thermal energy in various forms, including sensible heat, latent heat, and thermochemical energy [7]. Among these, PCMs have been widely used as storage media due to their high energy storage density, ability to store and release thermal energy at a constant temperature, and long-term stability. These materials offer a remarkable advantage in thermal energy storage due to their unique ability to undergo phase transitions, changing their state from solid to liquid and vice versa while storing and releasing large amounts of energy in the process. The use of phase change materials in thermal energy storage offers several advantages. The most important advantage of PCMs, these materials have high energy storage densities compared to conventional materials, allowing for a more compact and space-efficient storage solution. As research continues to advance in this field, specifically on phase change materials, further innovations and their application in thermal energy storage hold the potential to accelerate the widespread adoption of solar power and contribute significantly to the global transition towards cleaner and greener energy solutions.

Integration of renewable energy systems into the systems already in use especially sourced from non-renewable, conventional sources plays a critical role in lowering fossil fuel use, reducing greenhouse gas emissions, and eventually reducing the effects of climate change.

This thesis aims to propose the development and integration of a phase change material thermal energy storage system into supercritical water desalination. Experimental work, simulation, and numerical work were involved in this study. Since solar energy is the main energy source for thermal energy storage, solar data is needed to make the required calculations for solar energy. System Advisor Model (SAM) software was utilized to access solar data. SAM is a software developed by the National Renewable Energy Laboratory (NREL) to model renewable energy systems including concentrated solar power (CSP), photovoltaic (PV), geothermal, wind, etc. SAM integrates the annual time series power production models into the financial models to assess the performance indicators and cost analysis for renewable energy projects [8]. The NREL also has a publicly accessible solar database named the National Solar Radiation Database (NSRDB) which contains solar radiation and meteorological data [9]. This dataset includes a type of data called Typical Meteorological Year (TMY). TMY contains the hourly data throughout the year. The collected TMY data through NSRDB was used to evaluate the amount of solar energy collected and eventually, the amount of solar energy utilized in the experiment.

The experiment of this study demonstrates the solar thermal energy storage for the supercritical water desalination system on a smaller scale. For the demonstration of solar thermal energy storage, a tank filled with PCM was used. The heat source in the experiment is an electric heater. This PCM tank was covered with a blanket-type electric heater to heat the phase change material to provide the required heat transfer for the operating fluid. The PCM tank used in the experiment has a coil pipe in it. Operating fluid passes through the coil pipe and receives the heat from the phase change material in the tank.

Chapter 2

Background

2.1 Desalination

The demand for freshwater has escalated due to population growth, changing climatic patterns, and limited resources. As a response to the scarcity of traditional freshwater resources, desalination is a promising solution to this matter. Desalination is the process of producing fresh water by extracting salts and minerals from brine/seawater.

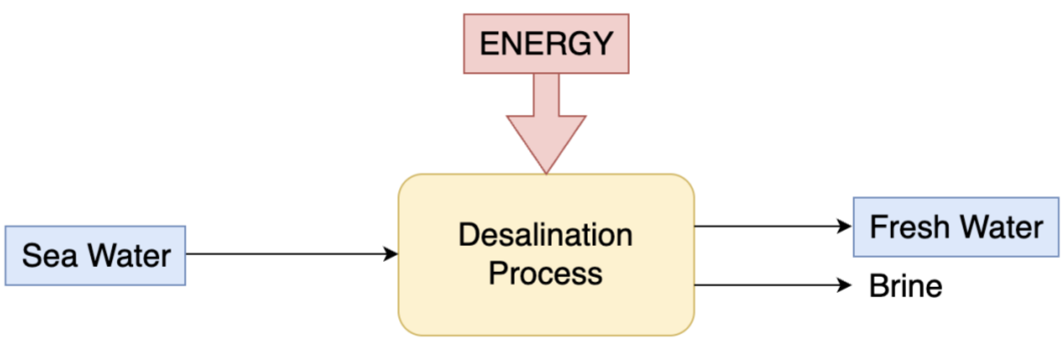

Figure 2: Desalination process diagram

The desalination technology has gained significance, especially in water-stressed regions where conventional freshwater resources are insufficient to meet the increasing demand. The environmental impact and economic feasibility of water desalination technologies are vital factors inspiring their widespread implementation and sustainability. Opportunities for integrating renewable energy sources into desalination, optimizing process efficiency, and developing novel materials are some key points to consider for the development of the desalination process. Additionally, the importance of interdisciplinary collaboration and policy support in advancing water desalination research and implementation is emphasized to achieve sustainable water management solutions.

There are several desalination techniques exist, each with distinct operational mechanisms and principles. Reverse Osmosis (RO), Multi-Stage Flash Distillation (MSF), Multi-Effect Distillation (MED), Electrodialysis, and solar-powered desalination are some of the desalination methods. These methods vary in efficiency, energy consumption, cost-effectiveness, and applicability based on the conditions in the application location and available resources.

Reverse Osmosis (RO) is one of the most common desalination methods which uses a semi-permeable membrane that allows water molecules to pass through while blocking salts and impurities. RO methods the commonly preferred over the other alternatives because of their cost-effectiveness [10]. In Multi-Stage Flash (MSF) Distillation, seawater is heated under high pressure, causing it to evaporate. The steam is then condensed into fresh water, leaving the salts behind. This process occurs in multiple stages, each at a lower pressure, to enhance efficiency. Similar to MSF, MED uses multiple stages, but instead of varying pressure levels, it relies on different temperatures for evaporation. Heat from one stage is used to evaporate seawater in the next, maximizing energy efficiency. The electrodialysis technique involves passing seawater through ion-selective membranes under the influence of an electric field. It separates ions, allowing fresh water to pass through while retaining the salts. Lastly, in solar-powered desalination method uses solar panels to heat seawater, causing evaporation, and then condensing the vapor to obtain fresh water.

2.1.1 Supercritical Water Desalination

Supercritical water desalination (SCWD) is a ZLD technology that utilizes water in supercritical conditions (374°C, 22.1 MPa) to remove the salt and other mineral ingredients from seawater [11]. Under supercritical conditions, the properties of water change and it becomes non-polar, and the inorganic ingredients become insoluble in water [12]. The dissolved salts are then separated from the water, resulting in desalinated water. In the table below (Table 1) critical properties of some solvents are shown:

Table 1: Critical properties of some solvents

Solvent	Critical Temperature (K)	Critical Pressure (MPa)	Critical Density (g/cm^3)
Carbon dioxide (CO_2)	304.1	7.38	0.469
Water (H_2O)	647.096	22.064	0.322
Methane (CH_4)	190.4	4.6	0.162
Ethane (C_2H_6)	305.3	4.87	0.203
Propane (C_3H_8)	369.8	4.25	0.217

As mentioned in the paper written by van Wyk et al. [11], three main parts of SCWD are the heating section, the gravity separator, and the brine recovery. In the heating part, saline water is firstly pressurized and heated to reach the supercritical conditions.

SCWD has various advantages over other desalination methods. One of the most important advantages of SCWD is that it can be integrated with energy recovery systems to improve its efficiency. As mentioned earlier, with water in its supercritical state, it exhibits remarkable solubility, enabling the effective removal of salts from seawater without the need for additional chemicals or additives. This efficiency translates to reduced energy requirements compared to traditional desalination methods such as reverse osmosis. However, despite its promising potential, the equipment required for this method can be costly to install and maintain, contributing to higher operating expenses. Technical complexities arise from the precise control required over temperature and pressure conditions during operation, which can complicate system design and increase the risk of operational issues. And more importantly, the high energy consumption required for heating and pressurizing water remains a substantial difficulty. Since the SCWD is a high energy-consuming process due to the high target temperature for brine, a high-temperature heater (>450°C) is needed for the system [13]. According to the research by van Wyk et al., compared to brine crystallizers, the net energy consumption for SCWD is double, assuming a 50% conversion efficiency of thermal energy to electricity [11], [13]. There are several studies performed due to the high energy consumption of SCWD and using thermal energy storage is one of them. Pumped thermal energy storage is one of the developing thermal energy storage technologies and is generally used for large-scale energy storage applications [13], [14], [15].

2.2 Solar Energy

The need for renewable energy increases because of the energy demand and the environmental impacts of non-renewable energy sources. These problems push us to use renewable energy sources/systems. Solar energy, wind energy, biomass, etc. are some of the continuously rising and developing renewable energy sources. Solar energy, deriving radiation from the sun is one of the most important and most common renewable energy sources in the world. As mentioned in a study (2023), 14% of the electricity generation from renewable sources is from solar energy in the European Union and it is the fastest-growing renewable energy source [16]. As the world faces the challenges of climate change and global warming, the importance of the utilization of renewable energy increases, and it becomes crucial and urgent. Solar energy is an abundant and endless resource that offers a solution to meet the increasing global energy demand as it minimizes the environmental reflections of conventional energy generation methods. As all the other renewable energy systems, efficient energy storage methods are essential for solar energy to reach their full potential. One of the very important challenges of solar energy is inconsistent solar radiation. This is one of the primary reasons indicating the importance of the improvements in energy storage technologies. These developments are essential to ensure a steady and dependable power supply, which makes it easier to integrate solar energy into conventional energy systems.

Solar energy includes many types of energy technologies that harness the abundant energy from the sun. These technologies/methods are broadly classified into two main categories: solar photovoltaic (PV) systems and solar thermal systems.

Photovoltaic (PV) solar systems employ sunlight to generate electricity through the photovoltaic cells. PV solar panels, typically containing silicon cells, absorb photons from sunlight, causing electrons to be released, creating an electric current. This direct conversion of sunlight into electricity is the ability of PV systems. This generated electricity by PV panels can either be used immediately, stored in batteries for later use, or fed into the grid. PV systems are adaptable and scalable. PV systems can be installed on rooftops, in solar farms, or integrated into various structures. In a study conducted by Chiang et al. [17], the author states that the performance of PV systems decreases by 0.5% for an increase of a degree in operating temperature.

On the other hand, solar thermal systems utilize sunlight to directly heat water or air for various applications. These systems typically contain solar collectors, which absorb sunlight and convert it into heat energy. In water-based thermal systems, sunlight heats a fluid which is then circulated to heat water for domestic use, space heating, or industrial processes. In air-based systems, sunlight directly heats air, which can be used for space heating or drying applications. Solar thermal systems are highly efficient for certain heating needs/applications and can significantly reduce the reliance on conventional heating fuels such as natural gas, propane, or electricity. They are often used in combination with other heating systems to provide cost-effective and environmentally friendly solutions.

2.2.1 Solar Thermal Systems

Solar thermal systems are a subcategory of solar energy technologies that harness the abundant and renewable resource of sunlight to generate heat energy for different applications, including water heating, space heating, and electricity generation. These systems typically employ solar collectors to capture and convert sunlight into usable thermal energy. Solar thermal collector types are classified as shown in the figure below:

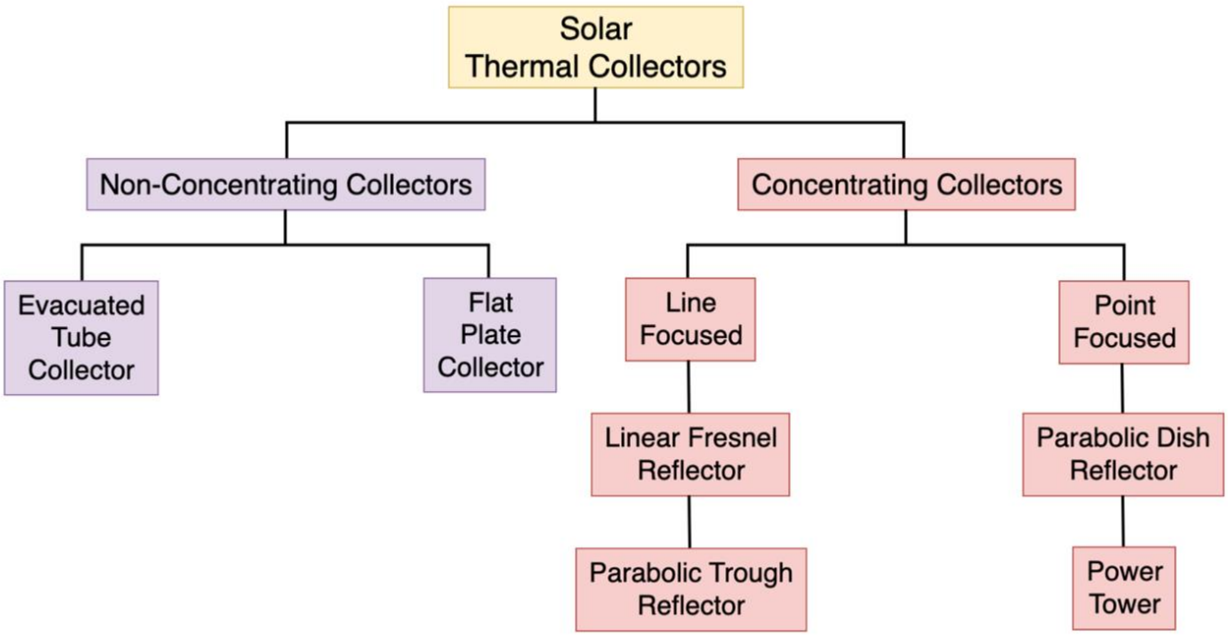

Figure 3: Classification of solar thermal collectors

In the various types of solar thermal collectors, flat-plate collectors stand out as the most widely used. They feature a straightforward design consisting of a flat, insulated metal box housing a dark-colored absorber plate, covered by a transparent layer of glass or plastic. When sunlight comes to the absorber plate, it heats a fluid circulating through tubes or channels in the collector, transferring thermal energy for heating purposes.

Another common type of solar thermal collector is the evacuated tube collector. This design includes rows of parallel glass tubes, each containing an absorber plate. By evacuating the space between the tubes, heat loss is minimized, resulting in better efficiency even in colder climates or under diffuse sunlight conditions. While evacuated tube collectors require higher initial costs compared to flat-plate collectors, their greater performance and resilience make them well-suited for a wide range of applications, particularly in regions with less promising solar conditions.

In contrast, concentrating collectors utilize mirrors or lenses to reflect and focus sunlight onto a smaller absorber area, achieving significantly higher temperatures compared to flat-plate or evacuated tube collectors. These collectors are commonly used in concentrated solar power (CSP) systems, where the concentrated solar energy is used to heat a fluid to drive a turbine for electricity generation. While concentrating collectors offer the potential for high-efficiency power generation, their complexity and cost often limit their utilization to utility-scale projects.

Solar thermal systems offer numerous advantages that contribute to their increasing adoption worldwide. Firstly, they provide a renewable and sustainable energy source, reducing reliance on limited fossil fuels and mitigating greenhouse gas emissions. Additionally, once installed, solar thermal systems have relatively low operating costs since sunlight is freely available and abundant. By displacing conventional heating fuels and electricity, solar thermal technologies contribute to energy independence and security while promoting environmental sustainability.

However, solar thermal systems also face certain challenges and limitations. High initial installation costs, particularly for systems with energy storage or complex components, can present a barrier to widespread adoption. Moreover, solar thermal systems are inherently dependent on sunlight availability, requiring backup heating systems for periods of low solar radiation or high demand. Additionally, maintenance requirements, including periodic cleaning and inspection of collectors and fluid systems, add to the overall operational considerations.

2.3 Energy Storage

Energy storage is a critical component of modern energy systems, allowing the capture and utilization of energy produced at one time for use at another. With the increasing integration of renewable energy sources like solar and wind power, energy storage systems have become essential for balancing supply and demand, mitigating intermittency. This capability is especially vital for renewable energy sources which are intermittent by nature, as they depend on factors such as weather conditions and daylight availability. It enables the decoupling of energy production from demand, allowing excess energy to be stored when supply exceeds demand and released when demand exceeds supply. It enhances grid stability, facilitates the integration of renewable energy sources, and supports a more flexible and resilient energy infrastructure.

Solar energy storage technologies play a critical role in ensuring a reliable and stable energy supply from solar sources, regardless of fluctuations in sunlight. Several methods of storing solar energy have been developed, each with its own advantages and limitations. These methods can broadly be categorized into thermal energy storage (TES) and electrical energy storage (EES) systems:

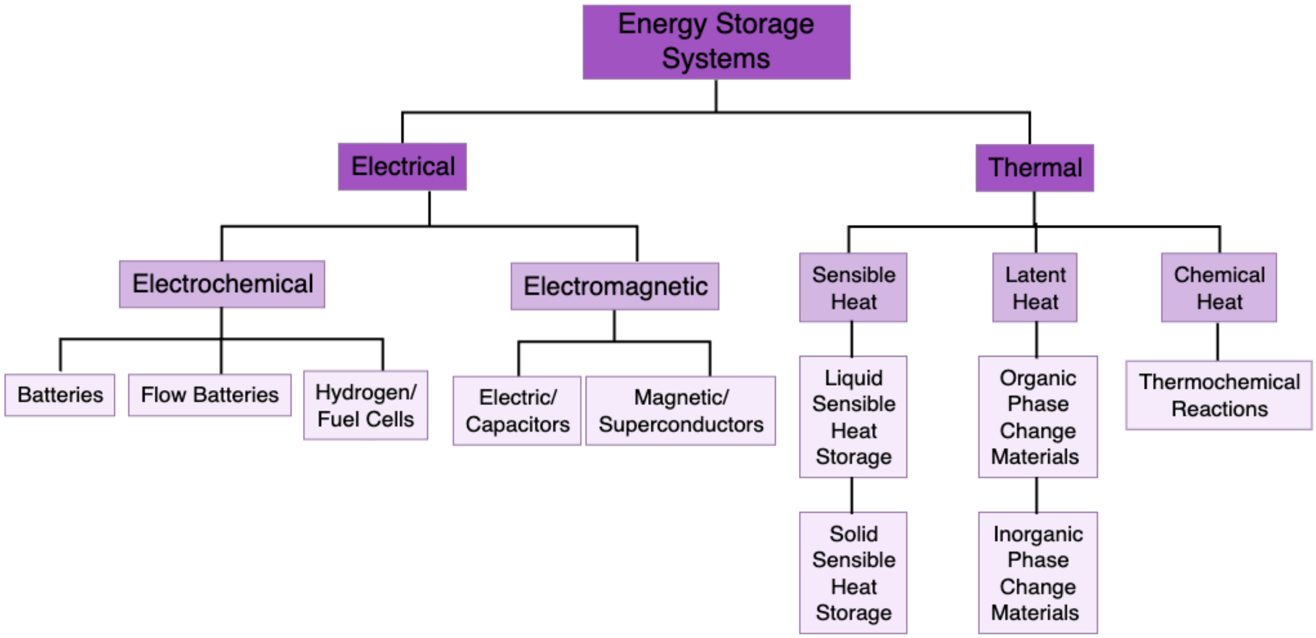

Figure 4: Classification of energy storage systems

2.3.1 Thermal Energy Storage

Thermal energy storage (TES) stands as a pivotal technology within the realm of energy storage, offering novel solutions for capturing and utilizing heat energy. This method addresses the intermittency of renewable energy sources like solar power, providing a stable supply of energy even when sunlight fluctuates. TES systems are capable of storing thermal energy during peak sunlight hours and providing it as needed, providing a reliable and consistent energy source. Thermal energy storage systems have been widely studied and developed for decades, and they are recognized as a viable option to support the integration of renewable energy sources. Thermal energy storage systems store thermal energy in various forms, mainly classified into 3 groups latent heat, sensible heat, and thermochemical energy [18].

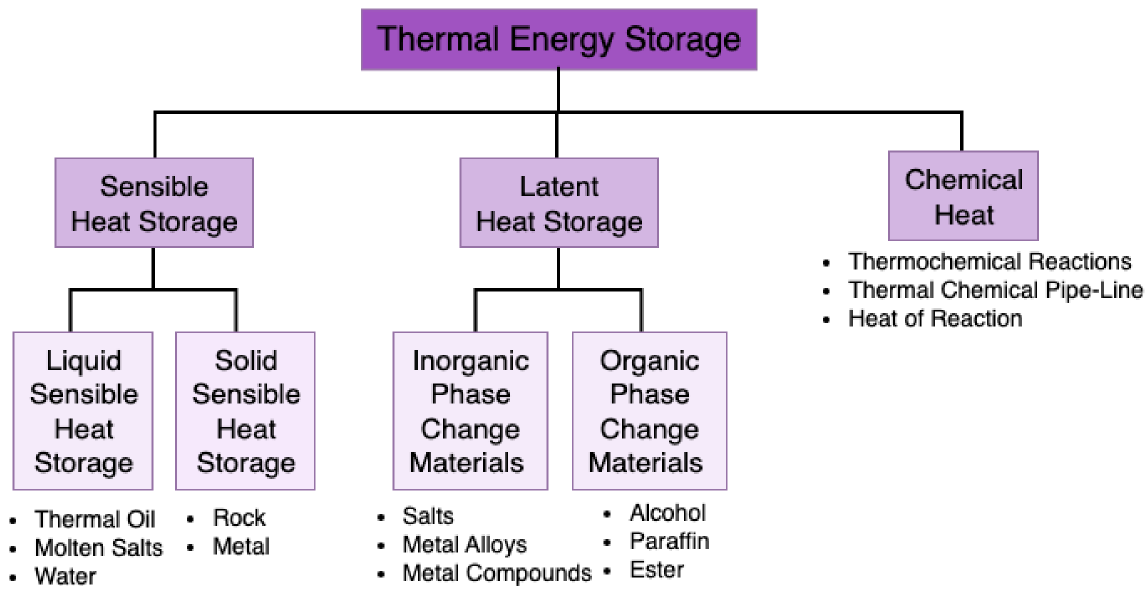

Figure 5: Subtitles of thermal energy storage

One noticeable approach in thermal energy storage is sensible heat storage, where thermal energy is stored by heating a material, such as water or molten salt, to high temperatures using solar collectors. These collectors absorb sunlight during peak production times, converting it into heat energy that is then transferred to the storage medium. This stored heat can be harnessed for various applications, including electricity generation through steam turbines or direct heating for industrial processes and space heating.

2.3.1.1 Latent Heat Storage

Latent heat storage is a type of thermal energy storage that utilizes the latent heat of a material to store and release thermal energy during phase transitions, such as melting or freezing. This process involves storing energy in the form of latent heat when a material changes phase and releasing it when the material returns to its original phase. This makes latent heat storage an effective method for storing thermal energy for later use, particularly in applications where a constant temperature is required or where energy demand fluctuates. Latent heat storage is one of the two most common types of thermal heat storage technologies [19], [20]. However, latent heat storage materials have 5 to 14 times higher energy storage density with lower temperatures [19], [21]. Because of this reason, a broad variety of research has been conducted on the thermal conductivity of different phase change materials (PCMs) [19].

2.4 Phase Change Materials

Phase change materials play one of the critical roles in thermal energy storage, as it enables the efficient storage and transfer of thermal energy. PCM is a material that can store and release large amounts of thermal energy during the melting and solidification processes, which occur at a constant temperature known as the phase change temperature. This ability to absorb or release heat during phase transitions makes PCMs valuable for thermal energy storage applications. By selecting an appropriate PCM with a suitable phase change temperature and specific heat capacity, the system can store thermal energy and release it to provide the required heat for the specific application. This effectively provides a thermal battery that can enhance the system's energy efficiency, reduce reliance on fossil fuels, and lower the operational costs and environmental impacts of desalination.

Organic phase change materials are a subset of latent heat storage materials derived from organic compounds. Organic PCMs are derived from carbon-based compounds and can include materials such as paraffin wax, fatty acids, and bio-based materials. These materials undergo phase transitions, typically from solid to liquid or vice versa, at specific temperatures (phase change temperatures). Organic PCMs offer several advantages, including high latent heat storage capacity, compatibility with a wide range of applications, and environmental friendliness compared to some inorganic alternatives such as metal compounds.

Inorganic phase change materials are substances' phase transitions typically from solid to liquid or from liquid to solid, at the phase change temperature of that specific material. Unlike organic PCMs, which are derived from carbon-based compounds, inorganic PCMs are composed of non-carbon elements such as metals, salts, or hydrates. These materials offer unique properties and advantages that make them suitable for some thermal energy storage applications. Inorganic PCMs are integrated into construction materials such as plasterboards, concrete, and roofing materials to improve thermal insulation and regulate temperatures in buildings. They are also employed in refrigeration and cold storage systems to maintain stable temperatures during the transportation and storage of food and pharmaceuticals.

2.4.1 Paraffin Wax

Because of its good thermal and energy storage properties with a transition temperature of 50–59 °C and latent heat of 210 J/g, paraffin wax is one of the most commonly used organic phase change materials [22], [23]. It is a mixture of hydrocarbons derived from petroleum or natural gas, with a molecular structure that allows it to undergo phase transitions at relatively low temperatures. Paraffin wax has a high latent heat of fusion, meaning it can store a significant amount of thermal energy during the melting process.

The use of paraffin wax as a phase change material is widespread in various applications, including building materials, thermal regulation in electronics, solar energy storage, and even in textiles for clothing with thermal regulation properties. Its adaptability, affordability, and availability make paraffin wax a preferred choice for many latent heat storage applications.

Furthermore, paraffin wax plays a vital role in thermal energy storage systems for applications such as solar water heaters, HVAC systems, and passive solar buildings. Beyond industrial uses, paraffin wax is also widespread in consumer products like candles, crayons, cosmetics, and pharmaceuticals, where its phase change properties are harnessed for specific functionalities.

Efforts are proceeding to address environmental concerns associated with paraffin wax by exploring bio-based alternatives derived from renewable sources. These bio-based variants offer similar phase change properties while reducing reliance on fossil fuels and mitigating environmental impact.

2.5 Heat Transfer

Heat transfer is a fundamental process in the field of thermodynamics, representing the exchange of thermal energy between systems or substances due to temperature differences. This transfer occurs spontaneously from regions of higher temperature to regions of lower temperature until thermal equilibrium is achieved. The study of heat transfer covers various mechanisms through which this energy exchange occurs.

Heat transfer starts from the random motion of particles within substances, showing as kinetic energy. When two systems or substances at different temperatures come into contact, this kinetic energy diffuses from the hotter to the colder system, driving the process of heat transfer. The fundamental principle of the transfer is the second law of thermodynamics, which dictates that heat naturally flows in the direction of decreasing temperature gradients, resulting in a net increase in entropy.

The second law of thermodynamics can be expressed in terms of entropy change and heat transfer. One common formulation of the second law is:

$$\Delta S_{total} \geq 0 \tag{1}$$

ΔS_{total} represents the change in total entropy. In the equation, states that the total entropy of a closed system and its surroundings either increases or remains constant over time, but it never decreases. When heat transfer occurs spontaneously from a region of a higher temperature to a region of a lower temperature, it tends to increase the entropy of the system and its surroundings.

This is because heat transfer results in a more disordered distribution of energy among the particles in the system, leading to an increase in entropy. Conversely, if heat were to transfer from a colder object to a hotter one, it would lead to a decrease in entropy, violating the second law of thermodynamics. Therefore, the second law of thermodynamics, as represented by the equation, emphasizes the direction of heat transfer in natural processes (from hot to cold), increasing the total entropy of the system and its surroundings, following the principles of thermodynamics.

Heat transfer contains various mechanisms through which thermal energy is exchanged between systems or substances. The primary types of heat transfer include conduction, convection, and radiation. Conduction involves the transfer of heat through a material medium without any discernible movement of the material itself. Convection, on the other hand, entails the transfer of heat through the movement of a fluid medium due to temperature differentials. Radiation represents the transfer of heat through electromagnetic waves, emitted by objects due to their temperature.

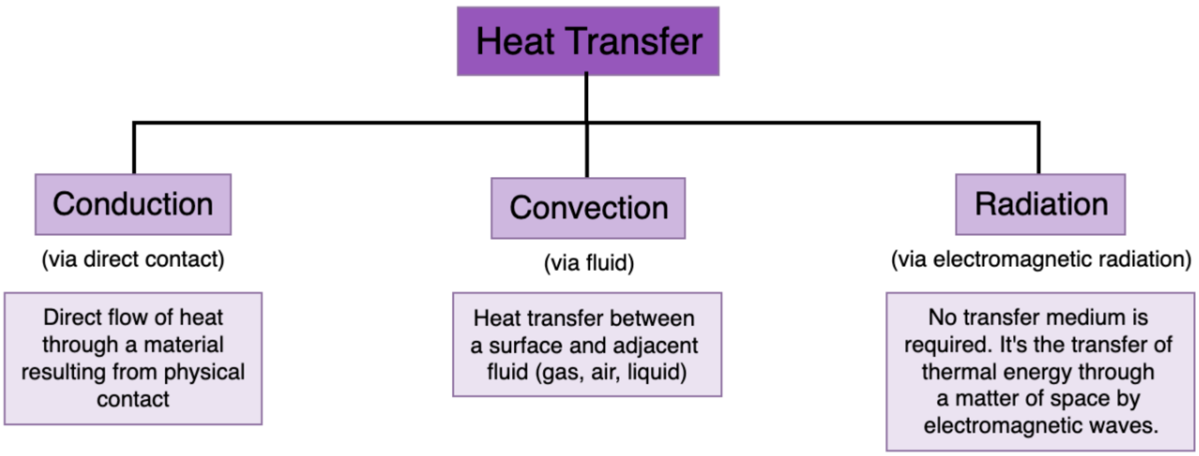

Figure 6: Heat transfer types

Conduction, one of the primary types of heat transfer, clarifies the process by which heat is transmitted through a solid medium with the vibration and collision of neighboring particles. This mechanism relies on the interactions between neighboring atoms/molecules within the material. The rate of conduction is influenced by factors such as the thermal conductivity of the material, the temperature gradient, and the cross-sectional area in which heat flows.

The rate of heat conduction can be described by Fourier's Law, which states:

$$Q = -kA\frac{\Delta T}{d} \tag{2}$$

Where “Q” is the rate of heat transfer (in watts, W), “k” is the thermal conductivity of the material (in watts per meter per kelvin, W/m.K), “A” is the cross-sectional area through which heat is transferred (in square meters, m^2), "ΔT" is the temperature difference across the material (in kelvin, K), and "d" is the thickness of the material (in meters, m).

The thermal conductivity "k" serves as a material property that orders how efficiently a substance can conduct heat. Materials with higher thermal conductivity values conduct heat more effectively than the ones with lower values. Additionally, the cross-sectional area "A" through which heat is transferred plays an important role in determining the rate of heat transfer. A larger area facilitates larger heat transfer, emphasizing the importance of considering the geometry of the system.

Convection is another type of heat transfer that involves the movement of fluids (liquids or gases) to transfer heat. Unlike conduction, which relies on direct contact between objects, convection occurs through the bulk movement of molecules within a fluid. This movement can be natural, driven by buoyancy forces due to temperature variations, or forced, induced by external forces such as fans or pumps.

The rate of heat transfer through convection can be described by Newton's Law of Cooling, which states:

$$Q = hA(T_s - T_\infty) \qquad (3)$$

Where "Q" is the rate of heat transfer (in watts, W), "h" is the convective heat transfer coefficient (in watts per square meter per kelvin, $W/m^2 \cdot K$), "A" is the surface area through which heat is transferred (in square meters, m^2), "T_s" is the surface temperature (in kelvin, K), "T_∞" is the fluid temperature far from the surface (in kelvin, K).

The rate of heat transfer “Q” is directly proportional to the temperature difference $(T_s - T_\infty)$ between the surface and the fluid. A larger temperature difference results in a higher rate of heat transfer. The convective heat transfer coefficient “h” represents the efficiency of heat transfer between the surface and the fluid. It depends on factors such as fluid properties, flow conditions, and surface geometry. Higher values of “h” indicate more efficient heat transfer. As in conduction, the rate of heat transfer is directly proportional to the surface area “A” through which heat is transferred. Increasing the surface area enhances heat transfer, as it provides more area for interaction between the surface and the fluid.

Convection plays a crucial role in many natural and industrial processes, including atmospheric circulation, HVAC (heating, ventilation, and air conditioning) systems, and heat exchangers. Understanding the principles of convection and its governing equation enables to design of efficient heat transfer systems, optimizes thermal management processes, and improves the performance of various engineering applications.

2.5.1 Heat Exchangers

Heat exchangers serve as a critical component in heat transfer processes, facilitating efficient heat transfer between fluids while minimizing energy loss. They find extensive use across various sectors including chemical processing, power generation, HVAC systems, and refrigeration. The fundamental function of a heat exchanger is to transfer heat from a hot fluid to a cooler one, or vice versa, thereby enabling temperature control and thermal management in various applications.

There are different types of heat exchangers exist, each designed to suit specific operational requirements and restrictions. Shell and tube heat exchangers represent one common design, comprising a bundle of tubes enclosed within a cylindrical shell. These exchangers simplify heat exchange between two fluids, one flowing through the tubes (tube-side fluid) and the other over the tubes within the shell (shell-side fluid). Plate heat exchangers employ a series of uneven metal plates to maximize surface area for heat transfer, making them compact and efficient. Finned heat exchangers utilize extended surfaces (fins) to enhance heat transfer by increasing the surface area available for thermal exchange. Double-pipe heat exchangers, characterized by two concentric pipes, are simpler in design and find utility in smaller-scale applications and experimental setups.

The heat transfer rate through a heat exchanger can be calculated using fundamental heat transfer equations, such as:

$$U = \frac{1}{\left(\frac{1}{h_1}\right) + (R) + \left(\frac{1}{h_2}\right)} \quad (4)$$

Where “h_1” and “h_2” are the convective heat transfer coefficients on the hot and cold sides, respectively, and “R” represents the thermal resistance due to conduction across the exchanger material.

The Logarithmic Mean Temperature Difference (LMTD) is widely used in heat exchanger design and analysis to determine the rate of heat transfer and to optimize the performance of heat exchangers. It provides a more accurate representation of the temperature driving force compared to using arithmetic mean temperature differences. The LMTD is calculated using the logarithmic temperature difference between the inlet and outlet temperatures of the hot and cold fluids. This calculation accounts for the varying temperature profiles along the length of the heat exchanger, providing a single characteristic value for the overall temperature difference. The Logarithmic Mean Temperature Difference (LMTD) equation is

$$LMTD = \frac{\Delta T_1 - \Delta T_2}{\ln{(\Delta T_1/\Delta T_2)}} \quad (5)$$

Where “ΔT_1" and “ΔT_2" are the temperature differences at the inlet and outlet of the heat exchanger.

The heat exchanger effectiveness (ε) is a parameter used to evaluate the performance of a heat exchanger by comparing the actual heat transfer achieved with the maximum possible heat transfer under ideal conditions. It calculates the efficiency with which a heat exchanger transfers thermal energy between the hot and cold fluids. The heat exchanger effectiveness typically ranges from 0 to 1, with a value of 1 indicating perfect heat transfer efficiency, where the actual heat transfer rate equals the maximum possible heat transfer rate. A lower effectiveness value indicates inefficiencies such as temperature imbalances or inadequate design. Lastly, the heat exchanger effectiveness (ε) equation is

$$\varepsilon = \frac{Q_{actual}}{Q_{max}} \quad (6)$$

Where "Q_{actual}" is the actual heat transfer rate and "Q_{max}" is the maximum possible heat transfer rate.

The number of transfer units (NTU) method is a widely used method in the analysis and design of heat exchangers. It provides a simplified effective means of quantifying the performance of a heat exchanger and predicting its effectiveness without the need for detailed temperature profiles along the length of the exchanger.

In the NTU method, the performance of a heat exchanger is characterized by two key parameters: the number of transfer units (NTU) and the heat capacity rate ratio (C). The NTU represents the size of the heat exchanger relative to the rate of heat transfer, while the heat capacity rate ratio reflects the relative thermal capacities of the two fluid streams involved in the heat exchange process.

The NTU method is particularly useful for analyzing heat exchangers with parallel or counter-flow configurations, where the temperature profiles of both fluids may vary along the length of the exchanger. By employing the NTU method, the effectiveness of the heat exchanger can be determined and its design parameters to achieve desired performance objectives.

The number of transfer units is calculated using the following formula:

$$NTU = \frac{1}{C-1} \cdot ln \frac{\varepsilon - 1}{(\varepsilon \times C) - 1} \tag{7}$$

$$C = \frac{C_{min}}{C_{max}} \tag{8}$$

$$NTU = \frac{U \times A}{C_{min}} \tag{9}$$

Where “UxA” is the overall heat transfer coefficient multiplied by the heat transfer area and “C_{min}” is the minimum heat capacity rate of the two fluid streams.

Chapter 3

Methodology

3.1 Numerical Methods

3.1.1 System Description

This study outlines a system comprising four primary components. The initial phase requires the gaining of solar data utilizing the System Advisor Model (SAM) and the National Solar Radiation Database (NSRDB), tailored to the precise geographical coordinates of the desalination location. Subsequently, within this initial part, the acquired solar data is employed to determine the incident solar energy at the designated location. Following this determination, the received solar energy serves as the basis for computation and simulation within the later stages of the study, namely the experimental part.

The following part of the study involves experimental endeavors, mainly focused on imitating solar energy through an experimental design explained in detail in the following sections. This experimental work primarily revolves around the smaller-scale utilization of solar thermal energy for heating the water by using solar thermal energy.

The experimental work of this research requires several key components, including a phase change material (PCM) storage tank equipped with an internal coil, a water reservoir, a circulation pump, a blanket-type heater, paraffin wax serving as the PCM, and necessary tubing and fittings to facilitate equipment interconnections. At ambient temperature and pressure, water is directed through the coil within the PCM storage tank via a circulating pump. An electric heater is designated to increase the temperature of the PCM, thereby enabling heat exchange between the PCM and the fluid (water). Temperature measurements at various stages throughout the experiment were precisely recorded, with the resulting data subsequently utilized for numerical analysis of heat transfer and the execution of MATLAB simulations to determine system performance.

Consequently, the study proceeded to the analysis of data gathered during the experimental work, involving the computation of heat transfer dynamics between the fluid within the experimental setup and the desalination system. Such calculations established a requirement for the MATLAB simulation in the following stage. The temperatures derived from these heat transfer calculations were employed as inlet parameters for the supercritical water desalination simulation conducted within the MATLAB environment.

The study covers an integration of a low-pressure phase change material solar thermal energy storage system into a high-pressure supercritical water desalination system. The experimental part of the study covers the low-pressure cycle, and the MATLAB simulation covers the high-pressure cycle. These two cycles are connected by a heat exchanger. During the heat exchanger calculations, the pressure difference was taken into consideration.

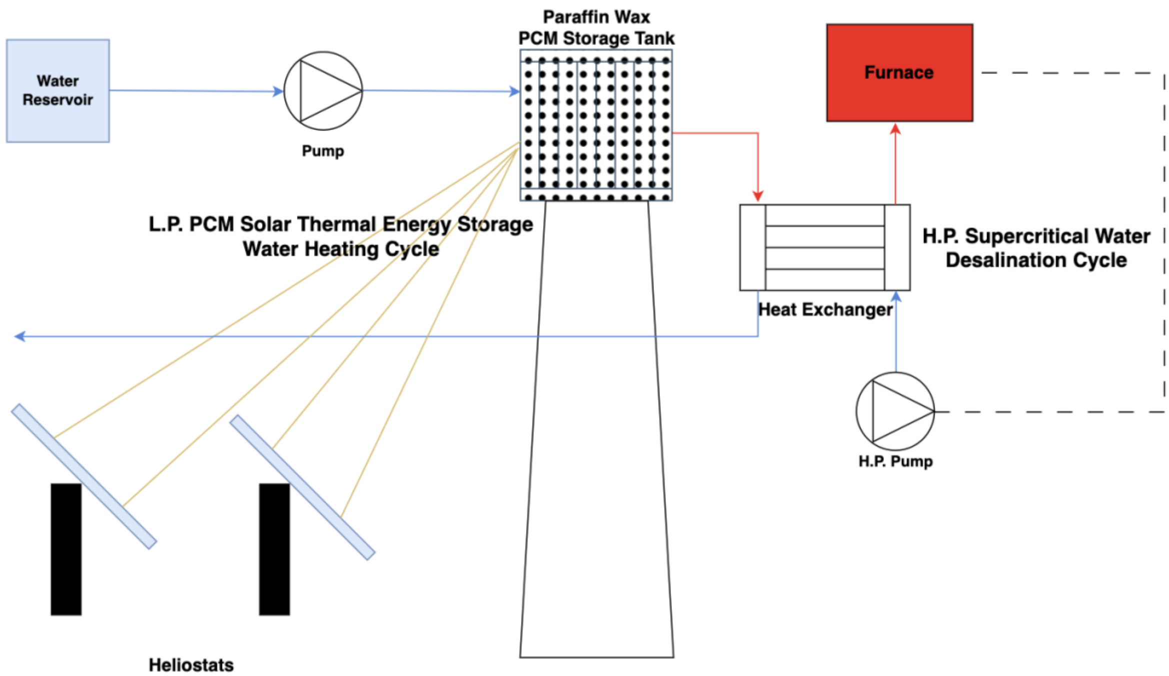

Figure 7: Overall system diagram

3.1.2 System Advisor Model (SAM)

System Advisor Model (SAM) is a software tool developed by the U.S. Department of Energy's National Renewable Energy Laboratory (NREL). It is designed to assist in the evaluation and analysis of renewable energy projects, particularly those involving solar, wind, geothermal, biomass, and other clean energy technologies. SAM provides comprehensive modeling capabilities to assess the performance, financial feasibility, and environmental impact of various energy systems.

SAM allows users to model the performance of renewable energy systems based on input parameters such as location, climate data, system design, and technology specifications. This enables users to predict energy output and system efficiency under different conditions. It also incorporates complex financial models to assess the economic feasibility of renewable energy projects. Users can evaluate factors such as project costs, financing options, incentives, and revenue streams to determine the financial attractiveness and return on investment (ROI) of proposed projects.

SAM obtains climate data from various sources, including publicly available meteorological databases, weather stations, satellite data, and global climate models. Some of the primary sources of climate data used by SAM include weather data sets provided by NREL, such as the Typical Meteorological Year (TMY), which includes hourly meteorological data representing typical weather conditions for a specific location over a one-year period.

SAM allows users to select the most appropriate climate data source and input the necessary meteorological data for their specific location and project requirements. This data is crucial for accurately modeling the performance and energy output of renewable energy systems under different weather conditions.

3.1.3 Solar Data

Solar energy is the main source of thermal energy systems. As mentioned in the introduction section, required solar data was obtained by using the System Advisor Model (SAM) which is a renewable energy modeling software developed by the U.S. National Renewable Energy

Laboratory (NREL). The National Solar Radiation Database (NSRDB) is also a public database published by NREL which contains solar radiation and meteorological data [9].

The data used in the study is "Typical Meteorological Year (TMY)" which contains the hourly data throughout the year. The TMY data is requested from the "NSRDB Viewer" on the official website [24]. The requested data contains the direct normal irradiance (DNI) in W/m^2, global horizontal irradiance (GHI) in W/m^2, and temperature in °C. The specifications of the data can be found below in Table 2.

Table 2: Specifications of the requested TMY data from NSRDB

Source	NSRDB
Location ID	1185124
Latitude	36.37
Longitude	-75.82
Time Zone	-5
Elevation	0

The collected TMY data for the specific location was used for calculating the solar energy amount. To determine the amount of solar energy and the temperature required to imitate the solar energy in the experiment, the following formula has been established:

$$Q = m \times \Delta H \tag{10}$$

Where “Q” is the rate of heat transfer, “m” is the mass of the substance, and “ΔH” is the enthalpy difference.

According to the collected TMY data for the specified location (Outer Banks, NC), the annual average direct normal irradiance (DNI) is 193.695 W/m^2 [24].

Daily and monthly DNI values and the heat map of DNI according to the hour of the day are as follows in the SAM interface from the NSRDB database [24].

Since the solar irradiation value is per hour, an average sunlight duration was needed for the same year to calculate the amount of daily average solar irradiation. The average sunlight duration was calculated by using a calculator tool developed and published by Global Monitoring Laboratories of the National Oceanic and Atmospheric Administration (NOAA), and the U.S. Department of Commerce. According to the information shared on the official website of NOAA, the calculations in the calculator are based on the equations in Astronomical Algorithms published by Jean Meeus [25], [26].

On the calculator provided by Global Monitoring Laboratories of the National Oceanic and Atmospheric Administration (NOAA), the latitude, longitude, time zone, and year were changed according to the specific application location of the study. The data obtained by using the calculator tool was used to calculate the average sunlight duration. The average sunlight duration in 2022 was found as 730.9163 minutes (12.18194 hours).

As a result, the daily average direct normal irradiance is 2,359.581 W/m^2 or 2.359581 kW/m^2.

The daily and monthly DNI and GHI values are shown in the graphs below and expectedly, the solar irradiance is higher during the summer than the winter months matching with the heat map.

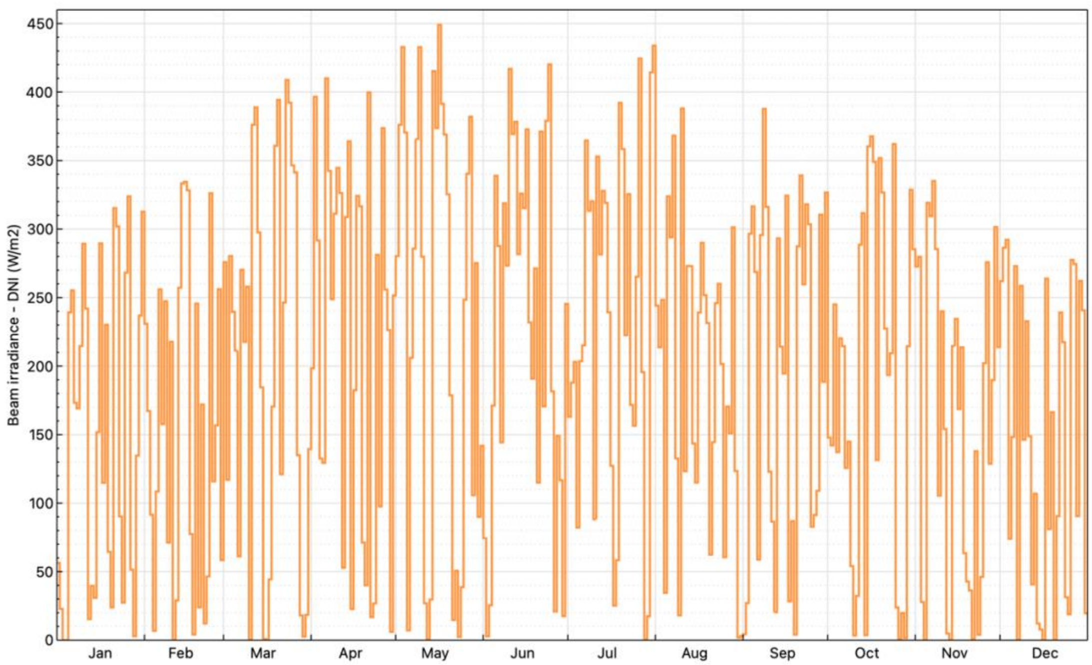

Figure 8: Daily DNI values at the location Outer Banks, NC

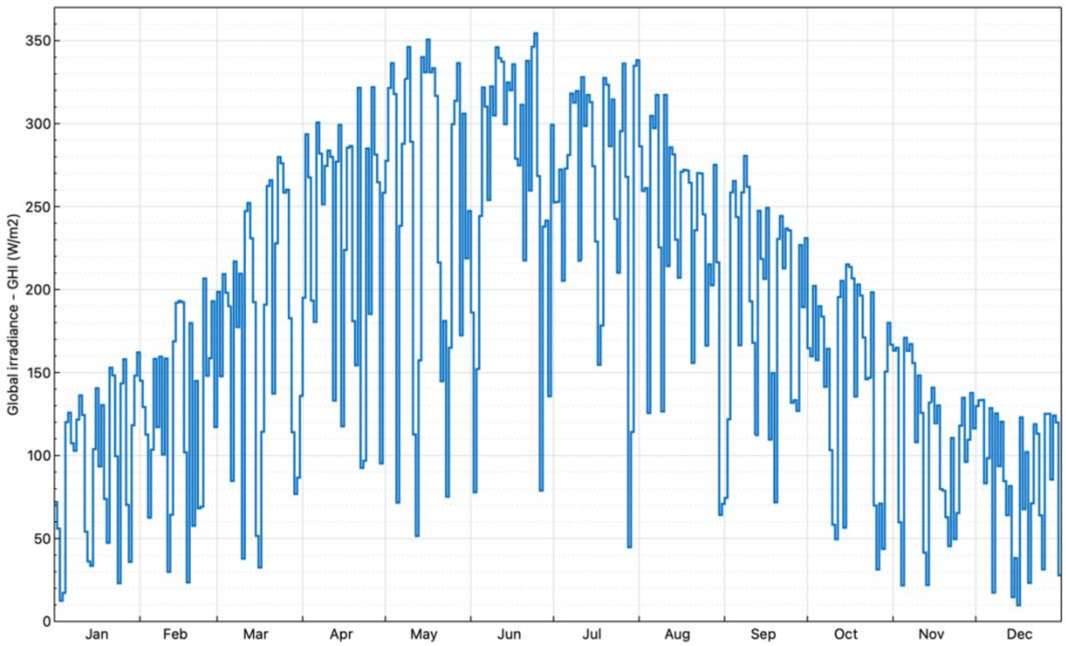

Figure 9: Daily GHI values at the location Outer Banks, NC

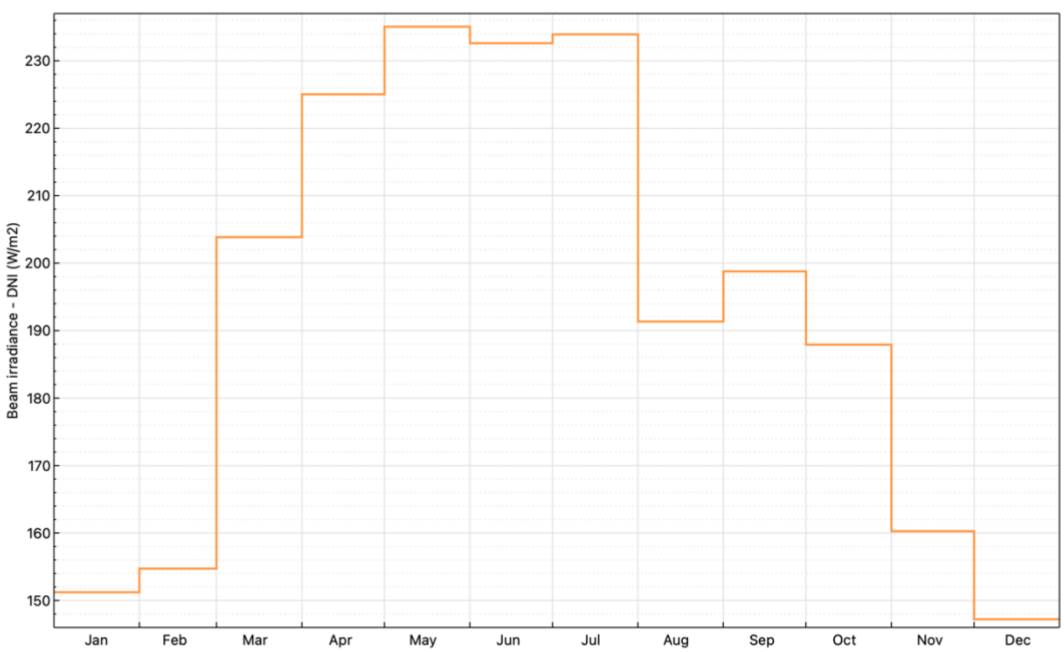

Figure 10: Monthly DNI values at the location Outer Banks, NC

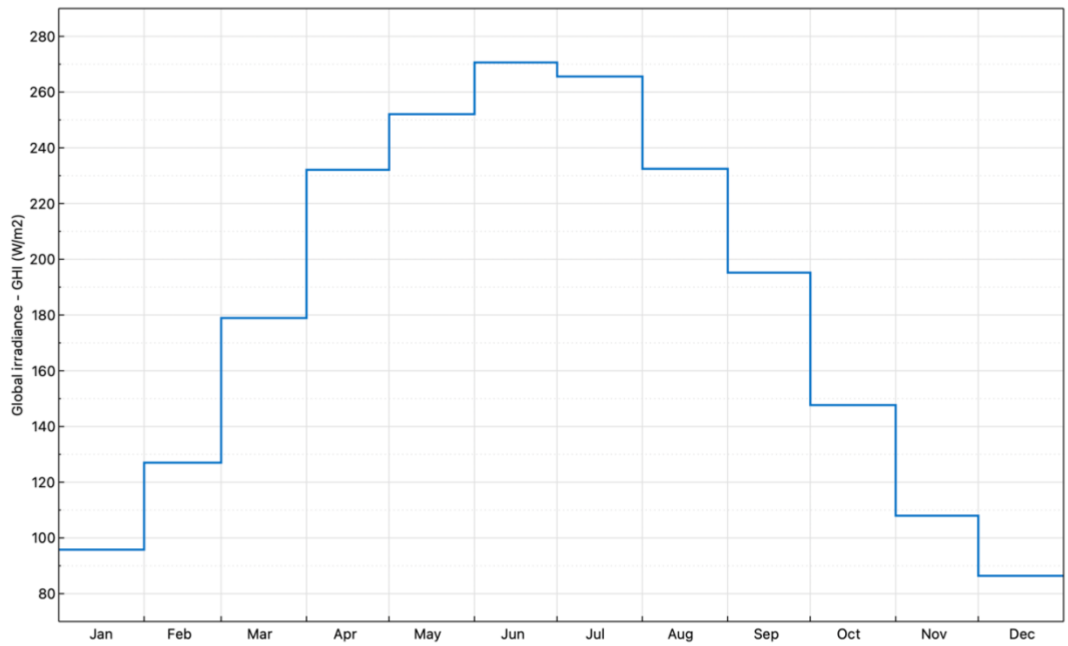

Figure 11: Monthly GHI values at the location Outer Banks, NC

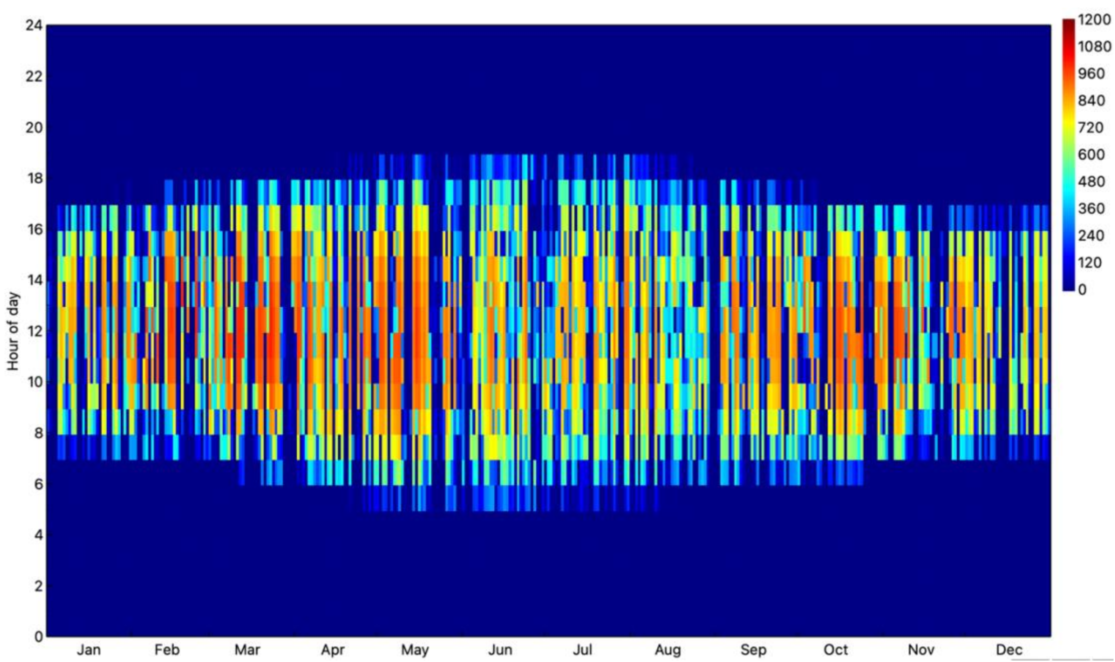

Figure 12: Heat map of DNI value according to the hour of day at Outer Banks, NC

3.2 Experimental Methods

3.2.1 Experimental System Description

In the experimental part of this study, as defined in previous sections, an experimental setup containing a phase change material (PCM) storage tank including a coil, a reservoir for the source water, a circulating pump, an electric heating, paraffin wax utilized as the PCM, and the necessary fittings was designated. The basic definition of the experimental setup fundamentally imitates the utilization of solar thermal energy to increase the temperature of the water.

A basic scheme of the experimental setup is as in the following figure and the details of the instrument used in the experiment are presented in the following sections.

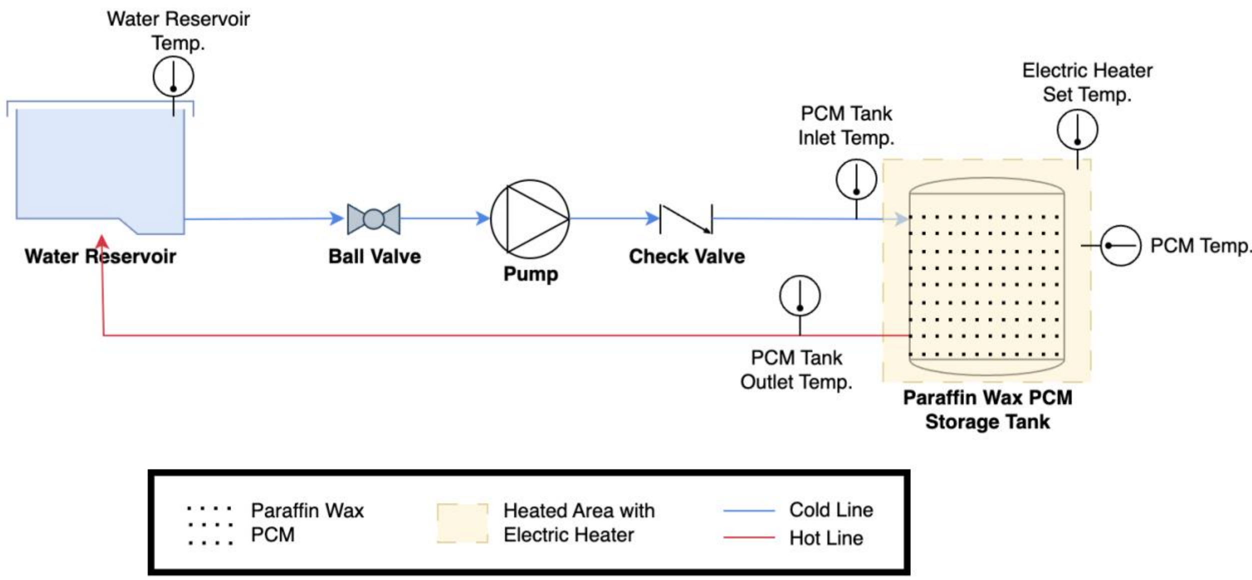

Figure 13: A basic schematic of the experimental setup

During the experimental procedure, water is directed from a reservoir toward the phase change material (PCM) storage tank. Within this tank, a blanket-type electric heater is employed to elevate the temperature of the PCM, consequently inducing a phase transition within the material. Due to its remarkable thermal conductivity, the PCM efficiently transfers heat to the water as it flows through the coil within the PCM tank. In conclusion, preheating the water for desalination by using solar thermal energy was imitated on a smaller scale. In this small-scale experimental setup, a smaller amount of water, and a smaller amount of PCM (Paraffin WAX) was used for experimental purposes.

Figure 14: Experimental setup in the High-Bay Laboratory

3.2.1.1 Phase Change Material Storage Tank

The phase change material (PCM) storage tank utilized in the experimental setup, constructed from 304 Stainless Steel with a 10-inch diameter, incorporates three 1/2-inch female national pipe thread (FNPT) connections. Remarkably, two of these connections are positioned at opposing extremities of the coil within the storage tank, while the third connection serves as a drain for the bucket segment of the tank. Originally designed as a "Condensing Coil Bucket" to cool a solvent/fluid using dry ice, as indicated in the manufacturer's description, the equipment was repurposed for the current experimental application [30].

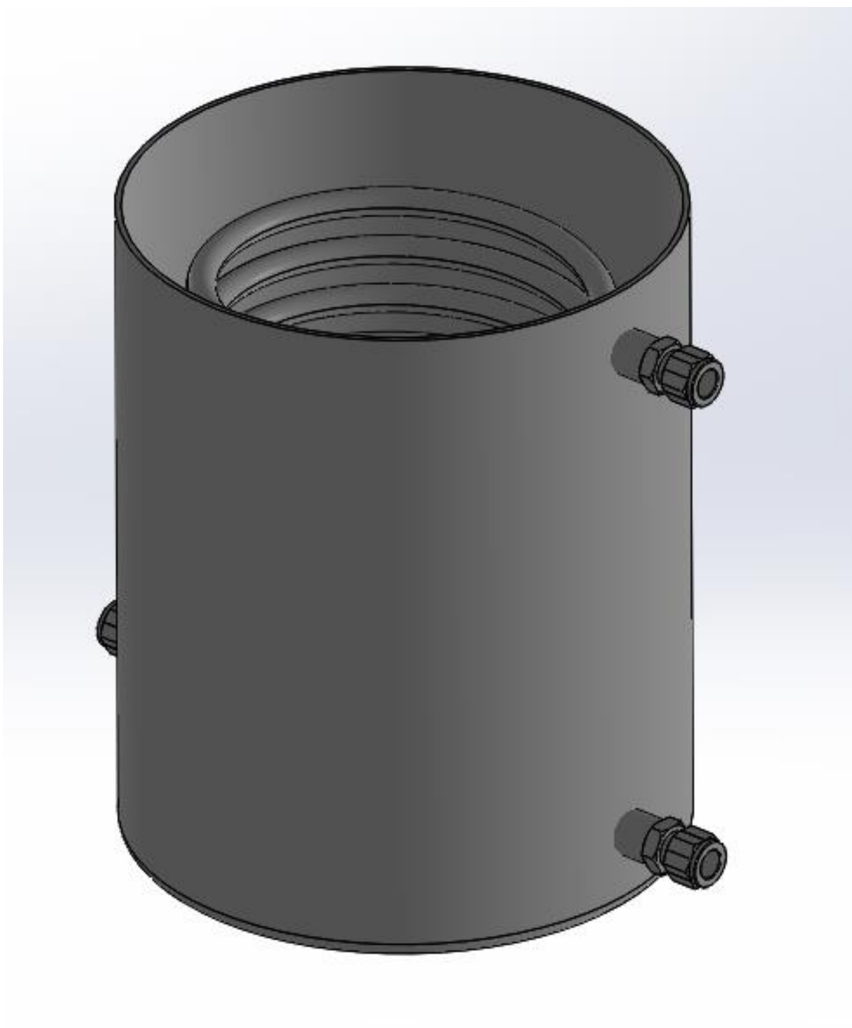

Figure 15: SolidWorks drawing of the PCM tank

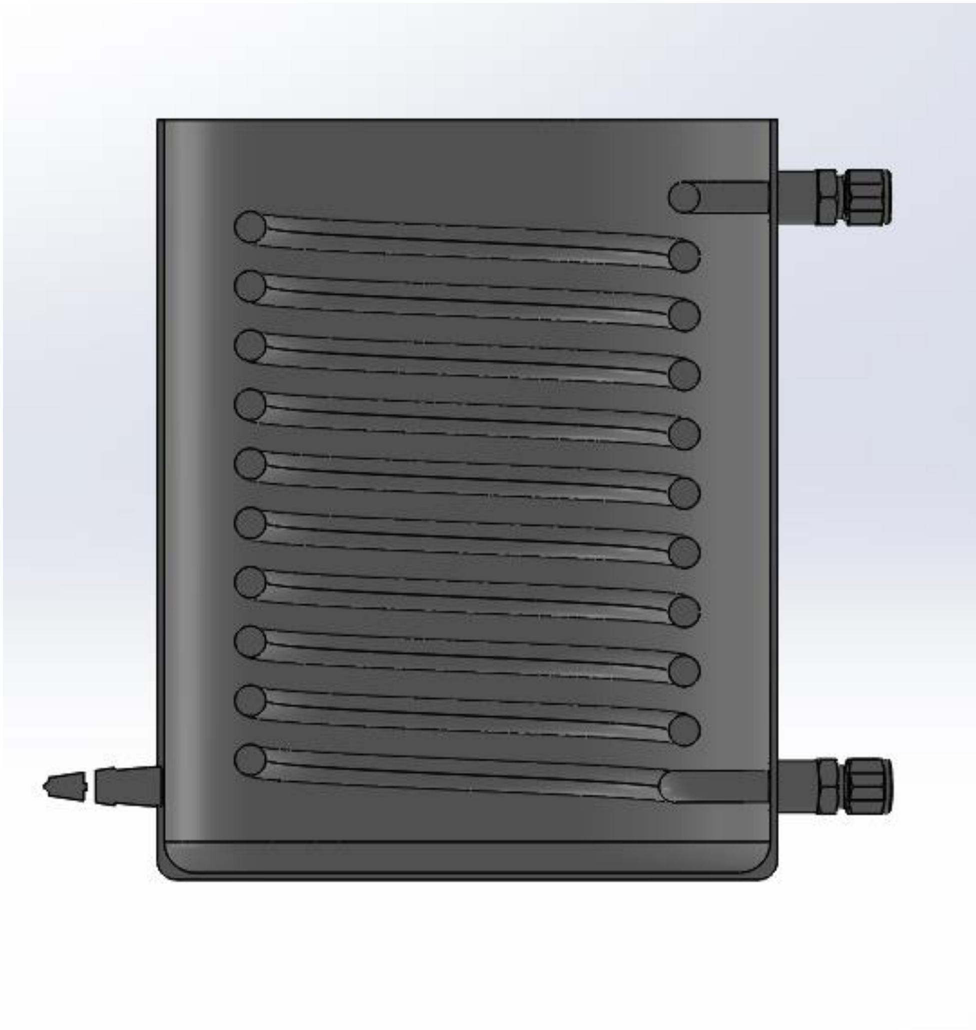

Figure 16: Cross-section of the PCM tank in SolidWorks

After connecting the electric heater and running some tests on the PCM tank without the paraffin wax, some heat loss was observed on the bottom surface of the tank and a heat barrier sheet was applied to the bottom at the inner surface of the tank for insulation purposes. This heat barrier sheet is made out of fiberglass with aluminum facing. Specifications of the product can be found in the table below.

Table 3: Specifications of the heat barrier sheet

Insulation Type	Sheet/Strip
Thickness	3/16”
Width	10”
Length	10”
Maximum Temperature	1750°F
Heat Flow Rate at 75°F	0.31 BTU
Material	Fiberglass
Color	Silver
Facing Material	Aluminum

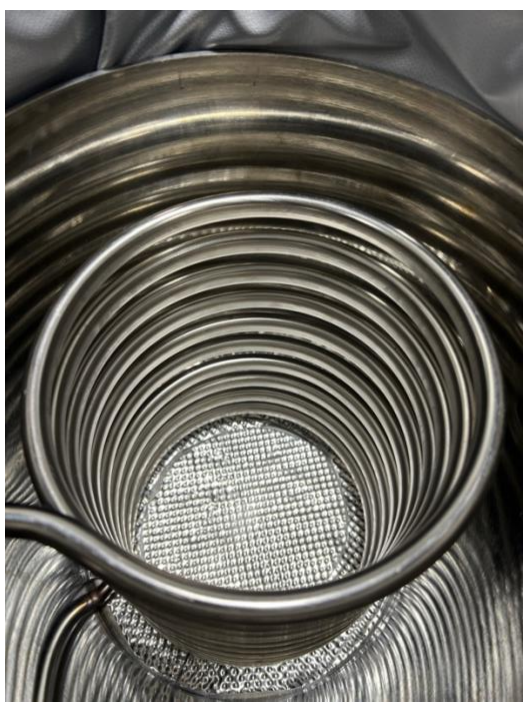

Figure 17: Fiberglass heat barrier applied to the PCM tank

3.2.1.2 Paraffin Wax as a Phase Change Material

Paraffin wax is a popular phase change material (PCM) utilized in various industries for its remarkable thermal storage capabilities. The paraffin wax used in this study's experimental work is manufactured by Thermo Fisher Scientific with a catalog number of 416770100.

Table 4: Specifications of the Paraffin Wax used in the experiment

Product Name	Paraffin, pure, wax, granular, ACROS Organics™
Catalog Number	416770100
Molecular Formula	$C_{21}H_{27}NO_3$
Molecular Weight	341.45
Appearance (Color)	White
Appearance (Form)	Pellets
Congealing Point	58°C to 62°C
Viscosity at 98.9°C	3 to 4.5 MPa.s
Thermal Conductivity	~0.19 to 0.35 W/m.K
Specific Heat [31]	2100 J/kg.K
Density [31]	900 kg/m^3

Figure 18: Photo of the paraffin wax used in the experiment

3.2.1.3 Blanket-Type Electric Heater

As mentioned in the previous sections, a blanket-type electric heat was assigned to provide the required thermal energy in the experimental setup. The used heater is manufactured for 5-gallon pails/drums for non-hazardous applications with the brand of InteliHeat. The heater operates on 120 volts and is capable of providing up to 350 watts according to the product's description on the official website of the manufacturer [32]. The heating jacket is equipped with an adjustable thermostat with a range of 32-194°F (0-90°C). Product specifications are provided in the table below.

Table 5: Specifications of InteliHeat heating jacket

Capacity	5 gallons
Color	Black
Material	Silicone coated glass cloth
To Be Used With	Metal
Temperature Reading	Fahrenheit (°F)
Voltage	120V
Power	350W
Dimensions	34.25"-40" W x 15.75" H
Weight	6 lbs.

Moreover, the heating jacket needed a modification because of the connections on the PCM tank to ensure the perfect fitment. An approximate 1 1/2” inch hole was drilled on the heating jacket and one of the connections was placed through the hole. A close-up photo of the modification is highlighted in the figure below.

Figure 19: A close-up photo of the hole drilled in the heating jacket

3.2.1.4 Circulating Pump

The circulating pump used in the experiment plays a critical role in the efficient transfer of heat between the phase change material (PCM) and the water. This pump is typically a centrifugal pump designed and was assigned to move fluid (water) continuously through the system.

In this experimental setup, the circulating pump is responsible for directing water from the water reservoir toward the PCM storage tank. Once inside the tank, the pump maintains the flow of water through the coil immersed within the PCM. As the water flows through this coil, it comes into contact with the PCM undergoing a phase transition due to the heat supplied by the electric heater.

The specifications of the circulating pump can be found in the table below.

Table 6: Specifications of the circulating pump

Pump Type	Centrifugal
Power Source	Electric
Phase	Single
Frequency	60 Hz
Voltage	120V AC
Current	0.5A
For Use With	Water
Maximum Flow Rate	4 gpm
Maximum Head	4.3 ft.
Maximum Pressure	150 psi
Temperature Range	35°F to 250°F
hp	1/100

3.2.1.5 Measurement Tools and Devices

Temperature measurements were obtained by using J-type thermocouples in the experiment. The J-type thermocouples were connected to the system by using a 1/4" 304 stainless steel low-pressure tee connector and 1/4” brass adjustable thermocouple compression fitting. There are two thermocouples connected with the tee connectors in-line and one thermocouple was assigned to measure the water temperature in the water reservoir.

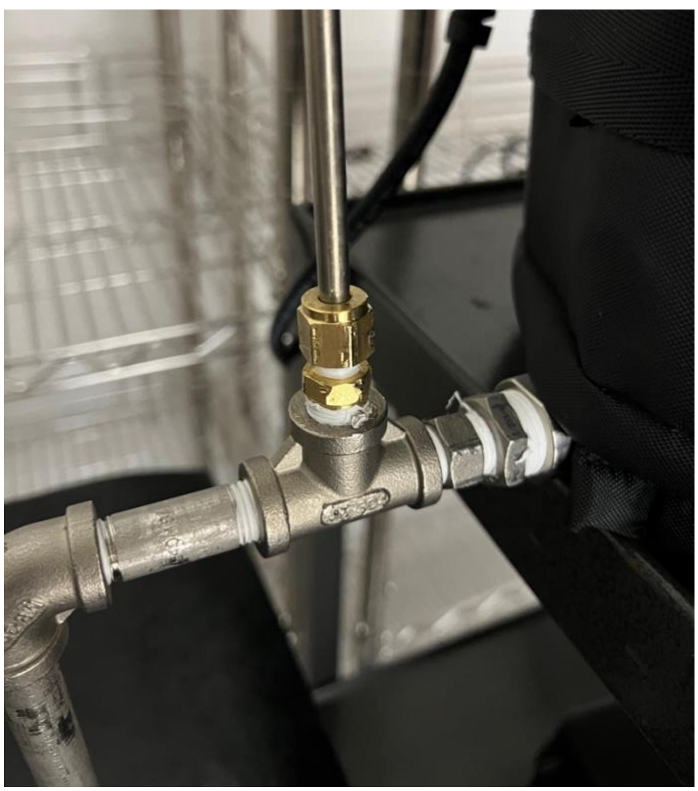

Figure 20: Thermocouple compression fitting and the tee connector in the experiment

These thermocouples were connected to a 12-channel datalogger manufactured by Extech with model number TM500. Extech TM500 supports 6 thermocouple types (J, K, T, R, E, S) and the data can be recorded simultaneously onto an SD card from all 12 channels [33]. According to the product specifications on the website, the datalogger has the following specifications for the J-type thermocouples [33].

Table 7: Extech TM500 specifications for J-type thermocouples

Temperature (Type-J)	0.1°/1°
Temperature (Type-J) Basic Accuracy	-148 to 2102 °F (-100 to 1150 °C)
Temperature (Type-J) Max. Resolution	±0.4% of reading (+1.8 °F/+1 °C)

Other than the temperature measurements, the flow rate was measured by using a beaker and a timer. The beaker filled up at the end of the line with the stream for one minute and measured the amount of water in the beaker. Adding an in-line flowmeter to the experiment was considered but it was found unnecessary since measuring it with a beaker was an option.

3.2.2 Experimental Process

In the experimental part of the study, solar radiation data sourced from the System Advisor Model (SAM) and the National Solar Radiation Database (NSRDB) were employed to determine if the applied temperature on the phase change material storage tank can be accessible in the application location. The heat was facilitated by the blanket-type electric heater. As described in the previous sections, the experimental work of the study was instrumental in obtaining the required temperature data critical for the following calculations, which were then integrated into the heat exchanger analysis. The outcomes derived from the heat exchanger computations were further utilized to conduct MATLAB simulations, so enabling the evaluation of differences in energy requisites for the furnace in the supercritical water desalination (SCWD) system. Therefore, the experimental work of this study assumed principal significance as it served as a crucial middle step facilitating consistent integration within the research outline.

The experimental procedures were performed under standard atmospheric pressure conditions (1 atm) and at ambient room temperature within the confines of the High Bay Laboratory, situated within the Life and Sciences Building on the main campus of East Carolina University.

Initially, the experimental setup was built, with all necessary measurement instruments. Following the connection of the measurement tools and devices, a series of preliminary test runs were performed to assess functionality compliance, ensuring the absence of leaks, electrical irregularities, and related issues.

The first trial was run without the PCM material (Paraffin Wax) in the PCM storage tank with 4 gallons of water at room temperature (25°C) in the water reservoir. The thermostat on the blanket-type electric heater was set to 60°C. The temperature readings were not logged during this trial; rather, the main purpose of this test was to check and assess parameters such as water leakage, heat dissipation from the PCM tank, water flow rate, and the identification of potential operational issues. The addition of the insulation material in Figure 21 within the phase change material storage tank occurred after this initial test run as a result of relatively high heat loss from the bottom and the top surfaces of the PCM storage tank.

The next test trial was also conducted without the inclusion of phase change material (Paraffin Wax) within the PCM storage tank, while increasing the volume of water in the reservoir by one gallon, thereby increasing from 4 gallons to 5 gallons. The initial temperature of the water within the reservoir was recorded at 21.1°C at the beginning of the test run. The thermostat controlling the blanket-type electric heater was set to maintain a constant temperature of 60°C. Three different temperature measurement points were designated within the experimental setup. The first temperature was within the water reservoir, the second temperature was at the water inlet to the PCM storage tank, and the third temperature was at the outlet of the PCM storage tank. Temperature measurements were systematically recorded at intervals of 30 seconds over 5 hours throughout the trial. Additionally, this trial served to assess the functionality of the datalogger and thermocouples. Practical adjustments were made, including relocating the water reservoir to a lower shelf to mitigate gravitational effects on water flow, besides switching the water inlet and outlet connections of the PCM storage tank.

The choice of avoiding to use of the phase change material (paraffin wax) was based on the requirement to prevent any phase change occurrences during the test trials, thus ensuring that the paraffin wax retained its thermochemical properties as much as possible for the later real experimental trials.

During the test trials, it was decided to have 5 measurement points on the experimental setup. The electric heater set temperature was added to the graph manually. These measurement points were as follows in the table below:

Table 8: Measurement points on the experimental setup

T1	Water Temperature in the Water Reservoir
T2	Electric Heater Set Temperature
T3	PCM Temperature 1
T4	PCM Temperature 2
T5	PCM Tank Outlet Temperature
T6	Ambient Temperature

The “PCM Temperature 1” refers to the temperature reading on the bottom part of the PCM tank and the “PCM Temperature 2” refers to the temperature reading on the top part of the PCM tank.

During the experiment, the power consumed by the electric heater was also manually recorded for use in the heat transfer analysis of the PCM tank with equal intervals and then the collected data was interpolated. The device used for this purpose is a REED brand power meter with a model number of R5090.

Also, the specifications of the REED R5090 power meter are shown in the table below:

Table 9: Specifications of the Power Meter

Voltage	AC 100V~150V
Current	MAX 15A
Rated Power	1800W
Frequency	60 Hz
Accuracy	±1%

In the experimental work of this study, a set of experiments was conducted according to the target temperatures. As mentioned above, the blanket-type electric heater simulates the solar irradiation and heat on the PCM storage tank to provide the target temperatures at the outlet of the PCM storage tank. This temperature value was used as an inlet temperature on the MATLAB simulation of the supercritical water desalination (SCWD) system. During the calculations, the accessibility of the target temperatures was also confirmed by using the solar data and the solar duration at the application location. In the experiment, the set temperature of the thermostat was adjusted to reach the target temperatures. In the table below, all the other variables of the experiment are shown.

Table 10: Variables of the experiment in each trial

	Target Temperature	**Phase Change Material**	**Amount of Used PCM**	**Heat Transfer Fluid**	**Amount of Heat Transfer Fluid**	**Flow Rate of Water**
Trial 1	30°C	Paraffin Wax	10 kg	Water (H_20)	5 gal. (approx. 18.927 kg)	200 mL/min.
Trial 2	35°C	Paraffin Wax	10 kg	Water (H_20)	5 gal. (approx. 18.927 kg)	200 mL/min.
Trial 3	40°C	Paraffin Wax	10 kg	Water (H_20)	5 gal. (approx. 18.927 kg)	200 mL/min.
Trial 4	45°C	Paraffin Wax	10 kg	Water (H_20)	5 gal. (approx. 18.927 kg)	200 mL/min.
Trial 5	50°C	Paraffin Wax	10 kg	Water (H_20)	5 gal. (approx. 18.927 kg)	200 mL/min.
Trial 6	55°C	Paraffin Wax	10 kg	Water (H_20)	5 gal. (approx. 18.927 kg)	200 mL/min.
Trial 7	60°C	Paraffin Wax	10 kg	Water (H_20)	5 gal. (approx. 18.927 kg)	200 mL/min.

3.2.3 Heat Transfer Calculations

In this part of the study, a set of calculations were performed to analyze the heat transfer in the PCM Tank. Mainly 4 different sets of calculations took place.

The first one is the calculations for the water circulating in the system. In this part, the amount of heat gained by water was calculated. These calculations were based on equation (2), similarly used for the solar calculations. After the calculations, the units were converted for the comparison purposes of the results of the other calculations.

The second calculation was performed to determine the amount of heat gained by the paraffin wax throughout the trials in the experiment. The units in the results of these calculations were also converted for comparison purposes. During the calculations, the average temperature for the PCM Tank was used.

The third set of calculations was performed to determine the total average amount of energy consumed by the blanket-type electric heater. To calculate the total average energy consumed, the average power meter reading throughout that trial was multiplied by the time for the trial.

Lastly, the fourth calculations are conducted on MATLAB to analyze the heat transfer in the PCM tank. The MATLAB code aligns with Fourier's Law, previously stated in equation (2).

The MATLAB code serves to calculate the rate of heat transfer through a cylindrical pipe, employing fundamental principles of conduction heat transfer. Initially, it establishes input parameters including the thermal conductivity of the pipe material, inner and outer diameters of the pipe, pipe length, and temperatures of both the phase change material (PCM) and water. Then, the code computes the temperature difference (ΔT) between the PCM and water temperatures, converting this value to Kelvin to facilitate further calculations. It then determines the radius of the pipe, followed by calculating the surface area available for heat transfer using the cylindrical pipe's dimensions. Utilizing Fourier's law of heat conduction, the code computes the rate of heat transfer (Q) through the pipe, considering the thermal conductivity, surface area, length of the pipe, and temperature difference in Kelvin. Finally, the calculated heat transfer rate is displayed in watts, providing insight into the heat exchange process within the cylindrical pipe. The MATLAB code can be found in Appendix A.

Other than that, the actual and ideal scenarios for the heat transfer in the PCM Tank were calculated, analyzed, and compared. The total ideal and the actual heat transfer were calculated for each trial. Then, the specific heat of the phase change material was taken into consideration and an analysis was made according to the selection of the phase change material. Since the study mainly focuses on the heat transfer in the PCM Tank, the selection of the phase change material plays a critical role. Paraffin wax with a 58-62°C phase change temperature was selected for this study.

3.3 MATLAB Simulation

In the study, a Simulink model was modified and designed for SCWD by Glosson using a model originally developed by Dr. Jinbo Chen from East Carolina University [34]. The original supercritical water desalination system modeled on MATLAB was designed as a two-stage system. The model includes a pump, a heat exchanger, a furnace, two reactors, and a condenser [34]. In the model developed by Glosson, the brine input comes from an RO (Reverse Osmosis) system and the pump pressurizes the input brine to supercritical conditions [34]. After the pressurization of the brine, a heat exchanger and a furnace were assigned to heat the fluid to supercritical conditions [34].

The MATLAB code and the Simulink interface were modified to serve the purpose of this study. The MATLAB code used in this research can be found in Appendix C. The first and most important modification to the MATLAB code was the fluid coming from the RO system. The brine was entered into the supercritical water desalination system as is. Also, the temperature of the fluid was manually entered into the simulation for each trial in the experiment.

Glosson used a modified MATLAB simulation and relied on the Reference Fluid Thermodynamic and Transport Properties Database (REFPROP) to determine the enthalpy values of various components. These components include feedwater enthalpy, pump enthalpy, furnace enthalpy, vapor enthalpies, concentrations, specific heats, and densities [34].

REFPROP is a commonly used software in thermodynamics and fluid properties analysis developed by the National Institute of Standards and Technology (NIST). It functions as a comprehensive tool for calculating the thermophysical properties of pure fluids and mixtures under many conditions, including temperature, pressure, and composition.

Chapter 4

Results and Analysis

4.1 Results

4.1.1 Weather Conditions at Outer Banks, NC

The application location chosen in this study is the East Carolina University Outer Banks Campus located at Outer Banks, NC with Coastal Studies Institute. This campus is located on the barrier island chain in Eastern North Carolina [35]. The weather data was obtained from the National Solar Radiation Database (NSRDB) and using the System Advisor Model (SAM).

The dry-bulb temperature increases with the increase of global horizontal irradiance and direct normal irradiance as expected. Also, the monthly profile of global horizontal irradiance and direct normal irradiance according to the hour of the day and the temperature profile of the location can be found in the following figures below.

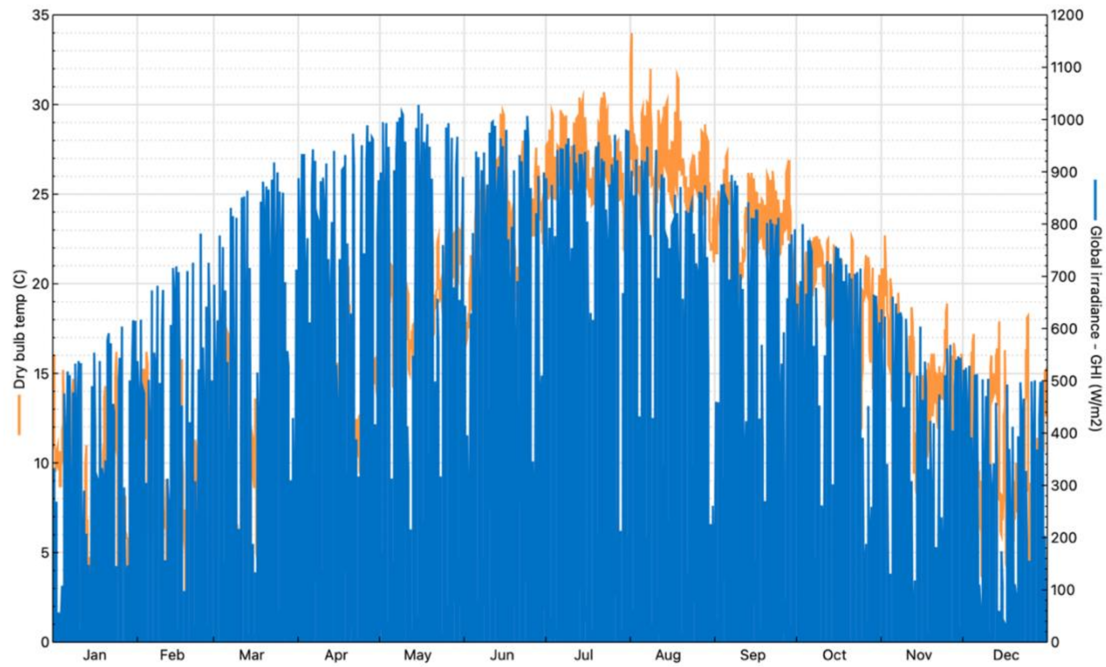

Figure 21: Change in Dry-Bulb Temperature (℃) and Global Horizontal Irradiance (W/m²)

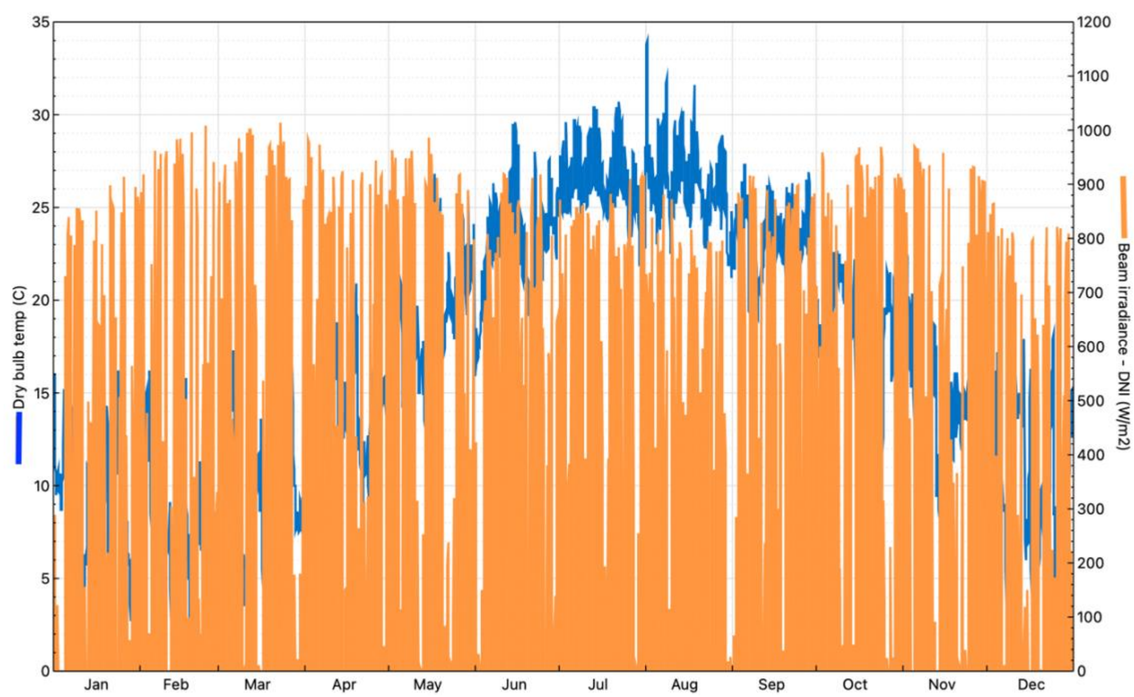

Figure 22: Change in Dry-Bulb Temperature (℃) and Direct Normal Irradiance (W/m2)

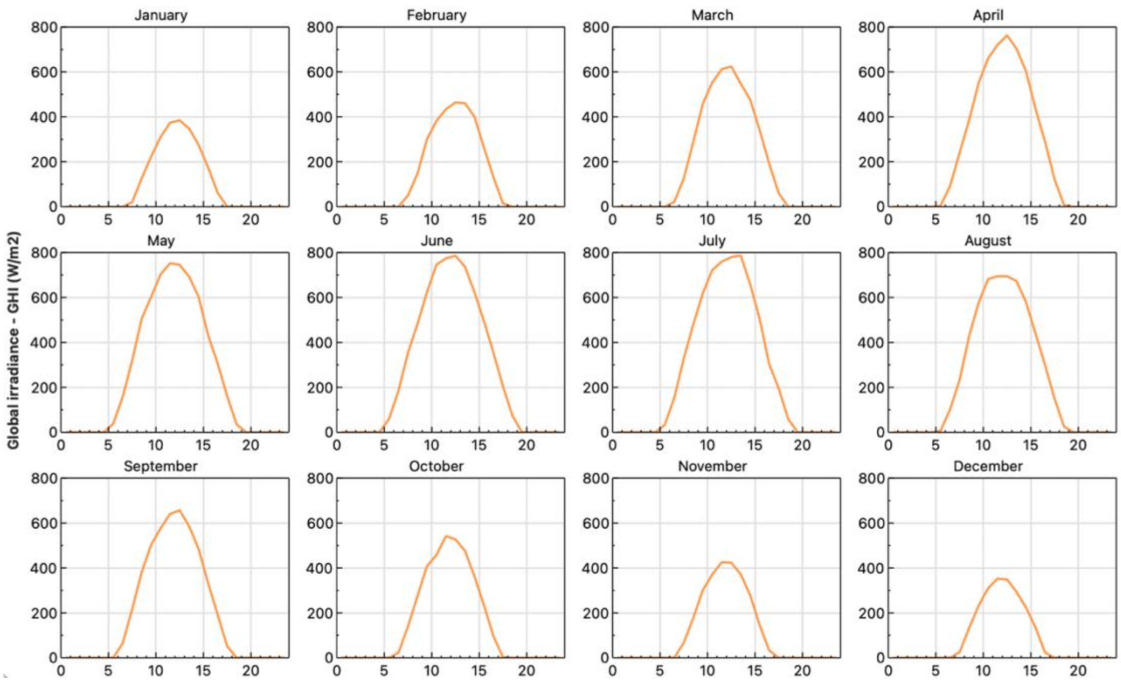

Figure 23: Monthly Global Horizontal Irradiance (W/m^2) for the hour of the day

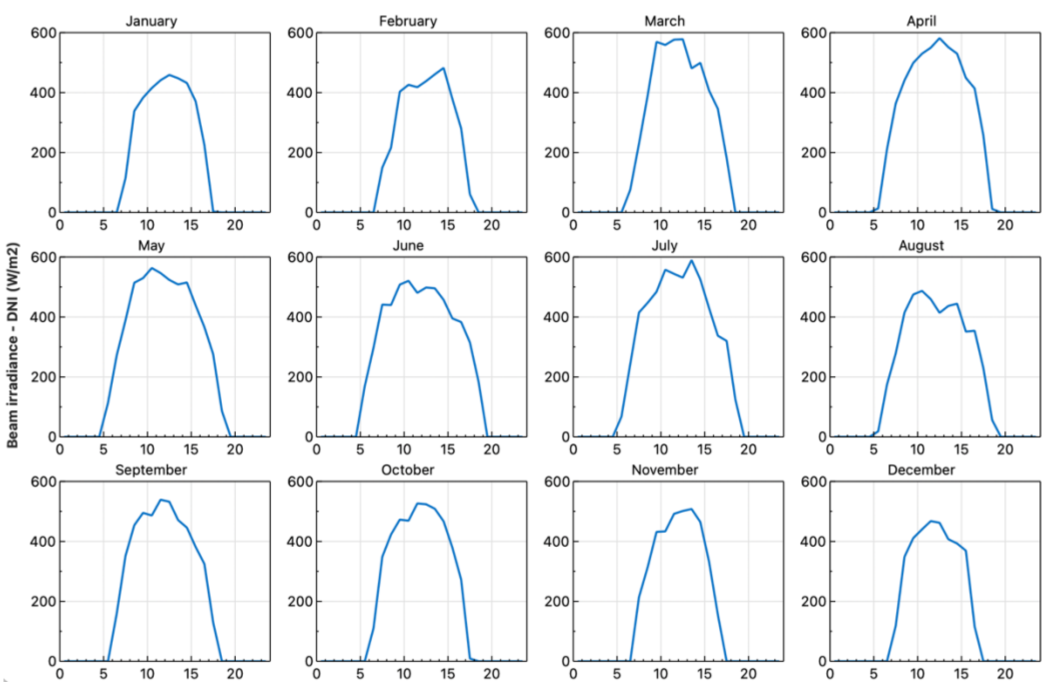

Figure 24: Monthly Direct Normal Irradiance (W/m2) for the hour of the day

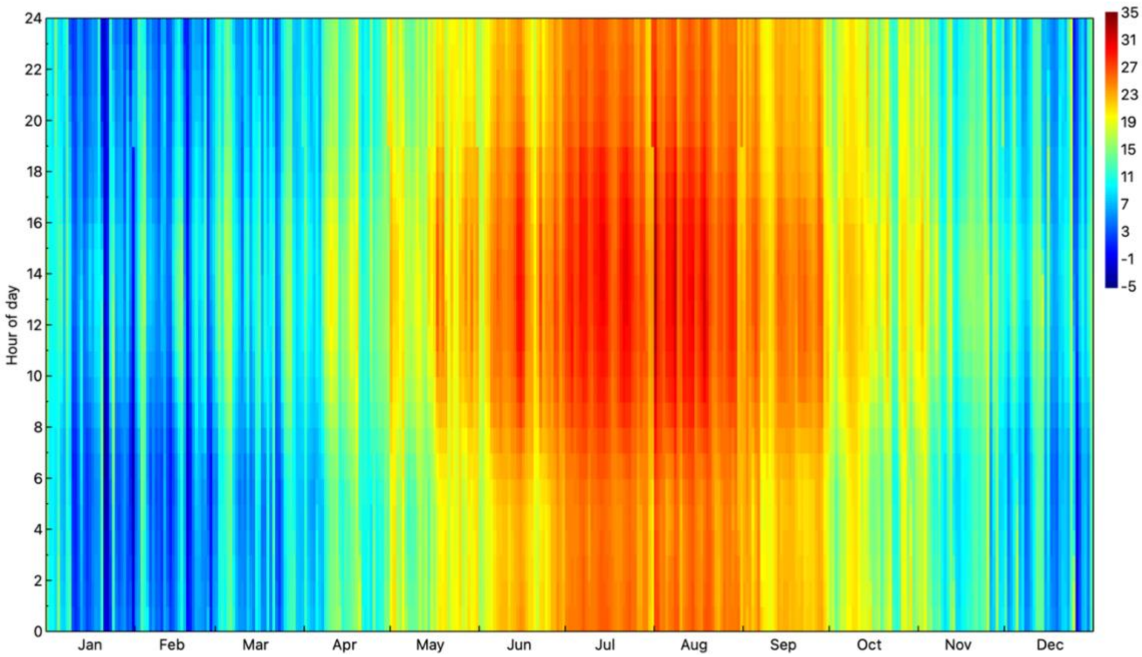

Figure 25: Heat map of the Dry-Bulb Temperature (℃) according to the hour of the day

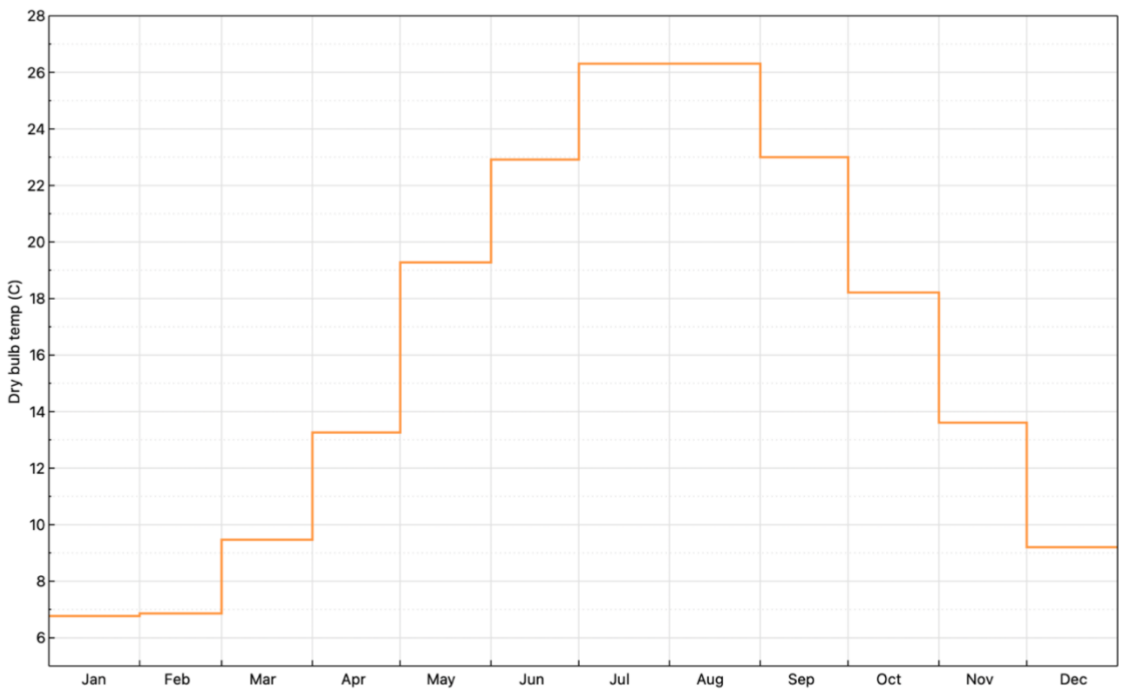

Figure 26: Average Dry-Bulb temperature (℃) profile throughout the year

4.1.2 Experimental Results

As described in the previous sections, in the experimental part of this study, a smaller scale of solar thermal energy storage was studied. To conduct the experimental work of the research, the solar data was collected at the location (Outer Banks, NC).

From the solar data, the rate of radiation emitted by the object at the specific location (Outer Banks, NC) was obtained as 193.695 W/m^2 as mentioned in the previous sections. With this data obtained by using the National Solar Radiation Database (NSRDB) and the System Advisor Model (SAM), the solar irradiation was converted into the unit of kJ/m^2 by using the unit conversion equation below.

$$\frac{kJ}{hm^2} = \frac{1000Ws}{m^2h(\frac{3600s}{h})} \tag{11}$$

$$\frac{kJ}{hm^2} = \frac{0.2777W}{m^2} \tag{12}$$

Or

$$\frac{3.6kJ}{hm^2} = \frac{W}{m^2} \tag{13}$$

So, the solar irradiation at Outer Banks, NC is equal to 697.302 kJ/h per m^2.

Since the average sunlight duration in 2022 was found as 12.18194 hours, the solar irradiance is 8494.491126 kJ/m^2.

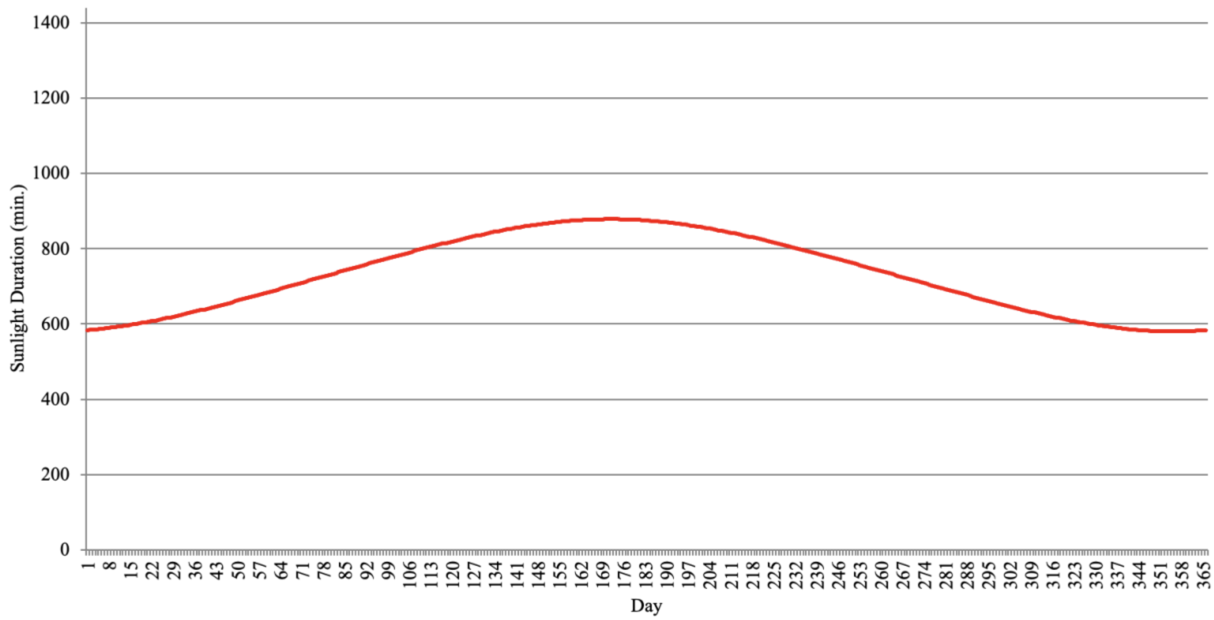

Figure 27: Sunlight duration(min.) as a function of the day of 2022

As seen in the graph above, the solar duration during the days of summer months is longer than the days of the winter months. As expected, the days are longer during the summer than in the winter.

Also, in the following graph, the sunrise and sunset times are shown for the specified location. It can be seen that the sunlight duration is longer in the summer due to the bigger difference between the sunrise and sunset time.

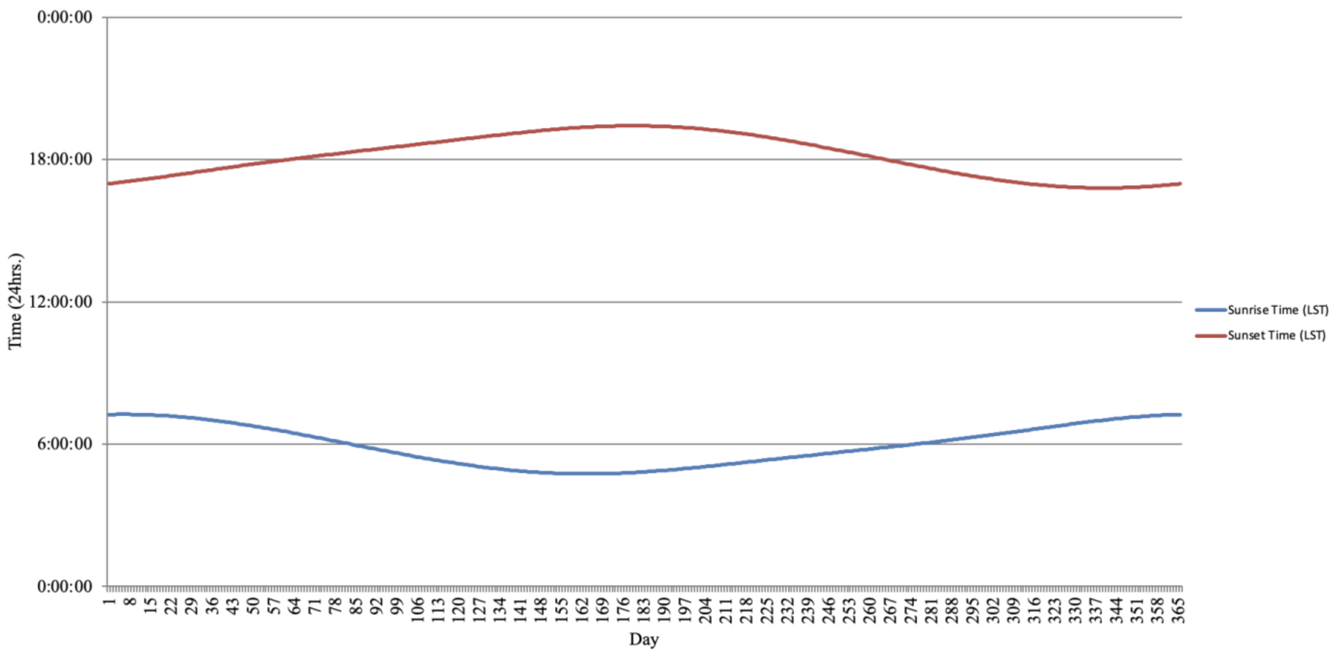

Figure 28: Sunrise and Sunset time as a function of the day of 2022

Some of the temperature measurements in the experiment are shared in the table below. The temperature measurements shared in the table below are shared to provide an overview of the collected data and the change in the outlet temperature of the PCM storage tank (T5) according to the target temperature. The temperature values added to the table below were picked from the dataset collected from the experiment to show the temperature profile. The values shown below are from the moments the T5 reached the target temperature.

Also, the power consumption by the blanket-type electric heater was recorded simultaneously.

Table 11: Some of the temperature measurements in the experiment

Target Temperature (°C)	T1 (°C)	T2 (°C)	T3 (°C)	T4 (°C)	T5 (°C)	T6 (°C)
30	20.6	90	33	36.4	30	20.7
35	22.3	90	48.3	47.8	35	19.9
40	21.6	90	51.5	44	40	21
45	20.1	90	49.5	59.9	45	20.7
50	21.8	90	57.8	61.9	50	20.8
55	20.6	90	50.3	61.9	55	20.4
60	21.9	90	57.3	61.5	60	19.5

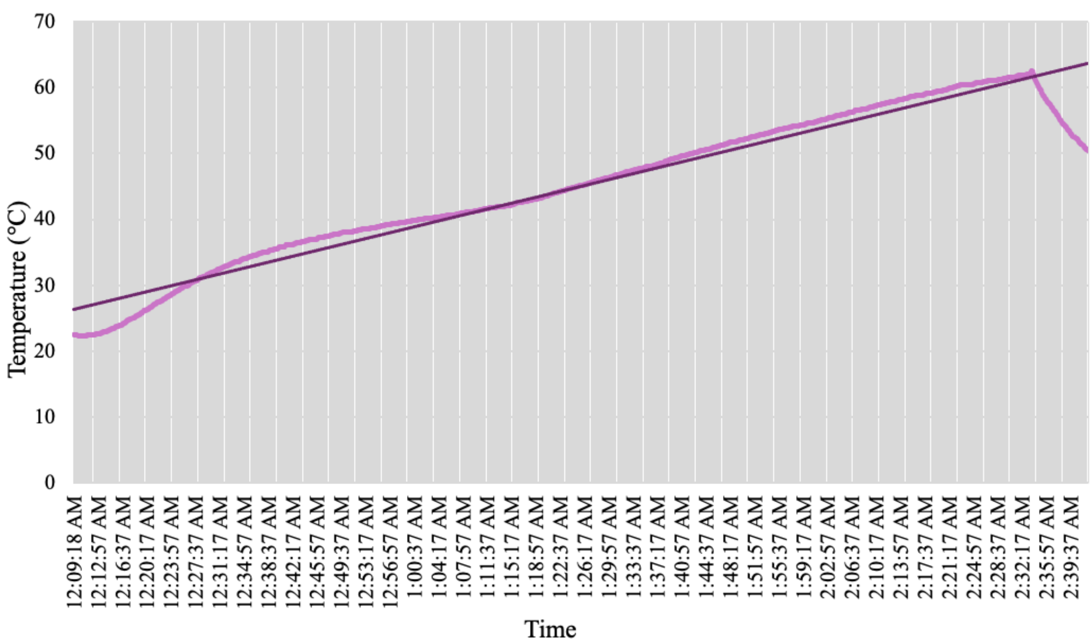

Figure 29: Trial 1 PCM Tank outlet temperature profile by time

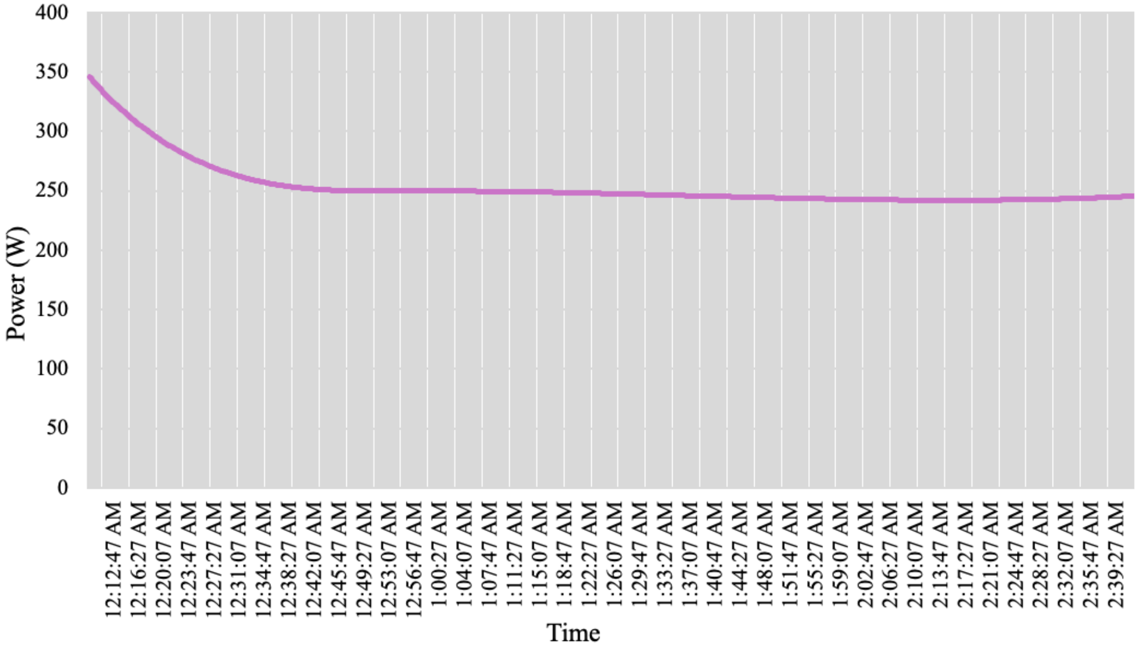

Figure 30: Blanket-type electric heater power consumption during Trial 1

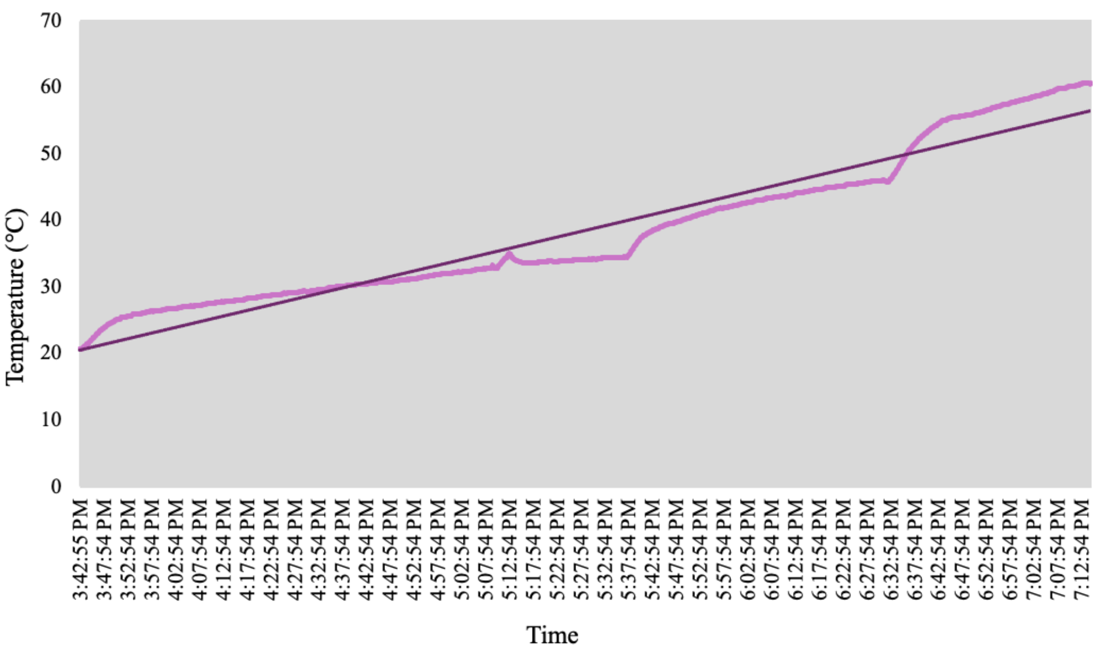

Figure 31: Trial 2 PCM Tank outlet temperature profile by time

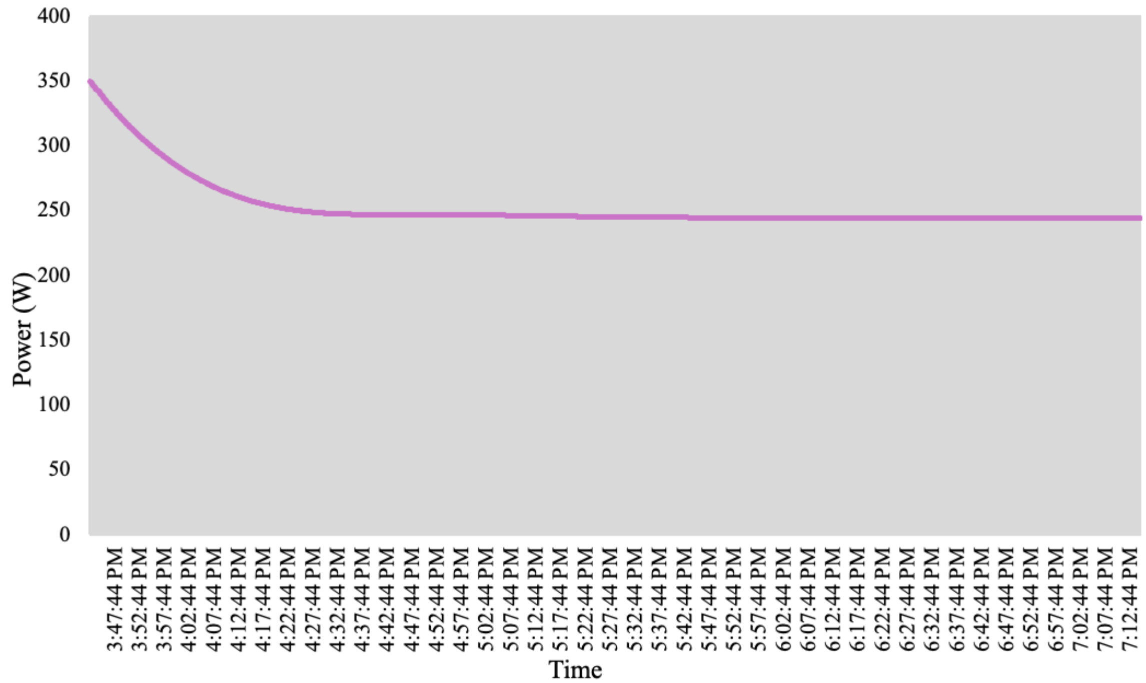

Figure 32: Blanket-type electric heater power consumption during Trial 2

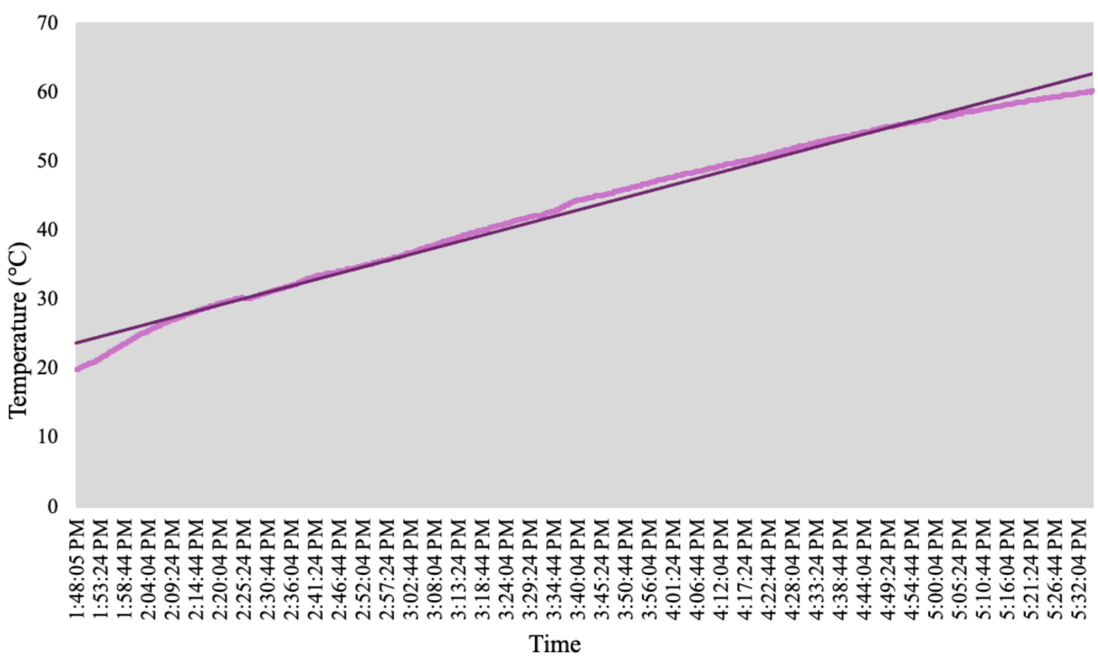

Figure 33: Trial 3 PCM Tank outlet temperature profile by time

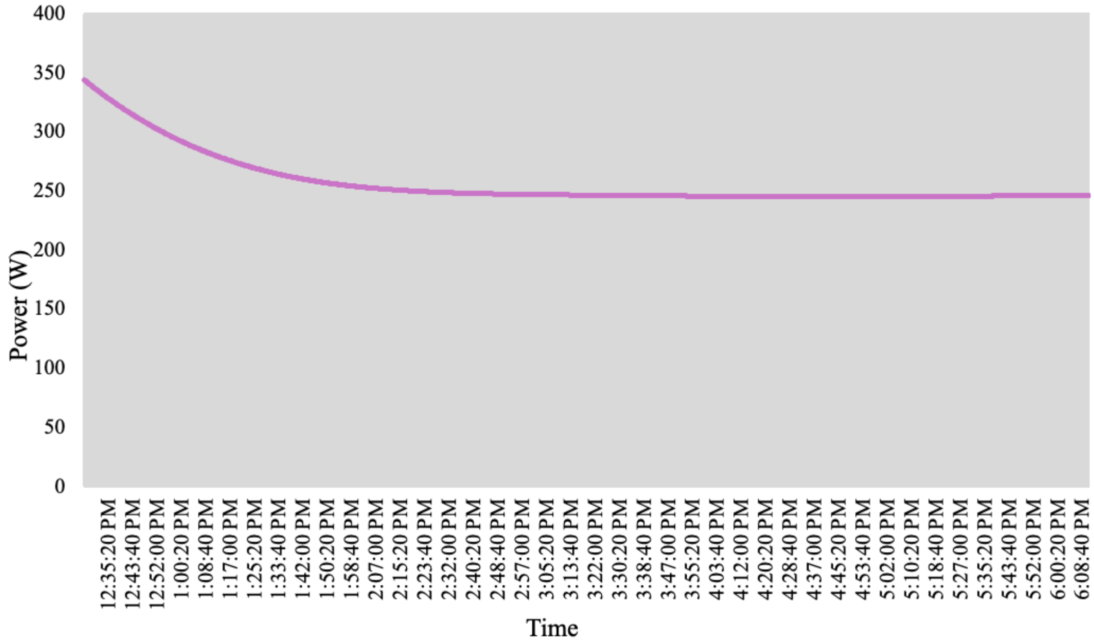

Figure 34: Blanket-type electric heater power consumption during Trial 3

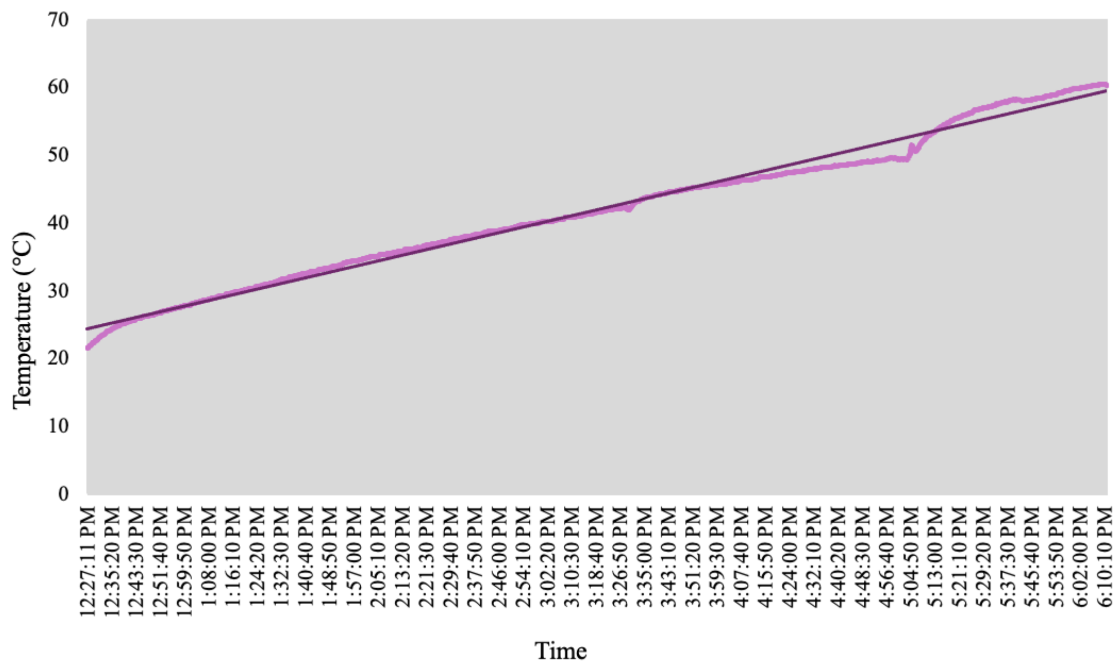

Figure 35: Trial 4 PCM Tank outlet temperature profile by time

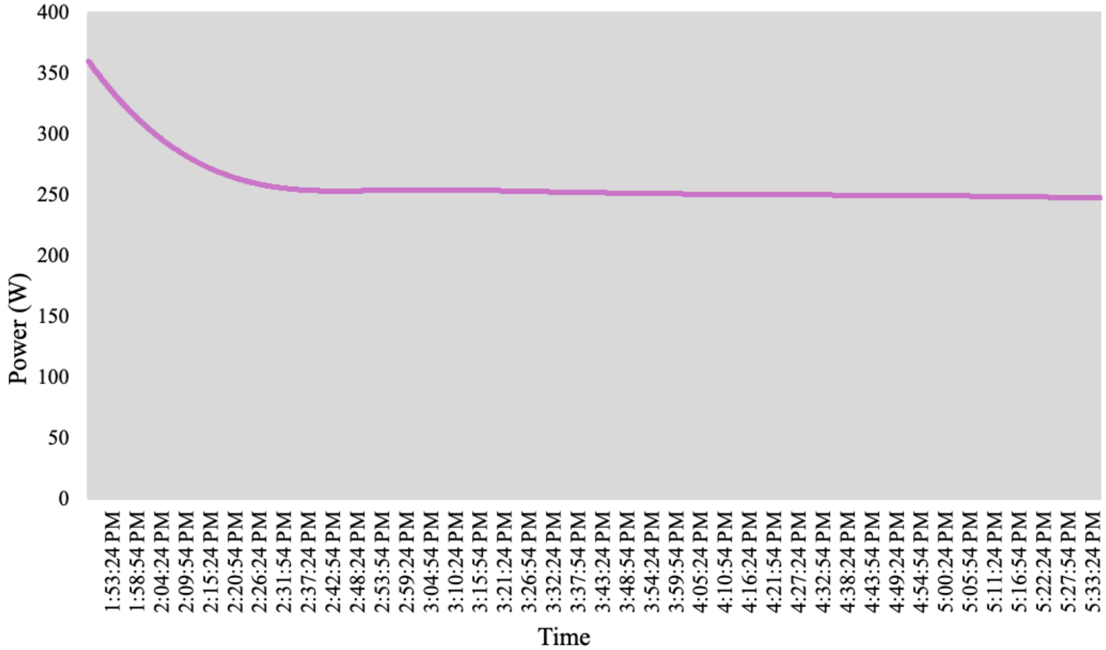

Figure 36: Blanket-type electric heater power consumption during Trial 4

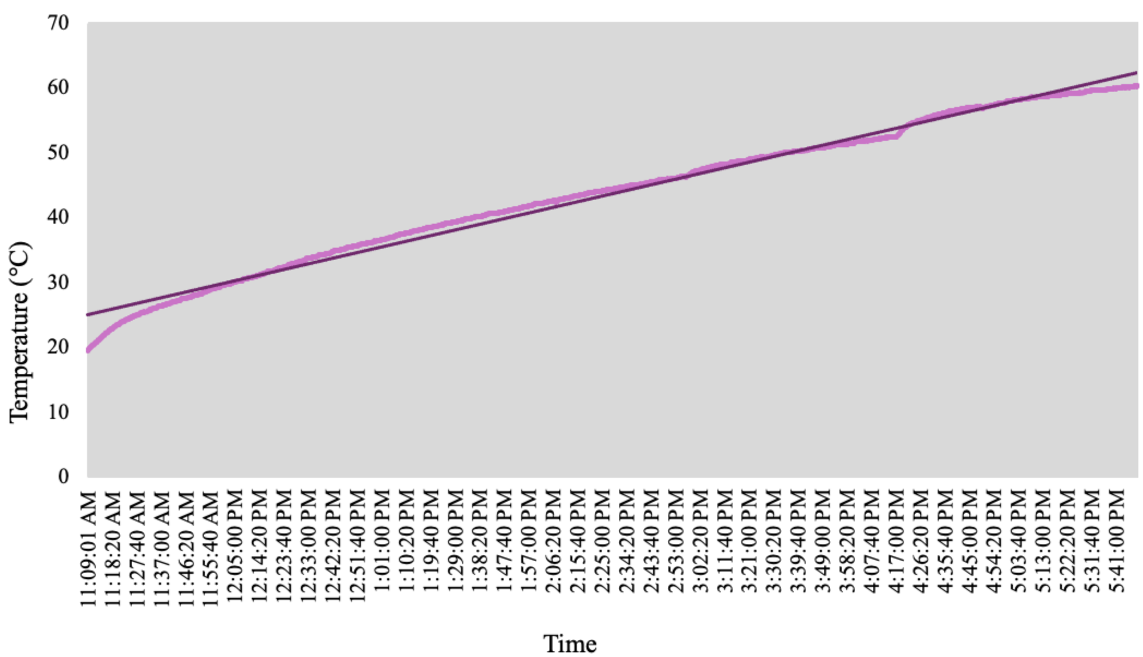

Figure 37: Trial 5 PCM Tank outlet temperature profile by time

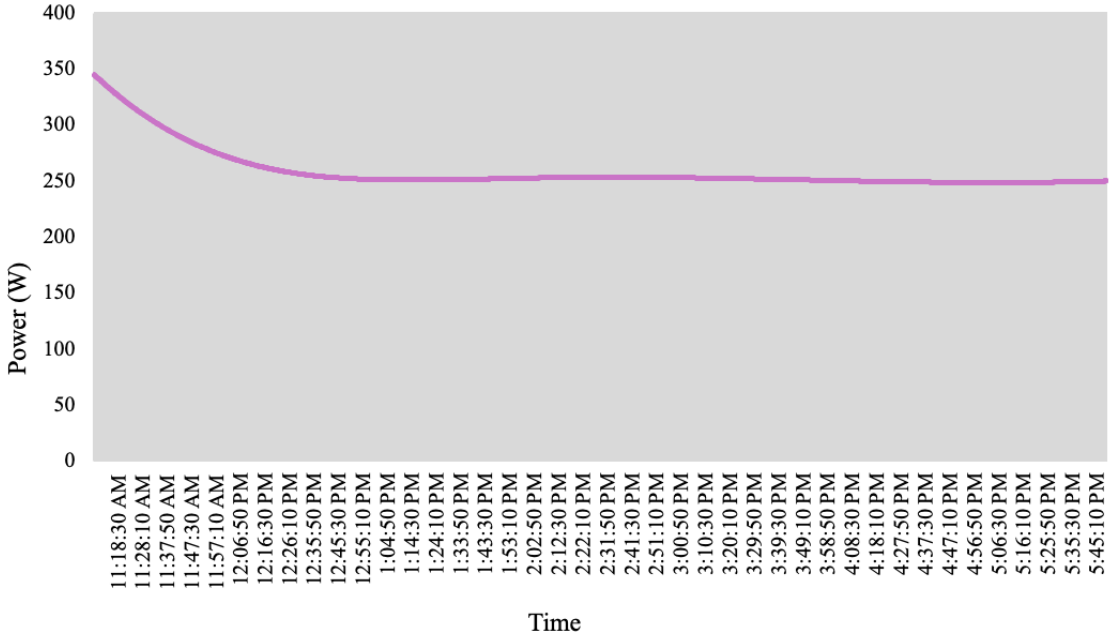

Figure 38: Blanket-type electric heater power consumption during Trial 5

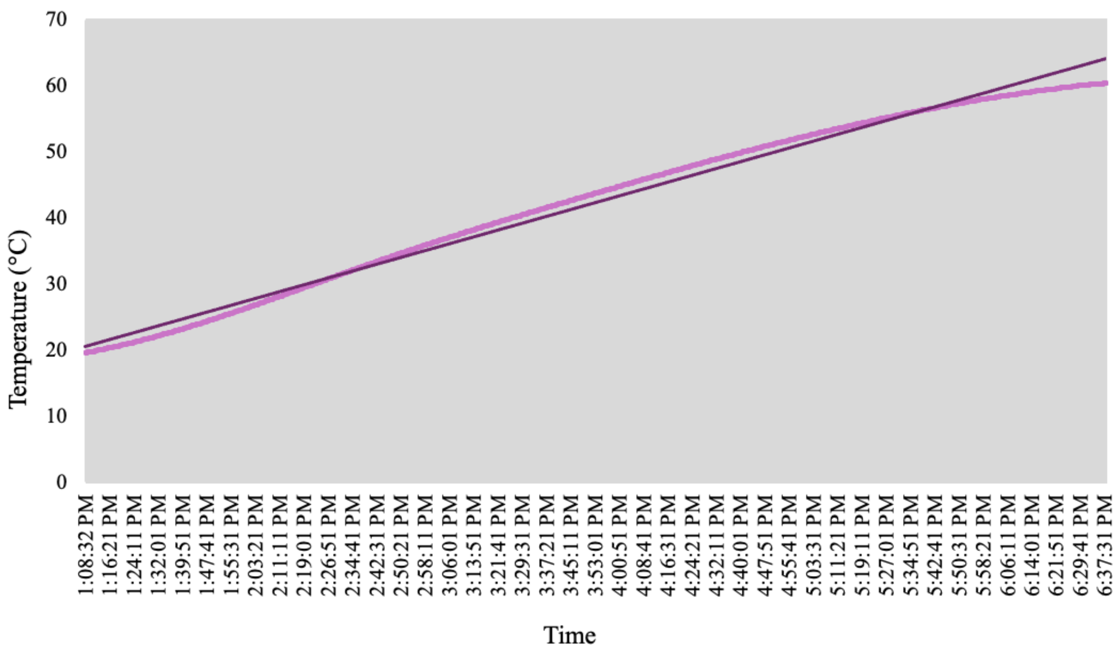

Figure 39: Trial 6 PCM Tank outlet temperature profile by time

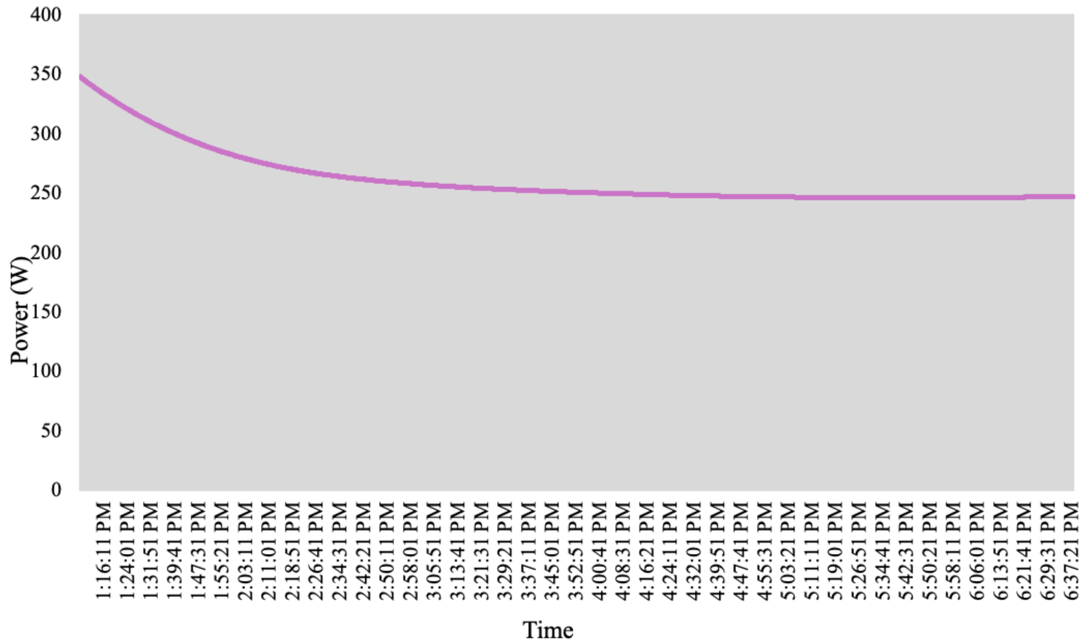

Figure 40: Blanket-type electric heater power consumption during Trial 6

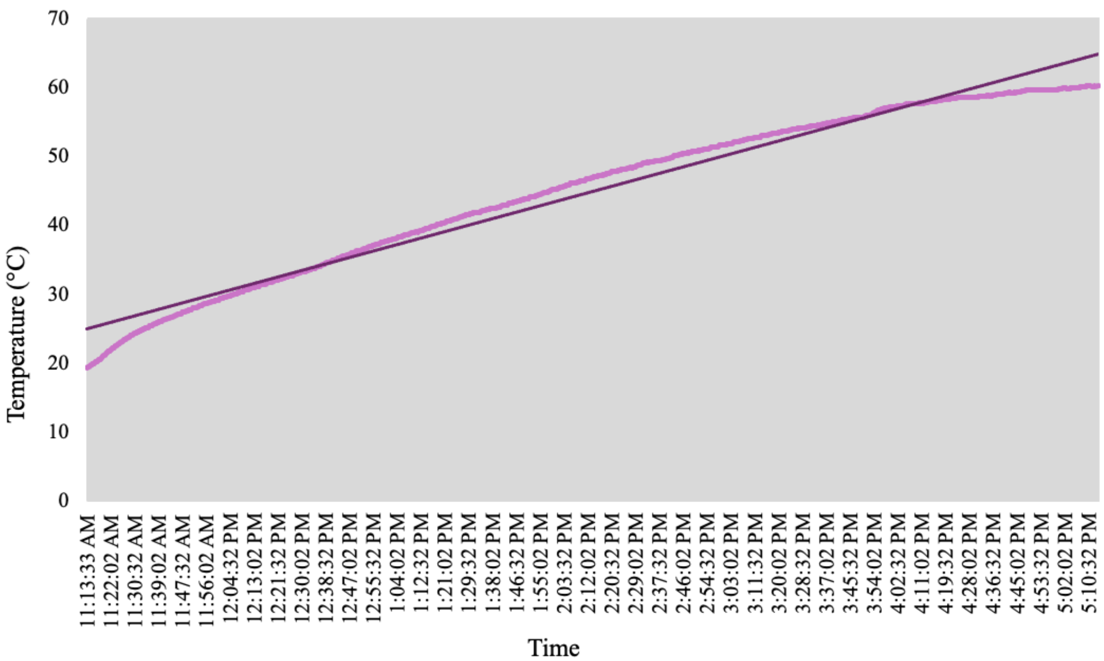

Figure 41: Trial 7 PCM Tank outlet temperature profile by time

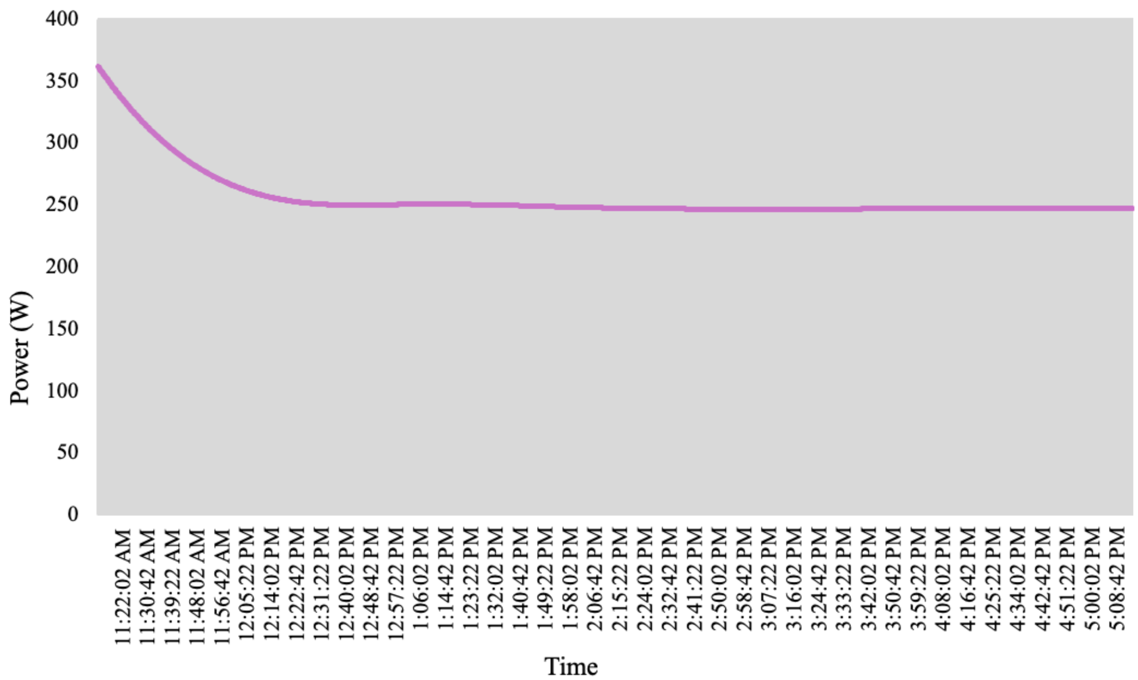

Figure 42: Blanket-type electric heater power consumption during Trial 7

In the graphs above, the trials of the experiment and the power consumption of the electric heater are shown. Expectedly, the water temperature at the PCM Tank outlet is rising over time. The longer water spends time in the coil, the longer it gains heat. Also, the power consumption of the electric heater is as expected. At the beginning of the trials, the electric heater consumes more power to provide the set temperature on its thermostat. Then, it regulates its power consumption according to the requested temperatures.

Other than that, the temperature change was also observed and recorded during the cooling down process of the phase change material. The following graph shows the change in average PCM temperature by time. Expectedly, the cooling down process takes longer than the heating of the phase change material due to material specifications.

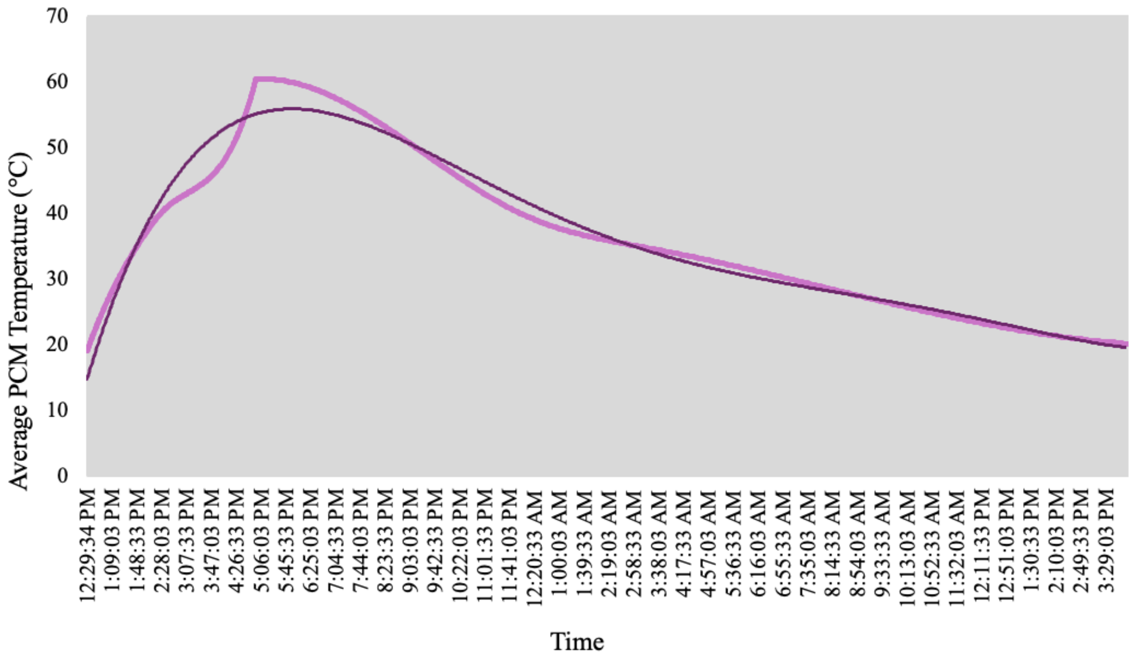

Figure 43: The change in the average PCM temperature during heating and cooling down processes

4.1.3 Numerical Results

The numerical part of this study is calculating the required heat to heat the water to the different target temperatures using the equation (12). The mass of the water used in the calculations was 18.927 kilograms which is the mass of 5 gallons (the amount of water used in the experiment) of water. Also, the lower temperature used in the calculations was 20 °C. Since the experimental work of this study is a smaller-scale application of the actual thermal energy storage system, a possible larger collector area in a real-life application should be considered while reviewing the calculations.

The specific enthalpy values of the liquid water were collected using the thermodynamic table. The values for the temperatures 35°C and 45°C were obtained by interpolation.

Table 12: Specific enthalpy values for the saturated water phase used in the calculations

Temperature T (°C)	20	30	35	40	45	50	55	60
Specific Enthalpy H_f (kJ/kg)	83.915	125.74	146.64	167.53	188.44	209.34	230.26	251.18

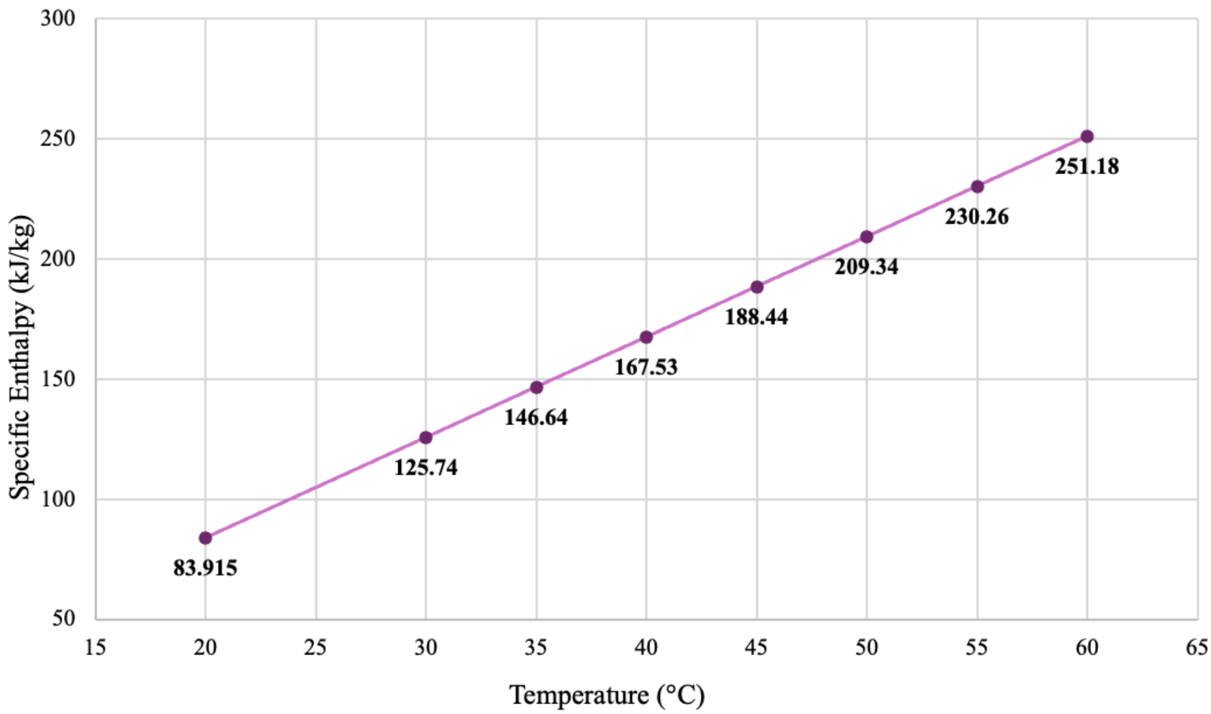

Figure 44: Specific enthalpy(kJ/kg) as a function of target temperature (℃)

The required heat for each target temperature was calculated by using the equation (12). As mentioned above, the calculated required heat is in kJ. Because of this reason, the change in the collector area should be considered while reviewing the calculations. Also, the minimum required collector area to provide the required temperature was calculated and added to the table below. Since the average solar irradiance at Outer Banks, NC is 697.302 kJ/h per m^2, the calculated required heat for each target temperature and collector area is as follows in the table below:

Table 13: Calculated required heat in kJ/h and collector area in m^2 for each target temperature

Temperature T (°C)	**Required Heat Q (kJ/h)**	**Required Area A (m^2)**
30	791.62	1.13
35	1187.19	1.70
40	1582.58	2.26
45	1978.34	2.83
50	2373.91	3.40
55	2769.87	3.97
60	3165.82	4.54

In the following graph, it shows that the required collector area increases with the increase in the required heat. Since the solar collectors are the main component to collect the sunlight, the results are expected to match with the basics.

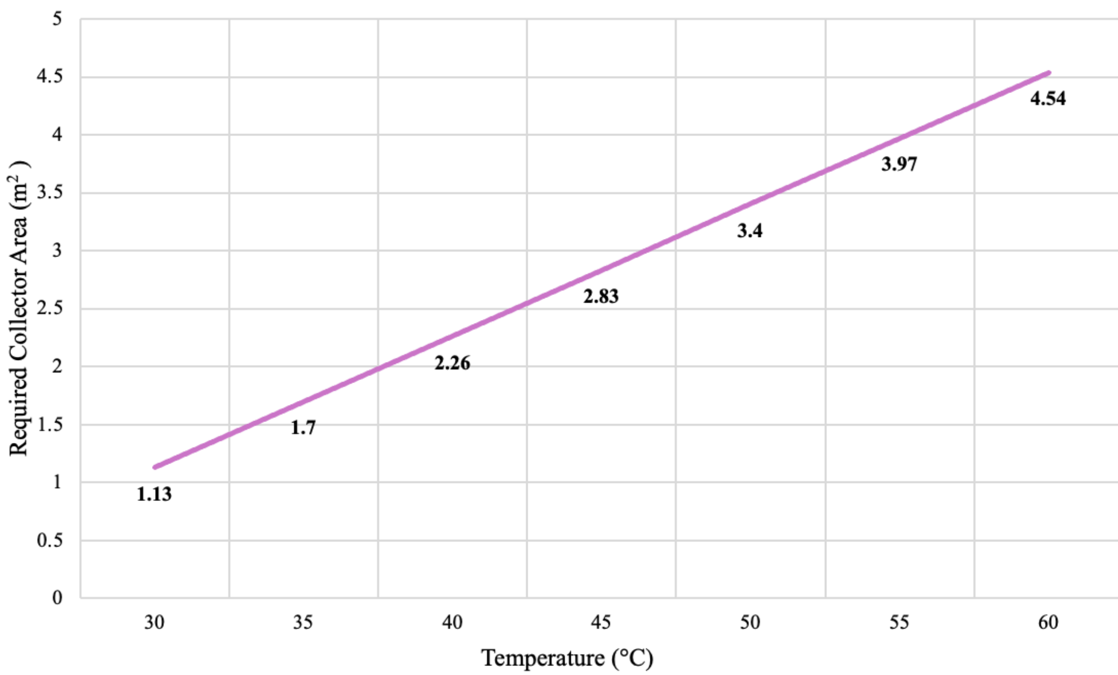

Figure 45: Required collector area (m^2) as a function of target temperature (℃)

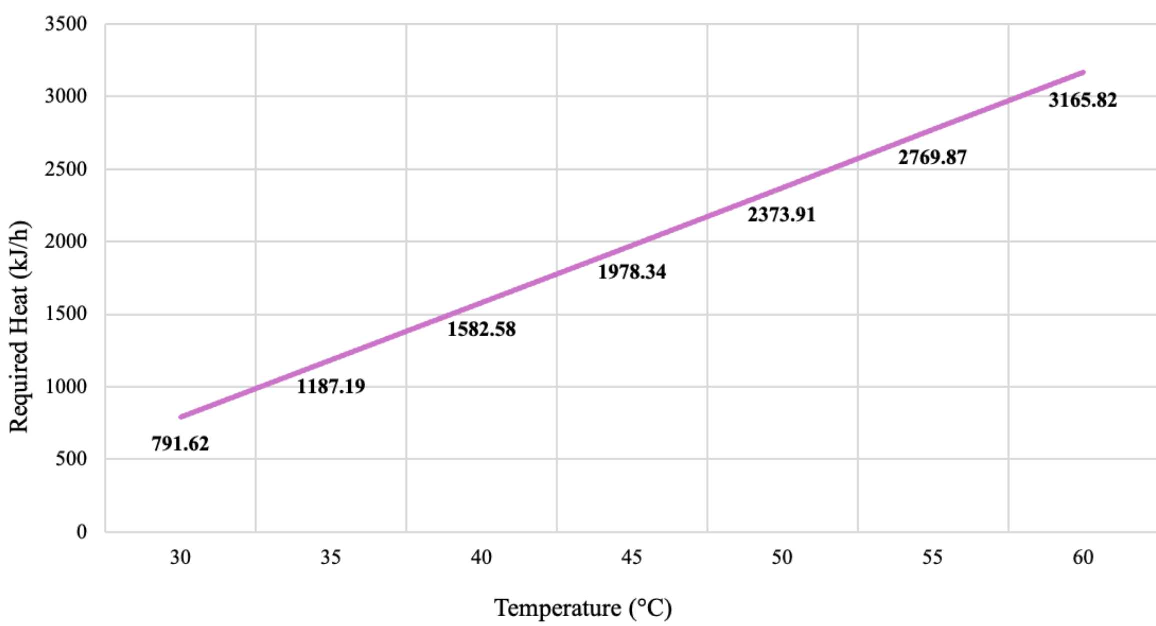

Figure 46: Required heat (kJ/h) as a function of target temperature (℃)

Heat exchanger calculations were conducted based on the specifications determined in the study by Trapani [27]. The variables used in the heat exchanger calculations are shown in the table below:

Table 14: The variables used in the heat exchanger calculations

Length (L)	1.6 m
Inner Diameter (D_i)	0.009525 m
Outer Diameter (Do)	0.01905 m
$C_{p, water}$	4184 J/kg.K
$C_{p, brine}$	3400 J/kg.K
$m_{c,i}$	0.0017 kg/s
$m_{h,i}$	0.003 kg/s
$T_{c,i}$	20 °C
U	~1000 W/m^2K

The temperatures in the heat exchanger according to the calculations are shown in the table below:

Table 15: Heat exchanger temperatures based on the calculations

T5 - PCM Tank Outlet Temp. (°C)	**$T_{H, IN}$ (°C)**	**$T_{C, IN}$ (°C)**	**$T_{C, OUT}$ (°C)**	**$T_{H, OUT}$ (°C)**
30	30	20	29.885	25.398
35	35	20	34.828	28.098
40	40	20	39.770	30.797
45	45	20	44.713	33.496
50	50	20	49.655	36.195
55	55	20	54.598	38.895
60	60	20	59.540	41.594

In the following table, the outlet temperature of the PCM storage tank and the calculated temperature values at the end of the heat exchanger are shown below:

Table 16: PCM tank outlet temperatures and heat exchanger calculation results

Temperature (°C)	**T5-PCM Tank Outlet Temperature (°C)**	**Heat Exchanger Outlet Temperature (°C)**
30	30	29.885
35	35	34.828
40	40	39.770
45	45	44.713
50	50	49.655
55	55	54.598
60	60	59.540

An Ansys Fluent simulation was run for the specific geometry and materials used in the experiment and the following results were obtained from the simulation. In the first figure below, the figure shows the temperature profile of the tank. The temperature values are as follows in a vertical cross-sectional area. The temperature profile is as expected. The temperature in the outer areas of the tank is relatively higher than in the center. Also, the temperature rise in water can be seen as well.

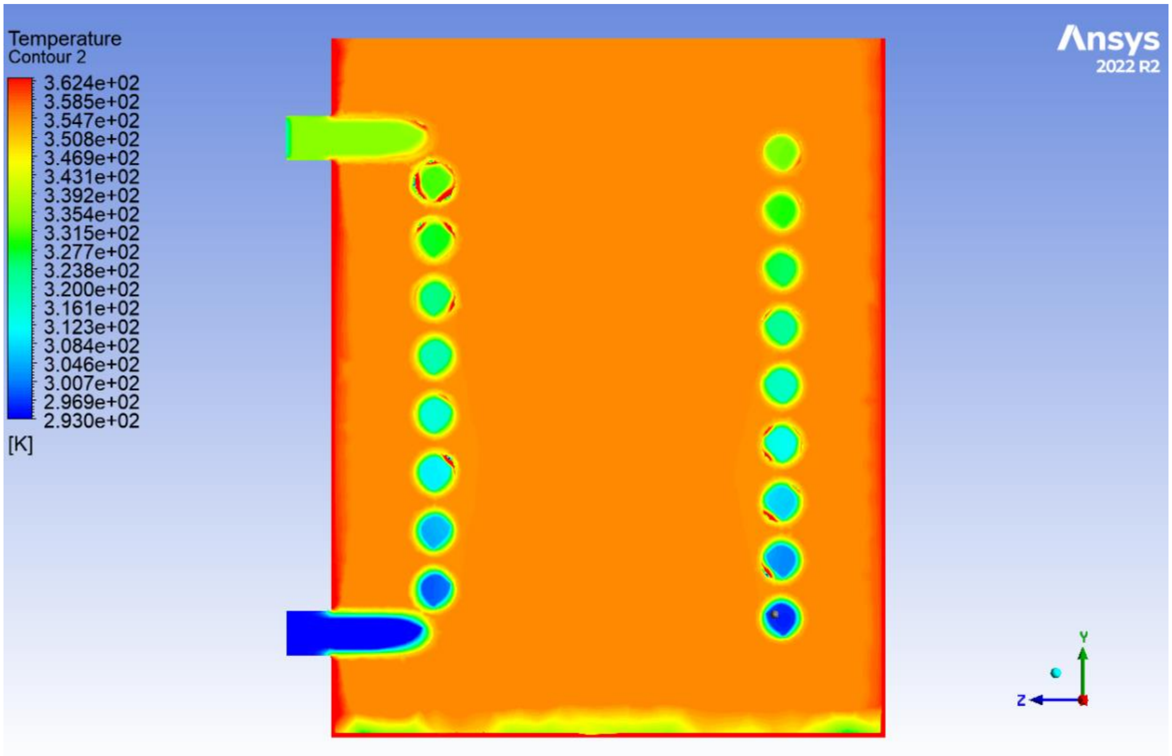

Figure 47: Temperature profile of the PCM tank in Ansys simulation

During the simulations on Ansys, the effect of using high-pressure water in the experimental setup was considered and the water pressure was set to 230 bar. The results of the simulation with the high-pressure water are as follows:

The results of the simulation with the high-pressure water are expectedly similar to the low-pressure simulation.

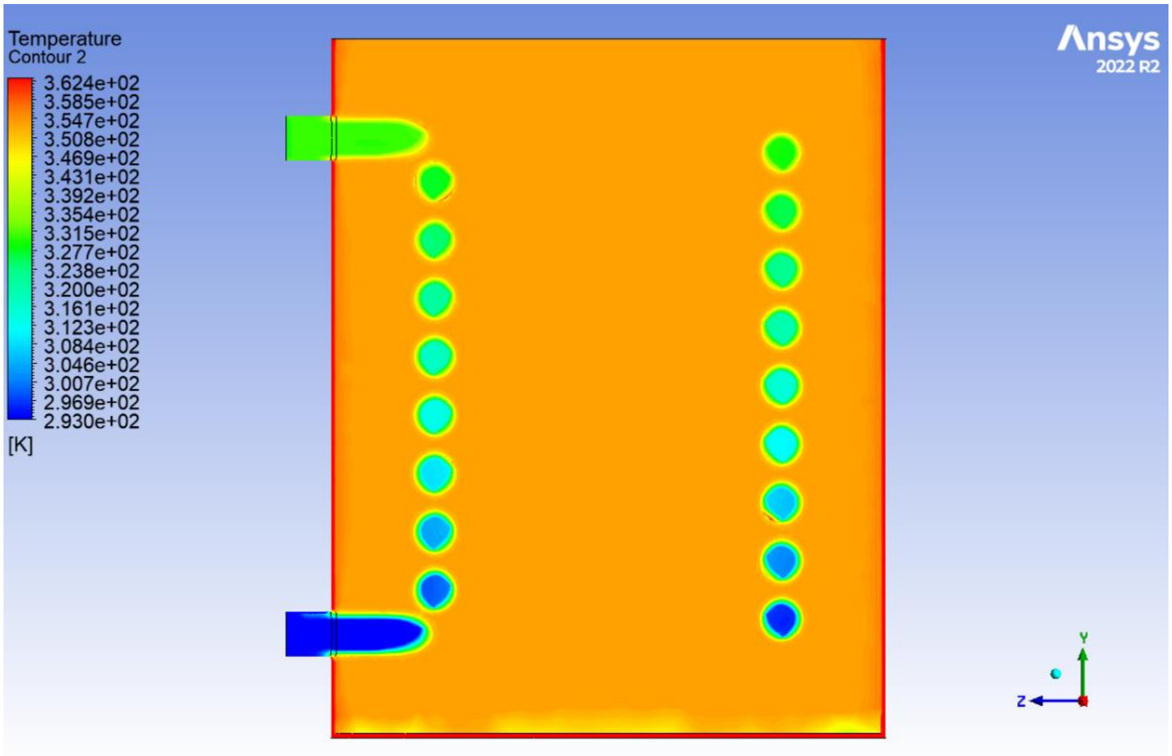

Figure 48: Temperature profile of the PCM tank in Ansys simulation (HP)

In the following figure, the applied heat to the PCM tank was the maximum heat reached at the specific application location. The result of the simulation is as expected. The temperature at the water outlet is higher than the temperature in the experimental setup.

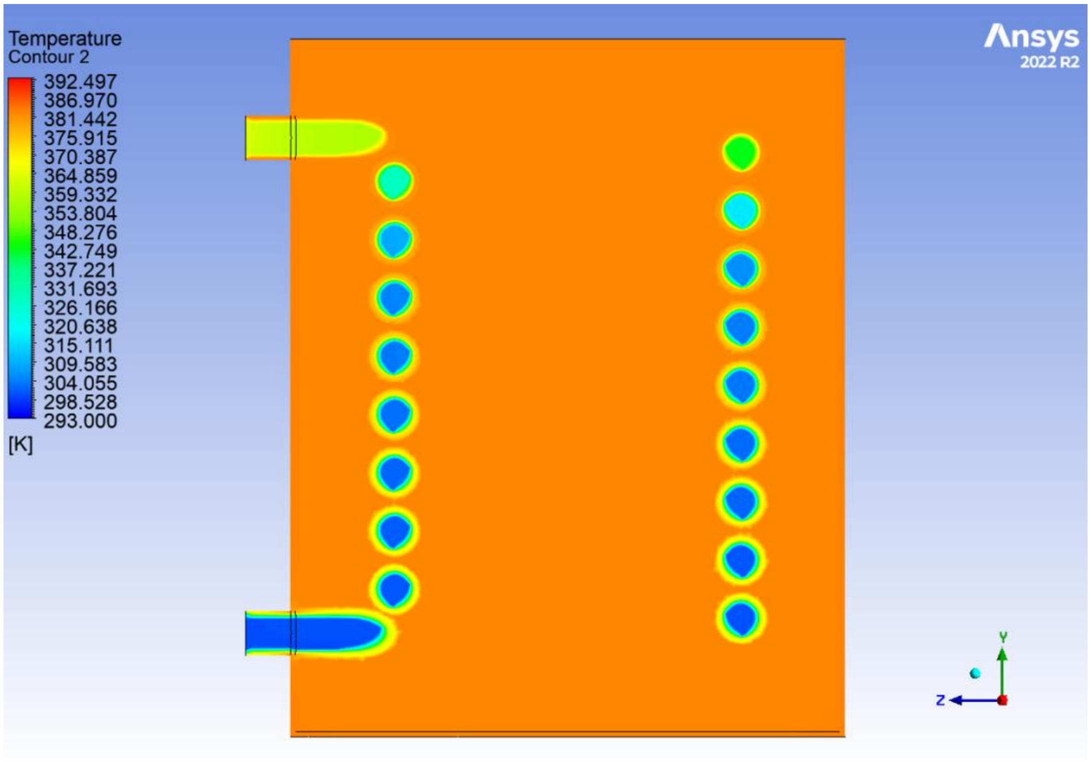

Figure 49: Temperature profile of the PCM tank in Ansys according to the location specifications

Another concept considered during the Ansys simulations was a double pipe flow with the phase change material in the outer pipe and the water in the inner pipe for the parabolic trough solar collectors. In this concept, the temperature profile of the pipes is as follows.

The temperature profile in the results is as expected. The water temperature rises in the flow direction as the heat transfer occurs between the phase change material and water.

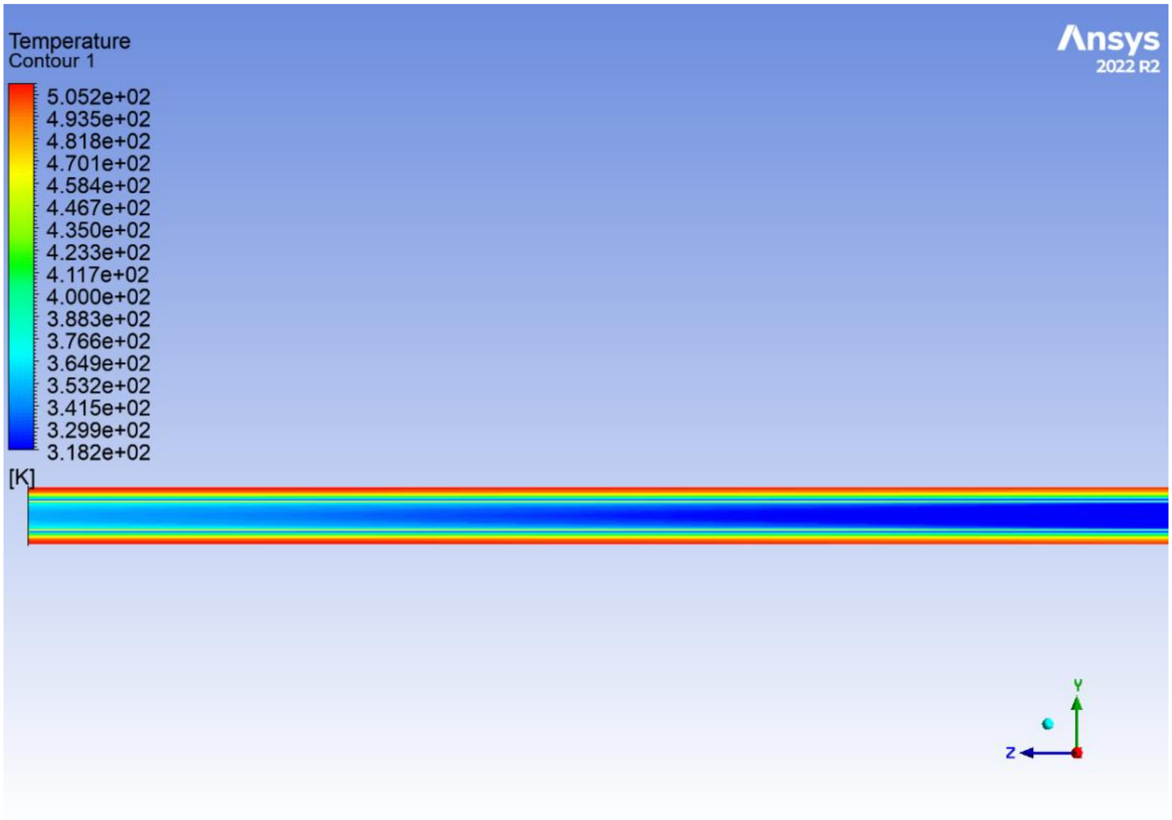

Figure 50: Parabolic trough solar collector concept simulation results for temperature profile

4.1.3 Heat Transfer Calculation Results

As mentioned in the methods section, the first set of calculations is for the heat gained by water for each trial. The enthalpy values for different temperatures were obtained by interpolation. The results are shown in the table below:

Table 17: Calculation results for the heat gained by water

Trial	Water Inlet Temperature (°C)	Water Outlet Temperature (°C)	Temperature Difference (°C)	Heat Gained by Water (J)	Heat Gained by Water (Wh)
1	20.2	30	9.8	776067.5664	215.574
2	20	35	15	1187858.52	329.960
3	19.1	40	20.9	1655082.871	459.745
4	19.1	45	25.9	2051035.711	569.732
5	18.9	50	31.1	2462826.665	684.118
6	19.2	55	35.8	2835022.334	787.506
7	18.8	60	41.2	3262651.402	206.292

In the second set of calculations, the heat gained by the paraffin wax as a phase change material was calculated with the same method. The specifications of the phase change material were shared in the previous chapters. According to the calculations, the results are shown in the table below:

Table 18: Results for the calculations of the heat gained by PCM

Trial	Average PCM Temperature (Cold) (°C)	Average PCM Temperature (at Target Temp. Reached) (°C)	Temperature Difference (°C)	Heat Gained by PCM (J)	Heat Gained by PCM (Wh)
1	27.9	34.7	6.8	142800	39.666
2	26.45	50.1	23.65	496650	137.958
3	22.5	49.75	27.25	572250	158.958
4	24.35	51.4	27.05	568050	157.791
5	22.7	59.85	37.15	780150	216.708
6	23	52.7	29.7	623700	173.25
7	21.9	59.4	37.5	787500	218.75

The third set of heat transfer calculations was performed to calculate the average total energy consumed during the trials according to the average power meter reading and the time passed until the target temperature reached the outlet of the PCM tank. The results are shown in the table below for this calculation:

Table 19: The average total ideal heat considering the power meter readings

Trial	T5- PCM Tank Outlet Temperature (°C)	Time (hrs.)	Average Power Meter Reading (W/h)	Average Total Ideal Heat (Wh)
1	30	0.28	253.79	71.0612
2	35	1.93	253.05	488.3865
3	40	1.5	257.04	385.56
4	45	3.35	258.82	867.047
5	50	4.42	258.78	1143.8076
6	55	5.25	256.78	1348.095
7	60	5.87	256.06	1503.0722

In the previous chapters, it was stated that a set of calculations were taken place for the heat transfer in the PCM tank. As mentioned before, a MATLAB code was employed for the calculations which can be found in Appendix A.

The results shared in the following table are from the moments when the PCM tank outlet temperature reaches the target temperature for that trial. In this fourth set of calculations, the heat transfer through the coil was calculated. The ideal value in the table was the heat transfer calculated using the PCM temperature. The actual heat transfer is the heat transfer calculated by using the water outlet temperature from the PCM tank. After the calculations, the ideal and the actual heat transfers were compared as well. In the following table, the ideal and the actual heat transfers for each scenario are shown.

Table 20: The ideal and the actual heat transfer for every trial in the PCM Tank

T5- PCM Tank Outlet Temperature (°C)	T3-T4 Average (°C)	T1- PCM Tank Inlet Temperature (°C)	Ideal Heat Transfer Rate (W)	Actual Heat Transfer Rate (W)	Time (hrs.)	Total Ideal Heat Transfer (Wh)	Total Actual Heat Transfer (Wh)
30	34.7	20.6	182.7406	179.7505	0.28	51.167	50.33
35	48.05	22.3	190.1520	181.8499	1.93	366.993	350.97
40	47.75	21.6	190.4064	185.4761	1.5	285.6096	278.214
45	54.7	20.1	195.7821	189.6112	3.35	655.87	635.197
50	59.85	21.8	197.9769	191.7106	4.42	873.731	847.36
55	56.1	20.6	196.3546	195.6549	5.25	1030.861	1027.188
60	59.4	21.9	198.0087	197.627	5.87	1162.311	1160.07

For the heat transfer calculations, the following specifications of the coil in the PCM tank were used:

Table 21: Specifications of the coil in the PCM tank

Material	304 Stainless Steel
Thermal Conductivity	16.2 W/m.K
Inner Diameter	0.01 m
Outer Diameter	0.015 m
Length	5.715 m

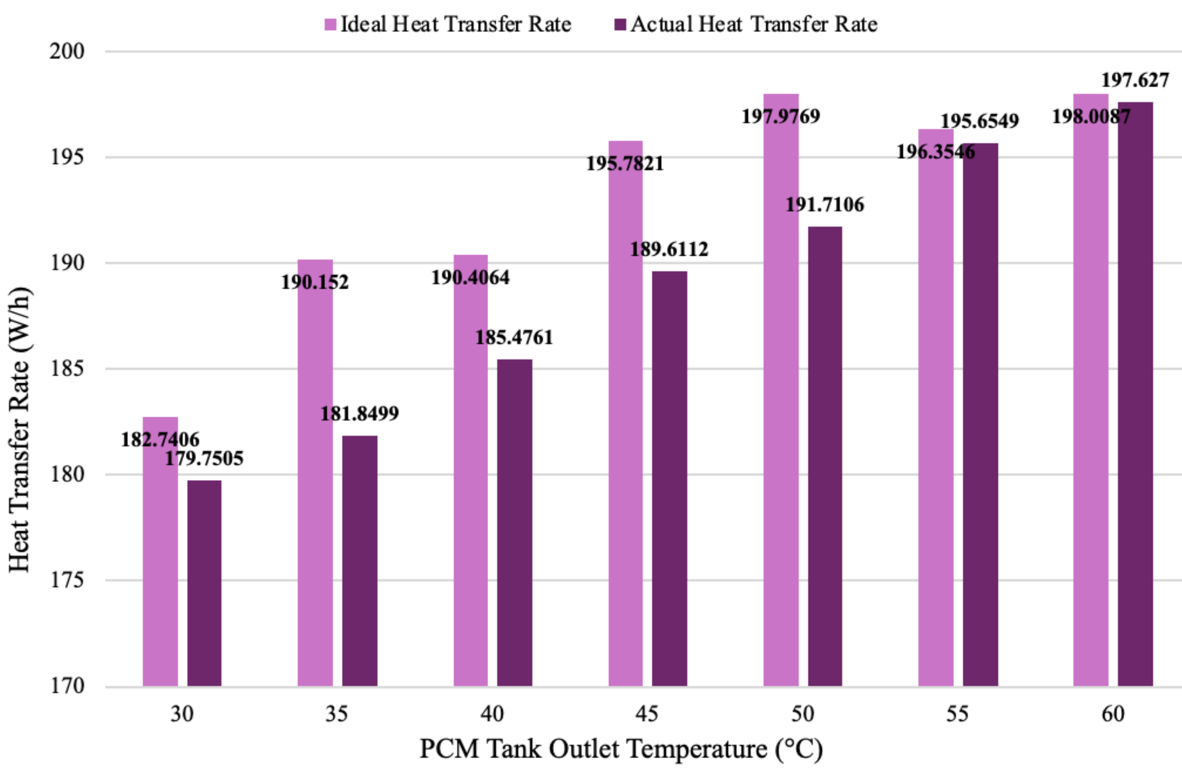

Figure 51: Comparison of the actual and the ideal heat transfer rate (W/h) in the PCM Tank

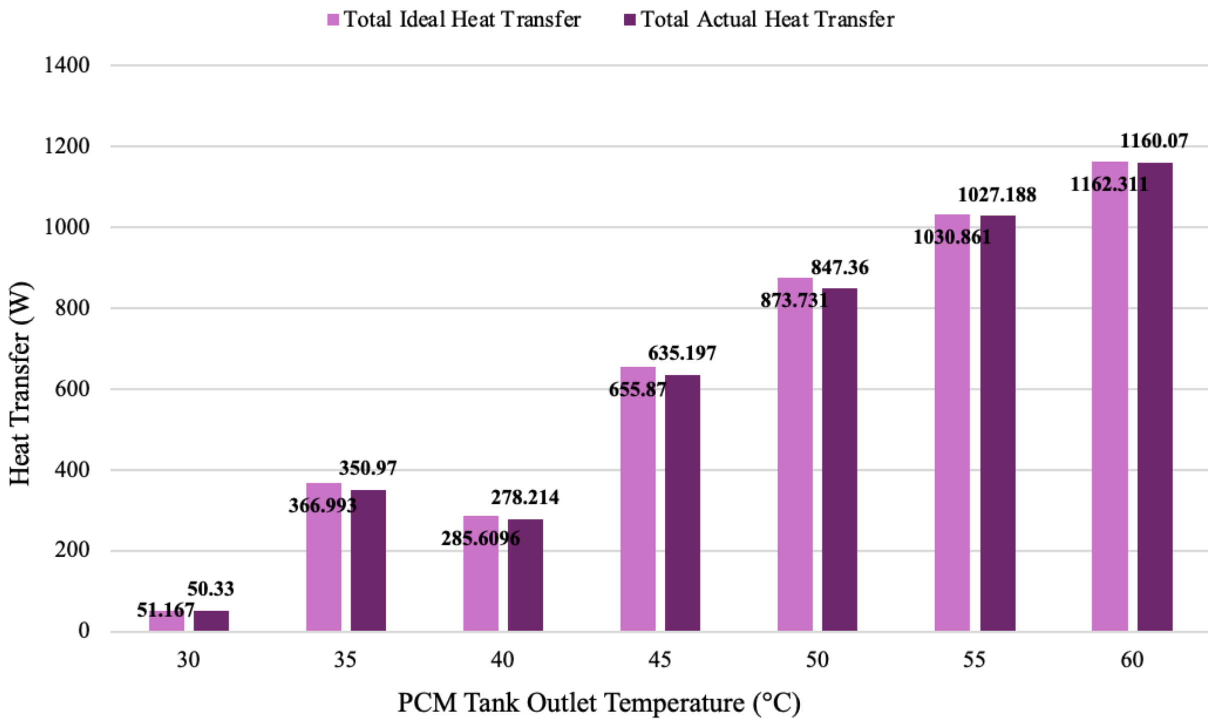

Figure 52: Comparison of the total ideal and actual heat transfer (W) in the PCM tank

The graphs above show heat gained by water comparing the use of energy to the PCM tank with the electric heater and the phase change material temperature. The results are as expected since the used energy is higher to heat the phase change material due to the losses during the energy conversion and the heat transfer. On the other hand, the phase change material cannot transfer all the heat to water due to the material properties of the PCM tank.

Also, a set of calculations was performed to determine the ideal amount of heat required to heat the PCM to 60°C. The method for the calculation was the same method used for calculating the heat gained by PCM calculations. As a result, the average ideal amount of heat for each trial was calculated as 233.33 W/h. To do the calculations, the total duration of each trial was taken as the time. However, the calculation by using the power meter reading was the actual average heat used during the experiment. The results are shown in the table below:

Table 22: Comparison of the average ideal heat required for PCM, and the actual amount of heat used in the experiment

Trial	**Trial Time (hrs.)**	**Average Power Meter Reading (W/h)**	**Ideal Amount of Heat Required (Wh)**	**Average Actual Heat (Wh)**	**Difference between the Ideal and the Actual Heat (Wh)**
1	2.55	253.79	594.991	647.164	52.173
2	3.53	253.05	823.655	893.266	69.611
3	3.78	257.04	881.9874	971.611	89.6236
4	5.73	258.82	1336.980	1483.038	146.058
5	6.67	258.78	1556.311	1726.062	205.751
6	5.5	256.78	1283.315	1412.29	128.975
7	6.02	256.06	1404.646	1541.481	136.835

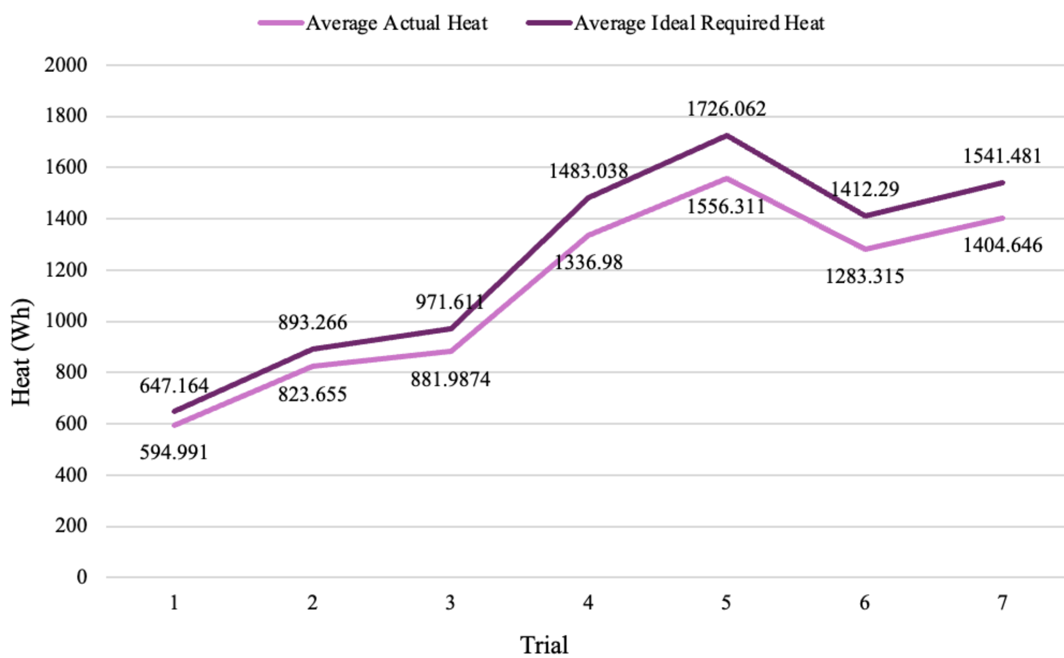

Figure 53: Comparison of the required ideal heat and the actual used heat for every trial in the experiment

The graph above shows the comparison of the required ideal heat to heat the phase change material to 60°C and the actual used energy during the experiment. As expected, the losses cause not to provide all the electric energy equivalent heat to the phase change material.

According to the calculations, the temperature difference between the ideal temperature of the PCM and the actual temperature reached was calculated as follows:

Table 23: The calculated temperature difference between the ideal and actual scenarios

Difference between the Ideal and the Actual Heat (Wh)	**Temperature Difference Between the Ideal and the Actual Scenarios (°C)**
52.173	8.944
69.611	11.933
89.6236	15.363
146.058	25.038
205.751	35.271
128.975	22.11
136.835	23.457

4.1.4 MATLAB Simulation Results

As mentioned, the MATLAB simulation was mainly used to determine the furnace consumption according to the water inlet temperature in the SCWD system. This water inlet temperature to the system was achieved by conducting the experiments and eventually the heat exchanger calculations. In this section of the study, the energy consumption of the furnace was obtained with and without the proposed PCM solar thermal storage system attached.

In the first scenario, the PCM solar thermal storage is not in use, and the water inlet temperature to the SCWD system is 20°C.

In the second scenario, the PCM solar thermal storage is in use. The obtained temperature values according to the heat exchanger calculations were plugged into the MATLAB simulation. The following results were obtained from the simulation and added to the table below.

Table 24: Furnace energy consumption according to the heat exchanger outlet temperature

Temperature (°C)	**Heat Exchanger Outlet Temperature (°C)**	**Required Energy without the PCM TES system (kW)**	**Furnace Energy Consumption with the PCM TES system (kW)**
30	29.885	1387	1329
35	34.828	1387	1300
40	39.770	1387	1271
45	44.713	1387	1242
50	49.655	1387	1212
55	54.598	1387	1183
60	59.540	1387	1154

In the following figure, the change in the furnace consumption is shown in a graph. The expectation of the change in the furnace consumption was a lower consumption when the feedwater temperature increased. Expectedly, the furnace consumption decreases when the feedwater temperature rises.

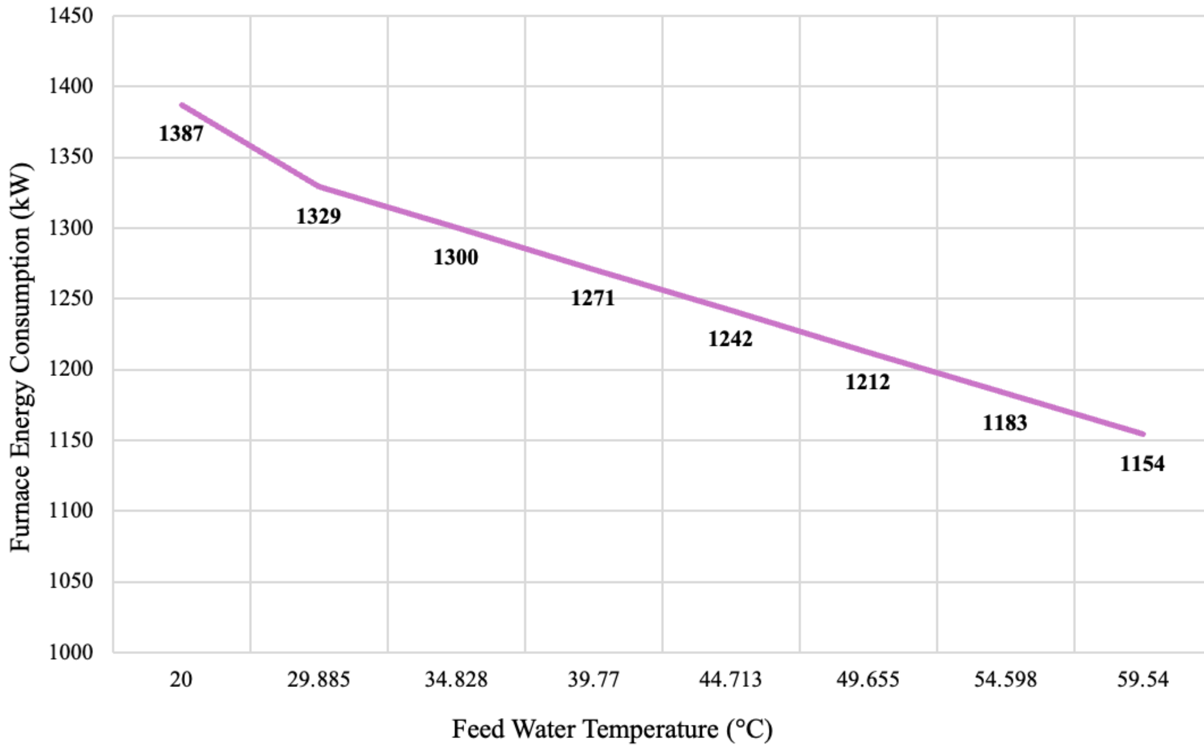

Figure 54: Change in furnace consumption (kW) due to the change in feed water temperature (°C)

In the graph above, the change in the furnace consumption due to the feedwater temperature is shown. As seen, the furnace consumption decreases with the increase in the feed water temperature as expected. The higher feed water temperature would require less energy consumption to reach the required temperature for the supercritical conditions.

4.2 Analysis

4.2.1 Economic Analysis

In the economic analysis calculations, the average industrial electric rate was taken as 7.84¢ according to the local provider at the specified location [36].

Table 25: Furnace energy consumption

Feed Water Inlet Temperature (°C)	**Furnace Energy Consumption (kW)**	**Furnace Energy Consumption** ($)
20	1387	108.7408
29.885	1329	104.1936
34.828	1300	101.9200
39.770	1271	99.6464
44.713	1242	97.3728
49.655	1212	95.0208
54.598	1183	92.7472
59.540	1154	90.4736

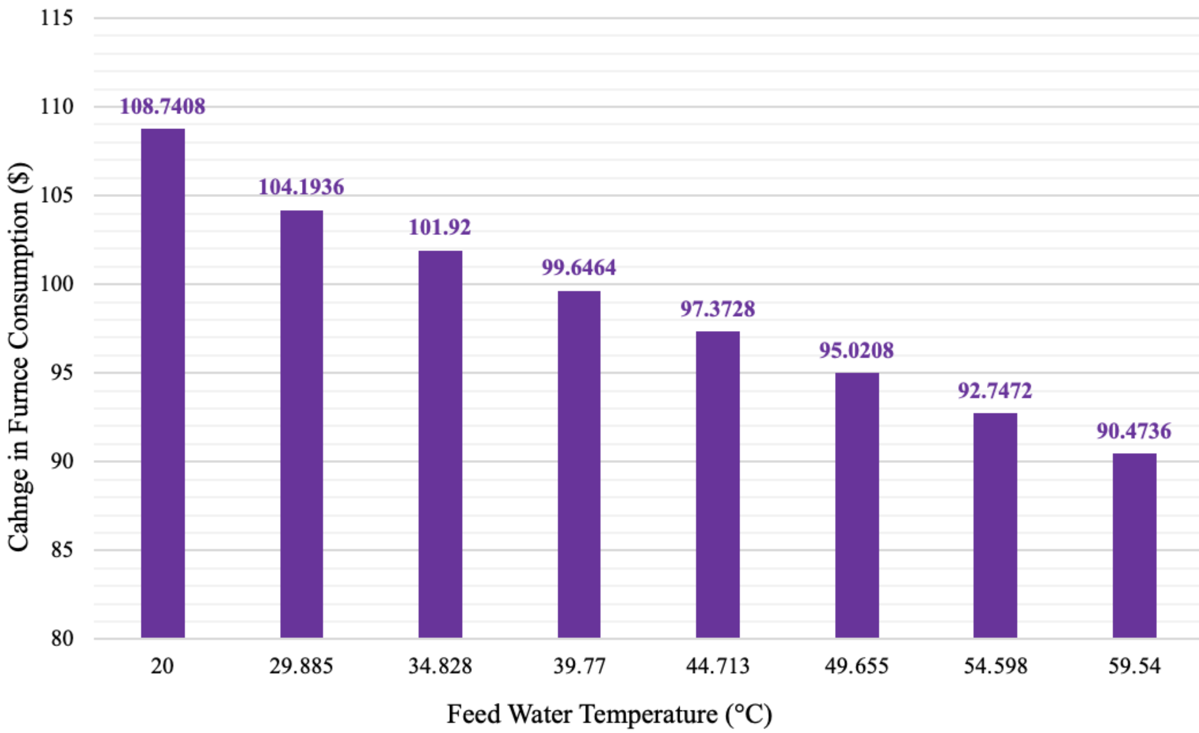

Figure 55: Change in furnace consumption ($) as a function of feed water temperature (°C)

According to the simulations, the furnace consumes less energy when the feed water temperature rises as expected. Simulations show that the difference between the feed water inlet temperature of 20 °C and the feed water inlet temperature of 58.54 °C is around 233 kW. According to the economic analysis based on the average electric rate in the application location (Outer Banks, NC), this difference is equal to a $18.2672 electric consumption difference. This difference provides a 16.7988% savings in the furnace energy consumption.

As seen in the graph above, the dollar value of the furnace consumption decreases with the higher feed water temperatures. Expectedly, the furnace would consume less to reach the required temperature for the supercritical water desalination when it receives the feed water at a higher temperature.

4.2.2 Error Analysis

In the experimental part of this study, there were many pieces of equipment used, and thermocouples were only one of them. The thermocouples used in the experiment are J-type thermocouples with a reading range of 32°F to 970°F (0°C to 521.11°C). According to the data provided by the manufacturer, these thermocouples have a ±0.75% accuracy and 1.3 seconds response time [37]. The power meter used to measure the power consumption of the electric heater during the experiment has a ±1% accuracy.

Other than the thermocouples, the other measurement device actively used in the experiment was the Extech TM500 12-channel datalogging thermometer. As mentioned in the previous sections, the datalogging thermometer has a temperature range of -148°F to 2102°F (-100°C to 1150°C), and the max resolution of ±0.4% of reading (+1.8°F/+1°C) [33].

Also, the last measuring device occasionally used in the experiment is a "Kamtop" branded digital dual-channel thermometer with the "TL253" model number. This thermometer has a temperature reading range of -210℃ to 1200℃（-346°F to 2192°F) for the J-Type thermocouples. It has a resolution of 0.1℃/℉＜1000℃; 1.0℃/℉≥1000℃ and an accuracy of ±0.1%+0.6℃ [38].

4.2.3 Environmental Analysis

The employment of a Phase Change Material (PCM) Solar Thermal Energy Storage System within the context of a supercritical water desalination system provides a remarkable reduction in energy consumption, calculated as 233 kW of electric savings achieved in the furnace operation. This reduction not only indicates a considerable enhancement in the savings of the desalination process but also brings positive impacts on environmental sustainability. By mitigating the demand for conventional energy sources, such as fossil fuels, the adoption of solar thermal energy storage systems contributes to a decrease in greenhouse gas emissions and associated environmental pollutants. According to a published calculator named "Greenhouse Gas Equivalencies Calculator" by the Environmental Protection Agency (EPA) the equivalent greenhouse gas amount is 978,984 kilograms of carbon dioxide (CO_2) [39].

Chapter 5

Conclusion

5.1 Evaluation of Work

This study analyzed the efficiency of paraffin wax as a phase change material (PCM) solar thermal energy storage to preheat the water before the furnace in a supercritical water desalination (SCWD) system. The utilization of PCM solar thermal energy storage aimed to mitigate the environmental impact and reduce energy consumption by the furnace operation and eventually the supercritical water desalination process. Solar energy was assigned (simulated in the experimental work) to supply the necessary heat for PCM, enabling heat transfer to the water and consequently decreasing the energy demand of the supercritical water desalination system. The primary objective was to promote environmental responsibility and endorse sustainability by decreasing furnace energy consumption while offering an effective solution for supercritical water desalination with the integration of paraffin wax as a phase change material.

To evaluate the efficiency of the proposed approach, a combination of experimental and numerical practices was employed. The numerical studies served as a bridge between solar data, experimental work, and MATLAB simulations. Solar data were analyzed and processed to determine the required parameters for the experimental work, facilitated by computational procedures described in the numerical work. Subsequently, experimental procedures took place to obtain temperature input data crucial for MATLAB simulations. Also, a heat transfer analysis in the PCM Tank took place after the experiment. The MATLAB simulation was then utilized for collecting the furnace consumption data, conducting the economic analysis, and the final analysis of the proposed study.

The solar data showed that the application location (Outer Banks, NC) has a solar irradiance of 193.695 W/m^2 (697.302 kJ/h per m^2). This data was combined with the solar duration hours (12.18194 hours), and the target temperatures in the experiment were decided as 30°C, 35°C, 40°C, 45°C, 50°C, 55°C, and 60°C considering the phase change temperature of the used paraffin wax.

In the experimental work of the study, decided target temperatures were reached at the outlet of the PCM storage tank, and the heat exchanger calculations were made. After the heat exchanger calculations, the temperatures were found at the inlet of the SCWD system. These inlet temperatures are the temperatures that go into the SCWD system. So, the MATLAB simulation was run by using these temperatures as feedwater temperatures of the system.

In the analysis of the experimental work, the lack of insulation and the possibility of choosing a different phase change material were observed. According to the calculations made based on the experimental data, the potential of reaching higher temperatures was clearly observed. Reaching higher temperatures is based on a few variables. One of the very first variables is the potential of solar radiation at the application location. The solar data shows that the application location (Outer Banks, NC) has the potential to provide the required thermal energy to reach higher temperatures. The second important variable is the phase change material selection. With a higher phase change temperature phase change material, a higher outlet temperature of the PCM Tank is possible. Also, the insulation of the PCM Tank plays a critical role in the experiment. To preserve the heat stored in the phase change material, the PCM tank should be insulated well.

The result and analysis of the MATLAB simulation were shared. According to the results of the simulation, an economic analysis was made. This economic analysis is based on the electricity rates in the application location (Outer Banks, NC) in the year of the research (2024). By using the electricity rate, the furnace consumption in every scenario was calculated and compared. According to the calculations, the furnace consumption with the use of the proposed system is 16.7988% lower on average than the furnace consumption without the use of the PCM TES system.

5.2 Future Work

The presented study focused on an investigation of the integrity of a phase change material thermal energy storage system within the context of a supercritical water desalination system. Both empirical experimentation and MATLAB-based simulation methodologies were employed to achieve a comprehensive understanding of the feasibility of the proposed system. Future attempts in this field are advised to extend the scope of experimental work and establish interconnections between the proposed system and supercritical water desalination setups, thus facilitating real-life observations regarding the integrity of these interconnected systems.

As mentioned in the evaluation of the work, the selection of the phase change material is one of the very important decisions for the study. Due to the solar radiation potential of the application location, different types of phase change materials can be selected in future studies.

Beyond the experimental investigations, improvements to the proposed system could be gathered by increasing liquid capacity depending on the specific application location. Customizing experimental outcomes based on the application's location can enhance the system’s performance. Furthermore, an additional possibility for future research lies in exploring alternative heat transfer fluids in the low-pressure system. This approach holds promise for advancing comprehension of the supercritical water desalination process and its compatibility with other heat transfer liquids.

References

[1] E. Jones, M. Qadir, M. T. H. van Vliet, V. Smakhtin, and S. mu Kang, “The state of desalination and brine production: A global outlook,” *Science of The Total Environment*, vol. 657, pp. 1343–1356, Mar. 2019, doi: 10.1016/J.SCITOTENV.2018.12.076.

[2] S. van Wyk, A. G. J. van der Ham, and S. R. A. Kersten, “Analysis of the energy consumption of supercritical water desalination (SCWD),” *Desalination*, vol. 474, p. 114189, Jan. 2020, doi: 10.1016/J.DESAL.2019.114189.

[3] D. A. (Donald A. Palmer, R. J. Fernández-Prini, A. H. Harvey, and International Association for the Properties of Water and Steam., *Aqueous systems at elevated temperatures and pressures : physical chemistry in water, steam, and hydrothermal solutions*. Elsevier Academic Press, 2004. Accessed: Apr. 29, 2023. [Online]. Available: http://www.sciencedirect.com:5070/book/9780125444613/aqueous-systems-at-elevated-temperatures-and-pressures

[4] S. van Wyk, A. G. J. van der Ham, and S. R. A. Kersten, “Analysis of the energy consumption of supercritical water desalination (SCWD),” *Desalination*, vol. 474, p. 114189, Jan. 2020, doi: 10.1016/J.DESAL.2019.114189.

[5] P. Sharan, J. D. McTigue, T. J. Yoon, R. Currier, and A. T. Findikoglu, “Energy efficient supercritical water desalination using a high-temperature heat pump: A zero liquid discharge desalination,” *Desalination*, vol. 506, p. 115020, Jun. 2021, doi: 10.1016/J.DESAL.2021.115020.

[6] S. O. Odu, A. G. J. Van Der Ham, S. Metz, and S. R. A. Kersten, “Design of a Process for Supercritical Water Desalination with Zero Liquid Discharge,” *Ind Eng Chem Res*, vol. 54, no. 20, pp. 5527–5535, May 2015, doi: 10.1021/ACS.IECR.5B00826/ASSET/IMAGES/LARGE/IE-2015-00826J_0009.JPEG.

[7] T. Kousksou, P. Bruel, A. Jamil, T. El Rhafiki, and Y. Zeraouli, “Energy storage: Applications and challenges,” *Solar Energy Materials and Solar Cells*, vol. 120, no. PART A, pp. 59–80, Jan. 2014, doi: 10.1016/J.SOLMAT.2013.08.015.

[8] A. Dobos, T. Neises, and M. Wagner, “Advances in CSP Simulation Technology in the System Advisor Model,” *Energy Procedia*, vol. 49, pp. 2482–2489, Jan. 2014, doi: 10.1016/J.EGYPRO.2014.03.263.

[9] M. Sengupta, Y. Xie, A. Lopez, A. Habte, G. Maclaurin, and J. Shelby, “The National Solar Radiation Data Base (NSRDB),” *Renewable and Sustainable Energy Reviews*, vol. 89, pp. 51–60, Jun. 2018, doi: 10.1016/J.RSER.2018.03.003.

[10] S. Yagnambhatt, S. Khanmohammadi, and J. Maisonneuve, "Reducing the specific energy use of seawater desalination with thermally enhanced reverse osmosis," *Desalination*, vol. 573, p. 117163, Mar. 2024, doi: 10.1016/J.DESAL.2023.117163.

[11] S. van Wyk, A. G. J. van der Ham, and S. R. A. Kersten, "Analysis of the energy consumption of supercritical water desalination (SCWD)," *Desalination*, vol. 474, p. 114189, Jan. 2020, doi: 10.1016/J.DESAL.2019.114189.

[12] S. van Wyk, A. G. J. van der Ham, and S. R. A. Kersten, "Potential of supercritical water desalination (SCWD) as zero liquid discharge (ZLD) technology," *Desalination*, vol. 495, p. 114593, Dec. 2020, doi: 10.1016/J.DESAL.2020.114593.

[13] P. Sharan, J. D. McTigue, T. J. Yoon, R. Currier, and A. T. Findikoglu, "Energy efficient supercritical water desalination using a high-temperature heat pump: A zero liquid discharge desalination," *Desalination*, vol. 506, p. 115020, Jun. 2021, doi: 10.1016/J.DESAL.2021.115020.

[14] J. D. McTigue, A. J. White, and C. N. Markides, "Parametric studies and optimisation of pumped thermal electricity storage," *Appl Energy*, vol. 137, pp. 800–811, 2015, doi: 10.1016/J.APENERGY.2014.08.039.

[15] A. Benato, "Performance and cost evaluation of an innovative Pumped Thermal Electricity Storage power system," *Energy*, vol. 138, pp. 419–436, Nov. 2017, doi: 10.1016/J.ENERGY.2017.07.066.

[16] S. Baghaei Oskouei *et al.*, "Solar-powered hybrid energy storage system with phase change materials," *Energy Convers Manag*, vol. 302, no. November 2023, p. 118117, Feb. 2024, doi: 10.1016/J.ENCONMAN.2024.118117.

[17] W. Chiang, I. Permana, F. Wang, H. Chen, and M. Erdenebayar, "Experimental investigation for an innovative hybrid photovoltaic/Thermal (PV/T) solar system," *Energy Reports*, vol. 8, pp. 910–918, Nov. 2022, doi: 10.1016/J.EGYR.2022.10.264.

[18] T. Kousksou, P. Bruel, A. Jamil, T. El Rhafiki, and Y. Zeraouli, "Energy storage: Applications and challenges," *Solar Energy Materials and Solar Cells*, vol. 120, no. PART A, pp. 59–80, Jan. 2014, doi: 10.1016/J.SOLMAT.2013.08.015.

[19] M. Fan, J. Wang, Z. Luan, X. Kong, J. Jia, and H. Li, "Experimental study on enhanced heat transfer performances and optimized strategies of cascade sensible-latent heat storage radiator," *Renew Energy*, p. 120088, Jan. 2024, doi: 10.1016/J.RENENE.2024.120088.

[20] M. Fan, J. Wang, X. Kong, H. Suo, W. Zheng, and H. Li, "Experimental evaluation of the cascaded energy storage radiator for constructing indoor thermal environment in winter," *Appl Energy*, vol. 332, p. 120503, Feb. 2023, doi: 10.1016/J.APENERGY.2022.120503.

[21] Z. Khan, Z. Khan, and A. Ghafoor, "A review of performance enhancement of PCM based latent heat storage system within the context of materials, thermal stability and compatibility," *Energy Convers Manag*, vol. 115, pp. 132–158, May 2016, doi: 10.1016/J.ENCONMAN.2016.02.045.

[22] R. Bharathiraja, T. Ramkumar, M. Selvakumar, and N. Radhika, "Thermal characteristics enhancement of Paraffin Wax Phase Change Material (PCM) for thermal storage applications," *Renew Energy*, vol. 222, p. 119986, Feb. 2024, doi: 10.1016/J.RENENE.2024.119986.

[23] S. P. Jesumathy, M. Udayakumar, and S. Suresh, "Heat transfer characteristics in latent heat storage system using paraffin wax," *Journal of Mechanical Science and Technology*, vol. 26, no. 3, pp. 959–965, Mar. 2012, doi: 10.1007/S12206-011-1017-4/METRICS.

[24] "NSRDB." Accessed: Feb. 11, 2024. [Online]. Available: https://nsrdb.nrel.gov/data-viewer

[25] N. G. M. L. US Department of Commerce, "ESRL Global Monitoring Laboratory - Global Radiation and Aerosols".

[26] J. Meeus, *Astronomical Algorithms*. Willmann-Bell, 1991. [Online]. Available: https://books.google.com/books?id=1smAQgAACAAJ

[27] M. J. Trapani, "EXPERIMENTAL DETERMINATION OF THERMOPHYSICAL PROPERTIES IN SUPERCRITICAL HEAT EXCHANGERS," 2023.

[28] "Engineering Page > Heat Exchangers > Typical Overall Heat Transfer Coefficients." Accessed: Mar. 26, 2024. [Online]. Available: https://www.engineeringpage.com/technology/thermal/transfer.html

[29] G. L. Dittman, "Calculation of brine properties," Feb. 1977, doi: 10.2172/7111583.

[30] "SS 304 Stainless Steel Condenser Coil Bucket | USA Lab." Accessed: Feb. 13, 2024. [Online]. Available: https://www.usalab.com/stainless-steel-10-condensing-coil-bucket-ss304-various-sizes-1-2-1-4/

[31] "(18) (PDF) Numerical investigation of thermal performance and phase change of wax paraffin layer surrounding water tank." Accessed: Apr. 03, 2024. [Online]. Available: https://www.researchgate.net/publication/316665948_Numerical_investigation_of_thermal_performance_and_phase_change_of_wax_paraffin_layer_surrounding_water_tank

[32] "Flexible Heating Jackets for 25L, 50L and 100L drums." Accessed: Feb. 15, 2024. [Online]. Available: https://www.inteliheat.com/25-100lhjs/

[33] "Extech TM500: 12-Channel Datalogging Thermometer | Teledyne FLIR." Accessed: Feb. 21, 2024. [Online]. Available: https://www.flir.com/products/tm500/?vertical=condition+monitoring&segment=solutions

[34] G. Glosson and F. Filho, "Simulating and Optimizing a Zero-Waste Wave-to-Water Desalination System," United States -- North Carolina, 2023. [Online]. Available: https://www.proquest.com/dissertations-theses/simulating-optimizing-zero-waste-wave-water/docview/2830117248/se-2?accountid=10639

[35] "ECU Outer Banks Campus | Integrated Coastal Programs | ECU." Accessed: Feb. 15, 2024. [Online]. Available: https://coastal.ecu.edu/obx-campus/

[36] "Business Rates | North Carolina - Electric | Dominion Energy." Accessed: Mar. 23, 2024. [Online]. Available: https://www.dominionenergy.com/north-carolina-electric/rates-and-tariffs/business-rates

[37] "Bendable Thermocouple Probe for Liquid and Gas, without Cable, Type J, Round Pin Connection, 6" x 1/4" Probe | McMaster-Carr." Accessed: Feb. 28, 2024. [Online]. Available: https://www.mcmaster.com/3856K27/

[38] "Kamtop Digital Dual Channel Thermometer – kamtop." Accessed: Feb. 28, 2024. [Online]. Available: https://www.kamtop.net/products/kamtop-digital-dual-channel-thermometer

[39] "Greenhouse Gas Equivalencies Calculator | US EPA." Accessed: Mar. 24, 2024. [Online]. Available: https://www.epa.gov/energy/greenhouse-gas-equivalencies-calculator#results

Appendix A: MATLAB Code for Heat Transfer

```
% Heat Transfer Calculations
k = TC_pipe; % Thermal conductivity of the pipe material (in W/mK)
inner_diameter = ID; % Inner diameter of the pipe (in meters)
outer_diameter = OD; % Outer diameter of the pipe (in meters)
length = L; % Length of the pipe (in meters)
PCM_T = T_1; % PCM Temperature (in Celsius)
water_T = T_2; % Water Temperature (in Celsius)
delta_T = PCM_T - water_T; % Temperature difference between inner and
outer surfaces (in Celsius)
% Convert temperature difference to Kelvin
delta_T_K = delta_T + 273.15;
% Calculate radius of the pipe
radius = (inner_diameter + outer_diameter) / 4;
% Calculate surface area of the pipe
surface_area = 2 * pi * radius * length;
% Calculate the rate of heat transfer
Q = (k * surface_area * delta_T_K) / length;
disp(['Rate of heat transfer: ', num2str(Q), ' watts']);
```

Appendix B: MATLAB Code for the Heat Exchanger

```
% Specifications
T_hot_in = T1;         % Inlet temperature of hot fluid (in Celsius)
T_cold_in = T2;        % Inlet temperature of cold fluid (in Celsius)
m_dot_hot = m1;     % Mass flow rate of hot fluid (in kg/s)
m_dot_cold = m2;   % Mass flow rate of cold fluid (in kg/s)
U = u1;              % Overall heat transfer coefficient (in
W/(m^2*K))
D_inner = ID;      % Inner diameter of pipe (in meters)
D_outer = OD;        % Outer diameter of pipe (in meters)
L = l1;               % Length of heat exchanger (in meters)
rho_hot = r1;      % Density of hot fluid (in kg/m^3)
c_hot = c1;          % Specific heat of hot fluid (in J/(kg*K))
rho_cold = r2;       % Density of cold fluid (in kg/m^3)
c_cold = c2;         % Specific heat of cold fluid (in J/(kg*K))
% Area of inner pipe (assuming it's a circular pipe)
A = pi * D_inner * L;
% Calculate the outlet temperature of the hot fluid
```

```
T_hot_out = T_hot_in - ((m_dot_cold * c_cold * (T_hot_in - T_cold_in))
/ (m_dot_hot * c_hot));
% Calculate the heat capacity rates
C_dot_hot = m_dot_hot * c_hot;
C_dot_cold = m_dot_cold * c_cold;
% Calculate the minimum heat capacity rate
C_min = min(C_dot_hot, C_dot_cold);
% Calculate the minimum heat capacity rate
C_max = max(C_dot_hot, C_dot_cold);
% Calculate the heat capacity rate ratio
C_ratio = C_min / C_max;
% Calculate the number of transfer units (NTU)
NTU = U * A / C_min;
% Calculate the heat exchanger effectiveness (epsilon)
epsilon = 1 - exp(-NTU * (1 - C_ratio)) / (1 - C_ratio * exp(-NTU * (1
- C_ratio)));
% Calculate the heat transfer rate
Q = epsilon * C_min * (T_hot_in - T_cold_in);
```

```
% Assuming fully developed flow and neglecting wall resistances, the
heat transfer area will be the surface area of the inner pipe
% Calculate the outlet temperature of the cold fluid
T_cold_out = T_cold_in + (Q / (m_dot_cold * c_cold));
% Display the results
fprintf('Outlet temperature of the hot fluid: %.3f Celsius\n',
T_hot_out);
fprintf('Outlet temperature of the cold fluid: %.3f Celsius\n',
T_cold_out);
fprintf('Number of Transfer Units (NTU): %.4f\n', NTU);
fprintf('Effectiveness (epsilon): %.4f\n', epsilon);
```

Appendix C: MATLAB Code for SCWD

```
% The original MATLAB code calculates all the parameters and simulates a Supercritical Water Desalination System. The code was obtained from Glosson, G. (2023). Simulating and optimizing a zero-waste wave-to-water desalination system (Order No. 30603347). Available from ProQuest Dissertations & Theses Global. (2830117248). Retrieved from https://www.proquest.com/dissertations-theses/simulating-optimizing-zero-waste-wave-water/docview/2830117248/se-2
% Obtained code and the parameters were modified according to the study's purposes by Emre U. Bal (May 2024).
FW_T=WPDS.SCW.FeedTemp;
% FW_T was changed manually for each experimental trial
FW_MW=WPDS.SCW.mw;
% FW_MW was changed to 20 percent
R1_P=WPDS.SCW.R1.P;
% Pressure for the Reactor 1 was kept as is
R1_T=WPDS.SCW.R1.T;
% Temperature for the Reactor 1 was kept as is
F_T=WPDS.SCW.FurnTemp;
```

```
% Temperature for the Furnace was kept as is
P_P=WPDS.SCW.PumpPres;
% Pressure for the Pump was kept as is
TankVol=WPDS.SCW.R1.TankVol;
%% Feed Water
%   Thermodynamic properties of the feed water at the specified
temperatures
%  and pressures were taken from REFPROP
[~,FW.Enthalpy_NaCl_Binary,FW.Cp_NaCl_Binary] =
NaCl_Thermodynamic_Properties_DWCopy(0,FW_T,FW_MW);
FW.Density_NaCl_Binary = 1000*(1.49108839858636E-10*FW_MW^6 -
1.06895640117344E-08*FW_MW^5 + 2.97518592873303E-07*FW_MW^4 -
3.51699375755743E-06*FW_MW^3 + 4.04032982714853E-05*FW_MW^2 +
6.86530444136224E-03*FW_MW + 9.99102279307635E-01);
%% 1st Reactor (R1) and 2nd Reactor (R2)
% The inputs and the functions for Reactor 1 and Reactor 2 were kept as
is to maintain the consistency of the simulation
R1.Input.P_select=R1_P;
R1.Input.T_select=R1_T;
R1.Input.wt_select=FW_MW;
```

```
R2.Input.wt_select=R1.Liquid_Concentration;
% Liquid from R1 feeds into R2
R2.Input.P_select=R1_P-10;
% Pressure difference between R1 and R2
R2.Input.T_select=R1_T;
% Set value replaces Phase_Isoconcen_diagram to speed up simulation
[R1.Salt_removal_percentage, R1.Dielectric_constant,
R1.Enthalpy_NaCl_Combined, R1.Enthalpy_NaCl_Vapor,
R1.Enthalpy_NaCl_Liquid, R1.Liquid_Concentration,
R1.Vapor_Concentration, R1.Liquid_fraction, R1.Vapor_fraction,
R1.Cp_NaCl_Vapor, R1.Cp_NaCl_Liquid, R1.Density_NaCl_Vapor,
R1.Density_NaCl_Liquid] ...
    =
NaCl_Two_Phase_Thermodynamic_Properties_DWCopy(R1.Input.P_select,R1.In
put.T_select,R1.Input.wt_select);
[R2.Salt_removal_percentage, R2.Dielectric_constant,
R2.Enthalpy_NaCl_Combined, R2.Enthalpy_NaCl_Vapor,
R2.Enthalpy_NaCl_Liquid, R2.Liquid_Concentration,
R2.Vapor_Concentration, R2.Liquid_fraction, R2.Vapor_fraction,
```

```
R2.Cp_NaCl_Vapor, R2.Cp_NaCl_Liquid, R2.Density_NaCl_Vapor,
R2.Density_NaCl_Liquid] ...
    =
NaCl_Two_Phase_Thermodynamic_Properties_DWCopy(R2.Input.P_select,R2.In
put.T_select,R2.Input.wt_select);
%% Pump
Pump.Input.P_select=P_P;
% P_P was kept as is
Pump.Input.T_select=FW_T;
% FW_T was changed manually for each experimental trial
Pump.Input.wt_select=FW_MW;
% FW_MW was changed to 20 percent
[Pump.Density_NaCl_Binary, Pump.Enthalpy_NaCl_Binary,
Pump.Cp_NaCl_Binary]...
    =
NaCl_Thermodynamic_Properties_DWCopy(Pump.Input.P_select,Pump.Input.T_
select,Pump.Input.wt_select);
%% Furnace
Furnace.Input.P_select=P_P;
% Furnace pressure kept as is
```

```
Furnace.Input.T_select=F_T;
% F_T was changed manually for each experimental trial
Furnace.Input.wt_select=FW_MW;
% FW_MW was changed to 20 percent
[Furnace.Density_NaCl_Binary, Furnace.Enthalpy_NaCl_Binary,
Furnace.Cp_NaCl_Binary]...
    =
NaCl_Thermodynamic_Properties_DWCopy(Furnace.Input.P_select,Furnace.In
put.T_select,Furnace.Input.wt_select);
R1.Liquid_fraction=R1.Liquid_fraction/100;
R1.Vapor_fraction= R1.Vapor_fraction/100;
R2.Liquid_fraction=R2.Liquid_fraction/100;
R2.Vapor_fraction= R2.Vapor_fraction/100;
SCW.R1=R1; SCW.R2=R2; SCW.Pump=Pump; SCW.Furnace=Furnace;
clear R1 R2 Pump Furnace    FW_T FW_MW R1_P R1_T F_T F_P P_P TankVol
```